Radio-over-Free-Space Optical Fronthauling for Cloud Radio Access Networks

RADIO-OVER-FREE-SPACE OPTICAL FRONTHAULING FOR CLOUD RADIO ACCESS NETWORKS

BY

KHALED AHMED, B.Sc., M.Sc.

A THESIS

SUBMITTED TO THE DEPARTMENT OF ELECTRICAL & COMPUTER ENGINEERING

AND THE SCHOOL OF GRADUATE STUDIES

OF MCMASTER UNIVERSITY

IN PARTIAL FULFILMENT OF THE REQUIREMENTS

FOR THE DEGREE OF

DOCTOR OF PHILOSOPHY

Doctor of Philosophy (2019) McMaster University

(Electrical & Computer Engineering) Hamilton, Ontario, Canada

TITLE:	Radio-over-Free-Space Optical Fronthauling for Cloud Radio Access Networks
AUTHOR:	Khaled Ahmed B.Sc., M.Sc. (Electrical and Electronic Engineering) Cairo University, Giza, Egypt
SUPERVISOR:	Dr. Steve Hranilovic
NUMBER OF PAGES:	xvi, 147

To my parents, my family, and friends

Lay Abstract

The upcoming generation of wireless communications, termed fifth generation (5G), promises faster data rates and lower latency. In order to achieve this, more base stations (BSs) have to be deployed which increases the cost and complexity of the network. A solution to this challenge is to install simple BSs, i.e. radio units (RUs), that collect signals from users and forward them to a central office (CO) for joint processing which is referred to as a cloud radio access network (CRAN). The fronthaul network in a CRAN connects the RUs to the CO and it can be implemented using different kinds of links. While there are several fronthaul media (e.g., radio frequency (RF), free-space optical (FSO) links, copper lines, satellite communications, and optical fiber (OF)), optical links provide high data rates that are promising to achieve the 5G requirements. In this thesis, a novel architecture of a CRAN is considered in which analog optical links, namely FSO links and OF links, are used for fronthauling. Performance improvement in terms of rate and reliability is investigated and optimized through different design tools. In response to the challenges introduced by the proposed architecture, such as the nonlinearities of analog FSO and OF links, various design parameters are proposed in the optimization problems to tackle those challenges. Furthermore, a network planning framework is introduced to provide guidance and insights on designing the network.

Abstract

The increasing demand on user rates in the fifth generation (5G) requires network architectures that can support high data rates with acceptable reliability. In order to increase the data rates in the presence of the current spectrum crisis, shrinking cells and reusing the spectrum is a proposed solution. Conventional implementation of dense cells requires a large number of expensive BSs to locally process and decode users' signals. Another limiting factor that degrades the performance in a dense network is the inter-cell interference. A cloud radio access network (CRAN) is a promising solution to those cost, complexity, and interference challenges. A typical CRAN architecture consists of simplified low-cost base stations (BSs), termed radio units (RUs), that collect the radio frequency (RF) user equipments' (UEs) signals and forward them over the fronthaul links to the central office (CO) where signal processing is done over shared resources. Besides the reduced cost and complexity of a CRAN, the joint processing at the CO enables joint interference mitigation techniques. However, the performance of CRANs depends critically on the availability of reliable fronthaul links with large bandwidth that may be expensive. Analog optical fronthaul links provide high data rates at lower cost and complexity since UEs' signals are optically analog-modulated without digitalization, however, they suffer from other channel impairments and nonlinearities.

In this thesis, analog optical fronthaul topologies are considered in which radio signals

are forwarded over free-space optical (FSO) links, termed radio-over-free-space optical (RoFSO) links, and optical fiber (OF) links, termed radio-over-fiber (RoF) links.

Firstly, a CRAN with mixed RF/RoFSO fronthaul is considered to investigate the performance improvement when RF fronthaul links are replaced one-by-one by RoFSO links. A novel joint optimization problem is introduced for the given architecture in which the weighted sum of UEs' rates is maximized by jointly designing RF and RoFSO links. The optimization problem is solved over different numbers of RF and RoFSO links and under various weather conditions. Under favorable weather conditions, the replacement of 1 RF link by a RoFSO link is shown to increase the 50th percentile of UEs' rates by 7 times.

Secondly, the reliability of a CRAN with two-hop RoFSO/RoF fronthaul links is derived along with other performance metrics such as the average bit-error rate and the cumulative distribution function of UEs' rates. For the given architecture, the Gaussian noise model of fiber nonlinearity is applied and an optimal OF average optical power is derived to minimize the outage probability. Using the optimal power, and under favorable weather conditions, the 50th percentile of user rate exceeds 1.5 Gbps.

Finally, a CRAN with passive all-optical two-hop fronthaul links is considered where optical signals from the first RoFSO fronthaul hop are passively coupled into the RoF fronthaul link. The fronthaul outage probability is derived in the context of network planning to provide guidance on designing a set of system parameters. Those parameters include coverage area radius, density of RUs, RoFSO gain, RoFSO optical power and RoF length.

Acknowledgements

To my family and friends, thanks for the continuous support not only during my PhD but also through my entire life.

To the committee members, Dr. Jun Chen and Dr. Tim Davidson, thanks for your insightful comments and advises during the last 4 years.

To my supervisor, Dr. Steve Hranilovic, and the post-doc, Dr. Ahmed Morra thanks for your guidance during those productive years.

Abbreviations

AF	amplify-and-forward
APD	avalanche photodiode
AWGN	additive white Gaussian noise
BER	bit-error rate
BS	basestation
CDF	cumulative distribution function
CO	central office
CSI	channel state information
CP	central processor
CRAN/C-RAN	cloud radio access network
DRAN	distributed radio access network
DSC	distributed source coding
EDFA	Erbium-doped fiber amplifier
EGBMGF	extended generalized bivariate Meijer G function
FSO	free-space optical
GN	Gaussian noise
GVD	group-velocity dispersion
INR	interference-to-noise ratio

IU	intermediate unit
MMW	millimeter wave
MW	microwave
NOMA	non-orthogonal multiple access
OF	optical fiber
PD	photodiode
PIN	p-type intrinsic n-type
PON	passive optical network
RF	radio frequency
RoF	radio-over-fiber
RoFSO	radio-over-free-space optical
RU	radio unit
RV	random variables
SINR	signal-to-interference-and-noise ratio
SMF	single-mode fiber
SNR	signal-to-noise ratio
UE	user equipment
WDM	wavelength-division multiplexing

Contents

List of Figures

Chapter 1

Introduction

The requirements of the fifth generation of cellular wireless networks (5G) are far more stringent than those of the forth generation (4G) systems (Andrews *et al.*, 2014; Gupta and Jha, 2015). Aggregate data rates need to be increased by roughly three orders of magnitude while the edge rates in 5G range from 100 Mbps to 1 Gbps as compared to 1 Mbps in 4G. Additionally, peak rates for users in 5G systems may also approach high limits of tens of Gbps. Both energy usage and latency in 5G networks must also be reduced by an order of magnitude to ensure stable operation and cost-effectiveness. In order to satisfy such an extreme increase in rates, cell densification, increasing the bandwidth, and improving the spectral efficiency are essential (Andrews *et al.*, 2014). Cell densification introduces other challenges such as the increased inter-cell interference which is the bottle neck for the performance of dense networks. Another limiting factor for the deployment of dense cells, is the cost of the added base stations (BSs). Cloud radio access network (CRAN) is a promising architecture that allows for better interference mitigation as well as decreasing the cost and complexity of BSs.

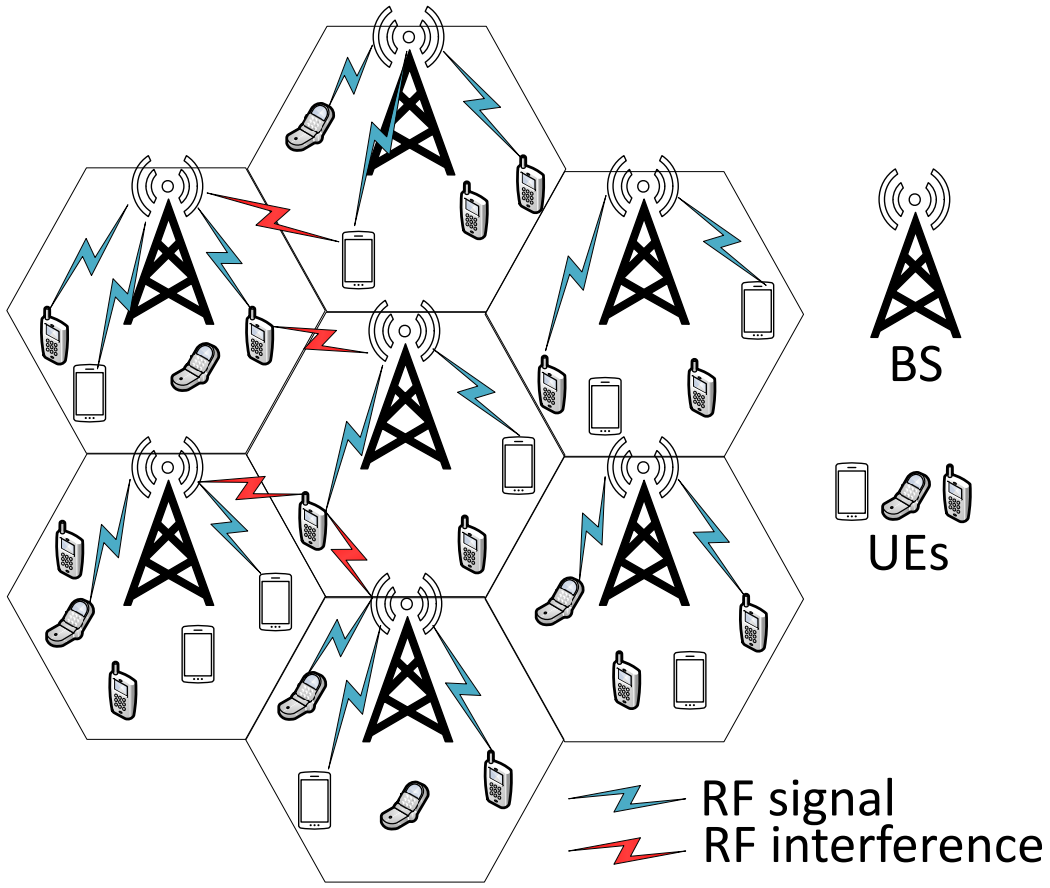

Figure 1.1: Architecture of a distributed radio access network.

1.1 Cloud Radio Access Networks

A traditional distributed radio access network (DRAN), such as distributed macro-cells in Fig. 1.1, consists of user equipments (UEs) that transmit radio frequency (RF) signals to the corresponding BSs. Each BS includes two parts for receiving and processing the signals. The first part is the radio unit (RU) which is responsible for receiving the RF signal and down-converting it to the baseband. The second stage is the baseband unit, or the digital unit, which performs sampling, quantization, and analog-to-digital conversion along with the required decoding and processing of the received signals (Wang *et al.*, 2016b). Since

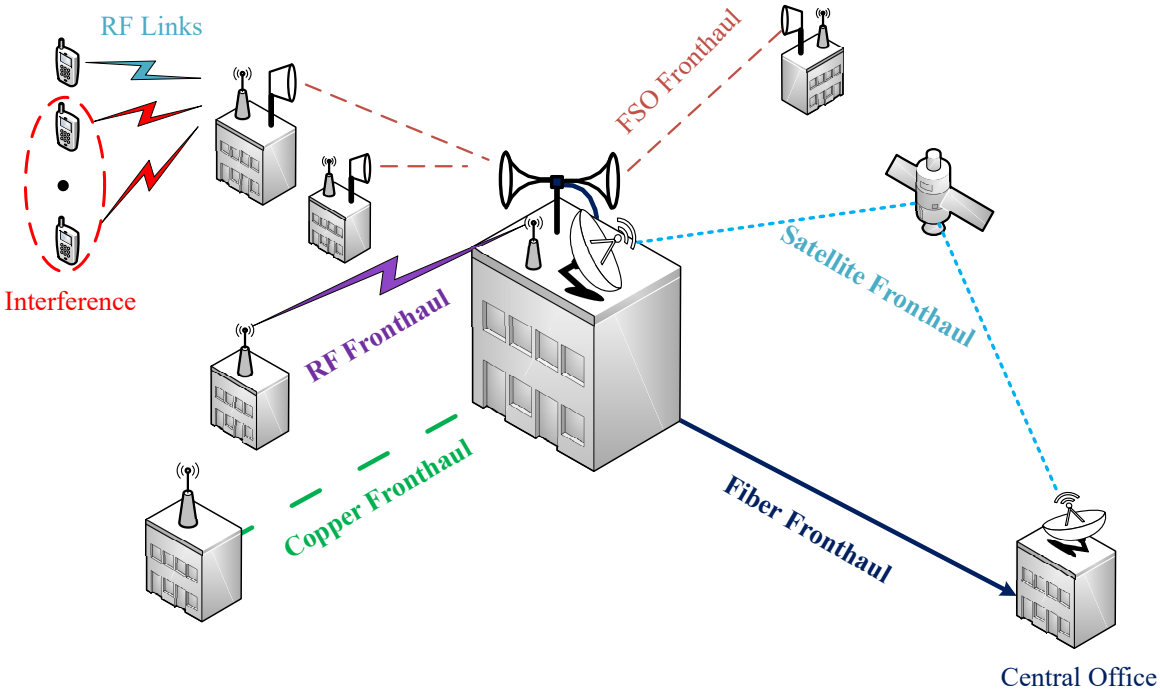

Figure 1.2: Architecture of a cloud radio access network.

all the processing is done locally, expensive and complex hardware is required at each BS. The total cost increases rapidly when a large number of BSs is deployed in a dense network which contradicts with the cost requirements of the 5G (Andrews *et al.*, 2014).

Unlike traditional DRANs, a CRAN can reduce the cost and complexity of the network by changing the structure and deploying simple RUs instead of the BSs. Figure 1.2 shows the basic structure of a CRAN which consists of two stages; the access network and the fronthaul network. In the access network, UEs transmit signals to the corresponding RUs via the RF channels. In the fronthaul network, RUs forward the received RF signals to the central office (CO) via the fronthaul links. The RUs apply one of the relaying protocols: amplify-and-forward (AF) in which the RF signals are amplified and forwarded in the analog form, decode-and-forward (DF) where the RF signals are digitized, decoded, then forwarded, or compress-and-forward (CF) where the RF signals are digitized, compressed

and then forwarded (Kim *et al.*, 2008). Finally, the CO is responsible for jointly processing and decoding all the received signals. Since UEs' signals are processed and decoded at the CO, joint interference mitigation techniques can be performed to improve the signal to interference and noise ratio (SINR) of the UEs. However, those techniques require exchanging an amount of channel state information which varies depending on the technique (Checko *et al.*, 2015). From the architecture perspective, as the processing units are centralized at the CO, the RUs operate as relaying nodes and do not require complicated nor expensive hardware to be installed locally. Such simple RUs reduce both the capital and operational expenses. They also improve the scalability of the network and make it feasible to integrate different units from various vendors (China Mobile, 2011). Furthermore, the CO can receive different user demands and allocate the resources, e.g., bandwidth, accordingly. The flexibility of resource allocation allows for better utilization of network resources (Demestichas *et al.*, 2013; Checko *et al.*, 2015). Thus, a CRAN can be a feasible solution to achieve the requirements of the 5G.

For a CRAN with compress-and-forward forthaul nodes, different source coding techniques can be used for signal compression. Distributed source coding (DSC) is favorable for the CRAN architecture since DSC allows for pushing the complexity towards the decoder. Thus, simpler RUs can be used while the heavy processing being performed at the CO. There are different techniques for DSC in the literature such as Slepian-Wolf, turbo, low-density parity-check, and Wyner-Ziv codes (Zixiang Xiong *et al.*, 2004). However, Wyner-Ziv performs better than turbo and low-density parity-check codes, i.e. lower probability of error, when the signals are correlated. While Slepian-Wolf sets the performance limit for lossless compression, Wyner-Ziv can approach that limit under general fidelity criterion. Thus, for a CRAN with interfering UEs in the access network, the fronthaul signals

are correlated and hence Wyner-Ziv is a promising DSC technique.

It is also remarkable to mention that there are other multiple access techniques that can improve the spectrum efficiency and reduce the effect of inter-cell interference. For example, non-orthogonal multiple access (NOMA) networks are promising to approach the 5G requirements (Saito *et al.*, 2013). However, CRAN has the advantage of centralized processing which reduces the cost and complexity of the radio units. Thus, among different architectures, CRAN is the main focus of this work.

1.2 Fronthaul Media

The high data rates provided by the CRANs rely on the availability of fronthaul links that can afford sufficient bandwidth, in the order of tens to hundreds of GHz (Gupta and Jha, 2015), with acceptable reliability, e.g., five-nines reliability (Agiwal *et al.*, 2016). The medium of those fronthaul links affects the rates, the cost and the bandwidth of the entire system. Thus, a careful choice of this medium, or alternatively a mixture of different media, is a critical point in designing the CRAN.

Figure 1.2 shows various fronthaul media in a two-hop CRAN while Table 1.1 shows a comparison between different fronthaul links. A leased copper link has low capital expense but it provides low data rates and requires high leasing cost. Furthermore, the cost increases linearly with the capacity. However, for applications that require low data rates with deterministic quality of service, such as voice traffic, a copper line would be favorable. A satellite link provides flexible coverage and can reach geographically challenging areas, such as an island, but it comes at a very high cost and with a long propagation delay. Wireless fronthauling using RF links has a low operational expense, however, the available bandwidth is small and often requires an additional cost of spectrum licensing. The

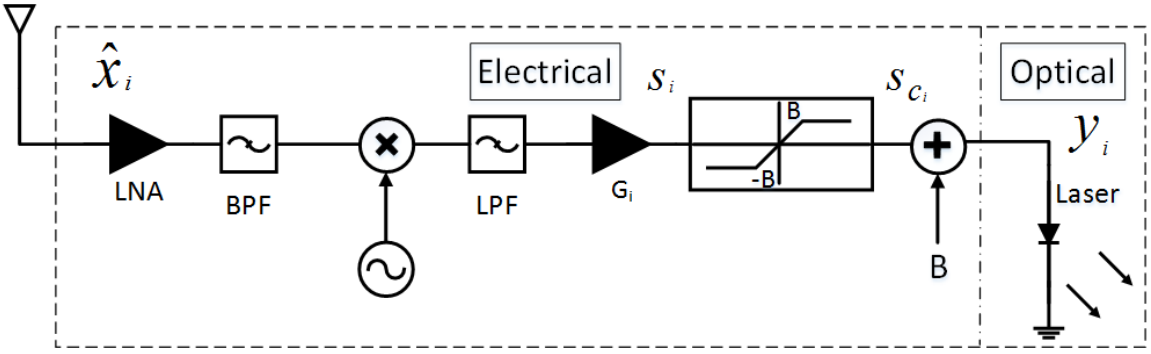

Figure 1.3: Architecture of analog RoFSO or RoF unit (Ahmed and Hranilovic, 2018).

millimeter-wave frohthauling provides high data rates due to its large unlicensed spectrum but it gets degraded by rain, requires expensive hardware, and operates well over short distances only. An optical fiber (OF) link is an ideal fronthaul medium providing high data rates and large bandwidth, however, deployment is not flexible and installation can be prohibitively expensive. An alternative fronthaul link, which combines some advantages of optical fiber and wireless fronthauling, is the free-space optical (FSO) link. Firstly, FSO fronthauling provides large unlicensed spectrum, on the order of GHz, that allows high data rates to be transmitted. Secondly, FSO links are immune to interference since the laser beam is narrow and highly directive. Thirdly, FSO units are also flexible to install, reusable, and cost-effective. On the other hand, FSO links get degraded by harsh weather conditions, such as thick fog. Thus, FSO fronthauling is a valuable candidate to be used in CRANs. Consequently, optical fronthauling, especially FSO, is the central topic of this thesis.

Table 1.1: Comparison between fronthaul media. Data is taken from (Siddique *et al.*, 2015; Tipmongkolsilp *et al.*, 2011).

Technology	Advantages	Limitations
Leased copper	Low capital expense.	Low data rates. High leasing cost. Price increases linearly with capacity.
Satellite	Flexible coverage. Solution for geographically challenging area, e.g. islands.	Low data rates.
RF links	Low operational expense.	Small bandwidth. Low data rate. Licensed spectrum fee. High initial cost.
Millimeter-wave	High data rates. Unlicensed spectrum.	Degraded by bad weather conditions (heavy rain). Not suitable for long distance links. Expensive hardware.
Optical fiber links	High data rates. Large bandwidth.	High installation cost. Not flexible. Last-mile problem.
Free-space optical links	High data rates. Large bandwidth. Cost effective. No regularity constraints.	Highly degraded by bad weather conditions (thick fog). Operates well over short distances. Requires line-of-sight.

1.3 Towards simpler RUs: analog and passive optical fronthauling

In dense networks, the cost, complexity, and energy of RUs become major design concerns (Andrews *et al.*, 2014). A digital RU requires the installation of sampling, quantization,

and decoding blocks. In addition to the high cost, designing high-speed analog-to-digital converters is more challenging at high data rates required by the 5G (Singh *et al.*, 2009). On the contrary, a simple low-cost RU, Fig. 1.3, can amplify-and-forward RF signals to the fronthaul network over analog links. For optical fronthaul links, amplifying and forwarding the RF signal without digitization is referred to as radio-over-fiber (RoF), for OF fronthauling, and radio-over-Free-space optical links (RoFSO), for FSO fronthauling (Pesek *et al.*, 2016).

1.3.1 Impairments of RoFSO and RoF links

Despite the benefits of RoFSO and RoF fronthauling, their impairments must be considered and addressed properly. Firstly, FSO links are sensitive to link range since the unguided laser beam experiences severe geometric loss. They also require a line-of-sight and proper alignment between the transmitter and the receiver to minimize the misalignment error. Additionally, FSO links are degraded by harsh weather conditions that may result in severe path loss. While clear weather is ideal for FSO links, foggy weather may introduce attenuation of up to 250 dB/km and reduce the visibility range to less than 100 m (Awan *et al.*, 2009). Furthermore, atmospheric scintillation, due to the changes in temperature and pressure, impact the FSO link (Farid and Hranilovic, 2007).

The OF link experiences a propagation loss due to the absorption and scattering along the link. Additionally, the Kerr-effect causes nonlinear interference to the transmitted signals in the OF (Poggiolini *et al.*, 2011).

At the detector side of both the FSO and the OF links, different kinds of noise are added depending on the detector and the signal power. If a p-type intrinsic n-type (PIN) photodiode is used, thermal noise dominates other types of noises. On the other hand, if

an avalanche photodiode (APD) is used at the detector, it amplifies the received signal. Since the shot noise is a function of the signal power, the amplification at the APD makes it dominate other types of noises. The PIN photodiode is favorable when the signal level is high enough and does not need further amplification at the receiver. However, if the received signal is severely attenuated, an APD is essential to compensate for the channel fading.

Analog transmission of RF signals over FSO and OF links, i.e. RoFSO and RoF, introduces new challenges to the network design. Practical constraints of the laser modulator must be taken into consideration. Due to the limited dynamic range of laser devices, the input signal must be clipped before the optical modulation as shown in Fig. 1.3. Clipping distortion degrades the signal and the amount of clipping increases with the amplitude of the signal. Thus, an amplifier prior to the clipper is required as its gain can be designed to manage this drawback. The amplifier gain must be chosen carefully to balance signal amplification with the clipping distortion. On the contrary, digital links do not experience clipping distortion. Digital signals can also be regenerated which makes digital links more immune to channel impairments. However, this comes at the cost of expensive and complex hardware required for digitization.

Previous work that considered RoFSO assumed a fixed amplifier gain (e.g., Anees and Bhatnagar, 2015b; Zedini *et al.*, 2014) which amplifies the RF signal by a constant value. Another approach, variable gain, is to normalize the incoming signal, given channel state information, then amplify it by a certain gain that satisfies a power constraint (e.g., Ansari *et al.*, 2013b; Soleimani-Nasab and Uysal, 2016). A middle ground between both approaches is to normalize the signal using average channel statistics instead of instantaneous values (e.g., Petkovic *et al.*, 2017). Those designs, however, did not consider designing the

amplifier gain from the perspective of managing the clipping distortion.

1.3.2 Passive optical network

A passive optical network (PON) consists of optical links, e.g. OF and FSO links, and optical passive elements that do not include any active devices (Lee *et al.*, 2006). The passive elements of the PON are responsible for collecting, coupling, and distributing optical signals between different stages and they are simpler and lower in cost compared with the active elements (e.g., Cai *et al.*, 2019; Zheng *et al.*, 2016). PON-based fronthauling decreases both cost and energy consumption of a CRAN (e.g., Wang *et al.*, 2016b; Tan *et al.*, 2017; Wang *et al.*, 2016a,c). On the other hand, PONs perform poorly over long distances at which multiple Erbium-doped fiber amplifiers (EDFAs) are essential to provide proper amplification at each OF span.

1.4 Rate-Range-Reliability trade-offs

In order to quantify the performance of a CRAN, a number of performance metrics need to be considered. On top of those metrics comes the data rate since it limits the applications and the quality of service (QoS) provided by the network which in turn define the communication generation it belongs to (Gupta and Jha, 2015). CRAN rate optimization has attracted considerable attention of the authors in (e.g., Park *et al.*, 2013; Najafi *et al.*, 2017; Zhou and Yu, 2016; Zhou and Yu, 2014) and it is considered in this thesis as well.

In a CRAN with time-varying wireless channels, such as FSO links with atmospheric scintillation (Farid and Hranilovic, 2007) or RF fading channels (Simon and Alouini, 2005),

maintaining high data rates is not guaranteed. Thus, besides rate analyses, another performance metric that addresses reliability of those links is required. The outage probability is a measure for the reliability of a communication link. The outage probability is defined as the probability that the rate falls below a certain threshold (Simon and Alouini, 2005). The essence of outage analysis is obvious in services that require consistent high rates such as interactive high-quality multimedia traffic (e.g., Zhang *et al.*, 2014; Agiwal *et al.*, 2016). Furthermore, the ergodic capacity is not an accurate measure for the quality of the FSO link due to the non-ergodicity of the FSO channel. On the contrary, the outage probability is essential for such block fading channels to quantify the reliability of the network. Thus the outage analysis of hybrid time varying channels, e.g. RF/FSO AF, is being carried out (e.g., Lee *et al.*, 2011; Ansari *et al.*, 2013a; Petkovic *et al.*, 2015; Anees and Bhatnagar, 2015b; Kong *et al.*, 2015; Zhang *et al.*, 2015; Soleimani-Nasab and Uysal, 2016; Trinh *et al.*, 2017; Samimi, 2019). The work in the literature can be extended to investigate the reliability of CRANs with RoFSO fronthaul links which is the main focus of this thesis.

Notice that, the higher the required rates, i.e. increasing rate threshold, the higher the probability of an outage which degrades the system reliability (Farid and Hranilovic, 2009). This trade-off is referred to as the rate-reliability trade-off. Additionally, the received signal strength is governed by losses in the wireless channel which become more severe with the length of the link. The degradation of the received signal decreases the SINR which in turn impacts both the delivered rates and the reliability of the link. Thus, range is the third branch of the trade-off, rate-range-reliability (Farid and Hranilovic, 2009). Selecting the range is a portion of a bigger problem, *network planning*, that considers different parameters related to the architecture of the network.

Planning FSO networks has not received much attention in the literature (e.g., Douik

et al., 2016; Smadi *et al.*, 2009). A cost minimization problem was addressed by Douik *et al.* (2016) by optimizing the deployment of radio and FSO backhaul links under rate and reliability constraints. Smadi *et al.* (2009) investigated the problem of allocating the FSO/RF gateways to minimize the number of links required to achieve a capacity constraint. However, none of the existing work has addressed network planning of RoFSO/RoF CRAN which is considered in this thesis. A novel network planning framework is introduced to design the coverage area (i.e. range), the density of RUs, the amplifier gain, the average optical power, the OF length, and other network parameters. The impact of each of those parameters on system reliability is investigated to provide guidance on planning the network. For example, for a given OF length and a reliability constraint, the coverage area, RU density, optical power, and amplifier gain are designed accordingly. Furthermore, in order to minimize the outage probability, an analytical expression for the optimum amplifier gain is derived.

Previous work on designing and planning CRANs has not addressed the nonlinearities of RoFSO and RoF links in the design problems despite their impact on the performance. Thus, those nonlinearities are addressed in this thesis in the context of rate maximization, outage minimization, and network planning.

1.5 Thesis Outline

This thesis provides a set of performance evaluation and system design tools for CRANs with mixed RF/RoFSO and hybrid RoFSO/RoF fronthaul links. As discussed in Sec. 1.4, a variety of performance metrics are considered such as user rates and outage probability. The objective of the design tools is to optimize those metrics, i.e. to maximize the rates and minimize the outage given a set of constraints. Furthermore, the thesis introduces a network

planning framework to design the CRAN fronthaul network and investigate the impact of various design parameters on the outage probability. The impairments of the RoFSO and the RoF, Sec. 1.3.1, are addressed and considered in the design problem. The nonlinearities associated with analog optical fronthaul links are included via Bussgang model (Bussgang, 1952), for the clipping distortion while a Gaussian noise (GN) model (Poggiolini *et al.*, 2011) is applied for the OF nonlinear interference.

This thesis is written in accordance with regulations for "sandwich" format. Besides the introduction, it includes three self-contained chapters. Each chapter has its own introduction, body, conclusion, and possibly appendices. The references from all chapters are collected in one bibliography list at the end of the thesis. The organization of the thesis is as follows:

In **Chapter 2**, a CRAN with mixed RF and RoFSO fronthaul links is considered. The RF links are digital links that follow the CF relaying protocol while the RoFSO links apply AF relaying protocol as explained in Sec. 1.3. In order to optimize the data rates of the CRAN, Sec. 1.4, a novel joint optimization problem is introduced in **Chapter 2**. The objective of the optimization problem is to maximize the summation of weighted user rates by designing the quantizers of the digital RF links and the amplifiers of the RoFSO links. In order to quantify the improvement due to replacing RF links with RoFSO links, the optimization problem is solved for different fronthaul structures starting from all-RF to all-RoFSO fronthauling. Furthermore, different weather conditions are considered to show the sensitivity of the RoFSO links to each of them. A year of weather data, quantized into four cases: clear, rain, snow, and fog, from two Canadian cities is considered to evaluate the impact and the frequency of each weather condition.

While **Chapter 2** motivates the use of RoFSO links, **Chapter 3** extends that by considering another type of hybrid fronthauling, namely two-hop RoFSO/RoF fronthahuling. The main objective of this chapter is to address the reliability problem, discussed in Sec. 1.4, with more focus on the effect of OF nonlinear interference as introduced in Sec. 1.3.1. The clipping distortion of the RoFSO and RoF links is addressed by assuming a conservative design of the gain that maintains a negligible clipping noise. Besides the outage probability analyses, other performance metrics are derived such as the cumulative distribution function of user rates, and the bit-error rate. Furthermore, asymptotic expressions of those performance metrics at high SNR are derived. Using the asymptotic expressions, an optimum average optical power is obtained for the OF to balance the level of signal power with the nonlinear interference.

A network planning framework of an uplink all-optical RoFSO/RoF C-RAN fronthaul is presented in **Chapter 4**. While the CRAN fronthaul media are the same as in **Chapter 3**, there are three main differences that make the architecture in this chapter unique. Firstly, as described in Sec. 1.3.2, a passive optical network is considered in which the received optical signals from RoFSO links are passively coupled into the RoF using an opto-coupler. Secondly, all RUs located in a circular area, defined as *coverage area*, forward the collected RF signals to an intermediate unit (IU) at the center of the coverage area via RoFSO fronthaul links which in turn passively couples the optical signals to the OF via the RoF link. Thirdly, in order to reduce the nonlinear interference in the OF, RUs within a certain radius, $r_{\min}$, from the IU scale down their average transmitted optical power such that the received power from any of them is the same as the power received from the RU at $r_{\min}$. Portion of the work in this chapter addresses the trade-off between reliability and range as mentioned in Sec. 1.4. The rest of the work focuses on providing network planning tools

to design and tune various system parameters such as the coverage area radius, the density of RUs, $r_{\min}$, the optical power, the length of the OF link, and the gain of the RoFSO links. An analytical expression of the fronthaul outage probability is derived and an approximate optimum RoFSO gain that minimizes the outage is obtained accordingly.

Chapter 5 concludes the thesis and presents the possible future directions and extensions to this work.

Further contributions and extensions to the work in **Chapter** 3 and **Chapter** 4 were not published but they are included in the **Appendices**. While the conservative design in **Chapter** 3 results into negligible clipping noise, the effect of clipping distortion is added in **Appendix** A. The derivation in **Appendix** A shows the required modifications to the analyses in **Chapter** 3 to include the clipping distortion which completes the analyses in **Chapter** 3. Numerical simulations are included in **Appendix** A to reflect the degradation due to the clipping distortion at different gain values. Simulation results also justify the assumption of the conservative gain design in **Chapter** 3 by showing the negligible effect of the clipping distortion at conservative gain values. In **Chapter** 3, in order to make the analyses tractable, no joint interference mitigation technique was considered. Thus, successive interference cancellation (SIC) is considered in **Appendix** B. Rate equations and Monte-Carlo simulations are provided for SIC decoding. The simulation results show the improvement in the CDF of UE rates due to SIC. The work in **Appendix** B is essential to reflect one of the key advantages of the CRAN by applying a joint interference mitigation technique at the CO. Furthermore, outage probability derivation of the fronthaul links from **Chapter** 4 is added in **Appendix** C for the case when the OF nonlinear interference becomes dominant over other noise sources. While the nonlinear interference term is not dominant for the given dimensions of the CRAN in **Chapter** 4, it may be dominant in a

different scenario when a long OF, e.g. tens or hundreds of km, is used and large optical power is transmitted. That scenario would trigger severe nonlinear interference and hence the added derivation would be more precise.

1.6 Description of Contributions to Publications

This thesis has been written in the form of a "sandwich thesis". Chapter 2 and 3 of this thesis are already published while Chapter 4 is currently submitted and under review. This section clarifies the contribution of each of the co-authors to the work.

Chapter 2: **C-RAN Uplink Optimization Using Mixed Radio and FSO Fronthaul**

Authors: Khaled Ahmed and Steve Hranilovic

Khaled Ahmed carried out all the research, analyses, derivations, and simulations in this paper. He also obtained all the graphs and did all the writing of this paper. Dr. Steve Hranilovic helped with editing the final version of the paper and guiding the research. The material in this chapter was published in *IEEE/OSA Journal of Optical Communications and Networking* (Volume: 10, Number: 6, Pages: 603 – 612, June 2018) (Ahmed and Hranilovic, 2018). The bulk of this work appears here, however minor modifications have been made to improve the clarity of the thesis. IEEE owns the copyright of the material in this chapter and it is permitted to be re-used in the thesis.

Chapter 3: **Impact of Fiber Nonlinearity on 5G Backhauling via Mixed FSO/Fiber Network**

Authors: Ahmed E. Morra, Khaled Ahmed, and Steve Hranilovic

This paper was primarily motivated by the postdoctoral fellow, Dr. Morra, who carried out a majority of the research, derivations, and simulations. Khaled Ahmed worked jointly

with Dr. Morra to make the derivations tractable by developing the following assumptions. First assumption is to use a conservative gain at the amplifiers to ignore the clipping distortion. The second assumption is to ignore the squared noise term with respect to the beating noise term. Khaled Ahmed also wrote portions of the code to verify the second assumption by comparing the two noise variances. Additionally, Khaled Ahmed performed the analyses to include the effect of the clipping distortion that was ignored in the analyses in this chapter. He also performed simulations, by modifying Dr. Morra's code, to provide results that reflect the clipping distortion and justify the conservative gain design. Analysis and simulations for the effect of clipping distortion are included in the **Appendix** A.

Furthermore, Khaled Ahmed wrote a subsection in the paper providing rate equations when SIC is applied and performed Monte-Carlo simulations to show the resulting improvement in the CDF of UE rates. However, those parts were removed late in the editing process. Although those rate equations and results do not appear in the final version of the paper, they are included in **Appendix** B. Khaled Ahmed had intellectual input as he helped to define the direction and the scope of the paper and provided guidance, and his simulations motivated the paper in **Chapter** 2. Finally, Dr. Morra wrote the first draft of the paper that was revised and modified by Khaled Ahmed and Dr. Steve Hranilovic afterwards. This paper was accepted and published in *IEEE Access* (Volume: 5, Pages: 19942 – 19950, 2017) (Morra *et al.*, 2017). The bulk of this work appears here, however minor modifications have been made to improve the clarity of the thesis. IEEE owns the copyright of the material in this chapter and it is permitted to be re-used in the thesis.

Chapter 4: **Network Planning of Uplink All-Optical Passive FSO/OF C-RAN Fronthaul**

Authors: Khaled Ahmed, Ahmed E. Morra, and Steve Hranilovic

Khaled Ahmed performed all the modelling, derivations, and simulations in this paper. Dr. Morra gave comments on the work and provided guidance on the application of the Gaussian Noise (GN) model of the fiber non-linearity. Khaled Ahmed wrote the first draft of the paper and modified it in accordance with Dr. Hranilovic and Dr. Morra's suggestions. Khaled Ahmed also added an extension to this work by providing the outage analysis for the case when the nonlinear interference dominates other sources of noise. The derivation is provided in **Appendix** C. The material in this chapter has been submitted to *IEEE/OSA Journal of Optical Communications and Networking* (11 pages, May 2019) and is currently under review.

Chapter 2

C-RAN Uplink Optimization Using Mixed Radio and FSO Fronthaul

In this chapter, the problem of CRAN rate optimization is addressed as discussed in Sec. 1.4. A CRAN with mixed RF/RoFSO fronthaul media is considered. A novel joint optimization tool is introduced to maximize the weighted sum of UE rates by jointly designing the quantizers of the digital RF links and the amplifiers of the RoFSO links. As discussed in Sec. 1.2, different fronthual media have benefits and limitations. In order to quantify the importance of the RoFSO links versus the RF links, the optimization problem is solved over different cases in which the RF fronthaul links are replaced gradually by RoFSO links. On the other hand, the degradation due to the impairments of the RoFSO links, Sec. 1.3.1, are considered in the design problem. The clipping distortion is included using the Bussgang's model and addressed in the optimization problem. Furthermore, the impact of different weather conditions on data rates is considered using weather measurements from Toronto, Ontario, and Gander airport, Newfoundland and Labrador, Canada.

The work in this chapter appeared in *IEEE/OSA Journal of Optical Communications*

and Networking (Volume: 10, Number: 6, Pages: 603 – 612, June 2018) (Ahmed and Hranilovic, 2018). Minor modifications have been made to improve the clarity of this work. IEEE owns the copyright of the material in this chapter and it is permitted to be re-used in the thesis.

Abstract Cloud Radio Access Networks (C-RANs) are a promising architecture for 5G systems in which simple radio units (RUs) fronthaul signals to a central processor (CP) for joint decoding. Although the C-RAN has reduced cost and complexity, high data rate fronthaul links are necessary. In this paper, we investigate the joint design of wireless fronthaul networks using both radio frequency (RF) and radio-over-free-space optical (RoFSO) links in the uplink of a C-RAN. Unlike earlier work which focuses on performance characterization of RF/FSO fronthaul networks, this paper presents a novel optimization approach to jointly design the quantizers for the RF fronthaul links and the amplifier gains of the RoFSO fronthaul links which suffer from clipping distortion. A subset of RUs fronthaul data via radio links using Wyner-Ziv source coding subject to a shared sum capacity constraint while other RUs employ RoFSO fronthaul which converts the incoming RF receptions to optical signals by analog modulation of a laser. The optimization problem jointly designs both RF fronthaul and RoFSO fronthaul links to maximize the weighted sum user rates. Simulation results of a simple C-RAN using measured weather data for two locations demonstrate that adding RoFSO links results in drastic improvements in end user rates but requires careful design of RF and RoFSO fronthaul links.

2.1 Introduction

Upcoming 5G networks will require huge increases in data rates while simultaneously demanding low latency and low energy consumption. In order to satisfy these requirements, approaches such as cell densification, increased bandwidth and improved spectral efficiency are essential (Andrews *et al.*, 2014).

The Cloud Radio Access Network (C-RAN) is a promising network architecture for 5G systems in which the processing of the signals is done in a central processor (CP) instead

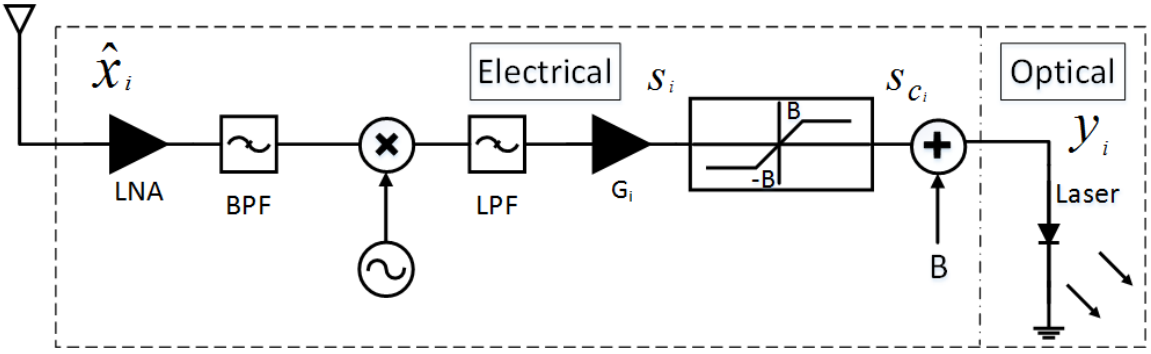

Figure 2.1: Architecture of a Radio-over-FSO Node.

of distributing processing over many basestations (BSs). Since the processing is moved to the CP, many simpler, lower cost radio units (RUs) are deployed to capture signals from user equipment (UEs) and to forward them to the CP. The CP can then perform joint encoding/decoding yielding significantly improved inter-cell interference mitigation, higher signal-to-interference-and-noise ratio (SINR) and ultimately end user rates (Andrews *et al.*, 2014).

The advantages of the C-RAN approach hinge on having high-speed, reliable fronthaul links. Although dedicated wired copper or fiber optic fronthaul links are ideal fronthaul media, their deployment is not flexible and installation can be prohibitively expensive. Wireless fronthaul using a radio frequency (RF) link has a low operational expense, however, the available bandwidth is small and often requires the additional cost of spectrum licensing. The use of free-space optical (FSO) links for fronthauling of C-RAN data has the advantage of high data rates, free spectrum, and immunity to radio interference. However, FSO links are sensitive to link range, require a line-of-sight and are impaired by weather, especially fog.

There has been considerable work to quantify the performance of the C-RAN architecture with a variety of media for fronthauling. Pham *et al.* (2015) considered using microwave, millimeter wave (MMW) links, optical fiber and FSO links for access and fronthaul networks and quantify the performance of given networks via the outage probability. Usman *et al.* (2014) studied a switching-based hybrid FSO/RF transmission and presented the average bit error rate (BER) of the system. Bhatnagar and Arti (2013) considered a hybrid satellite-terrestrial FSO cooperative link and derived an approximate average symbol error rate. In (Trinh *et al.*, 2017) and (Kong *et al.*, 2015) the authors studied and derived performance metrics for a mixed RF/FSO system with optical fiber fronthaul links (Trinh *et al.*, 2017) and a hybrid RF/FSO system with FSO fronthaul links (Kong *et al.*, 2015). A network-layer design for C-RAN fronthaul networks using RF/FSO links is presented in (Dahrouj *et al.*, 2015) under a cost constraint, however, the physical layer design of such networks is not explicitly considered. A common thread through earlier work has been the focus on quantification of the performance of C-RAN's with RF/FSO fronthaul while comparatively little work has been done on the joint design of such fronthaul systems.

Fronthaul using FSO can be readily implemented as a *radio-over-FSO* (RoFSO) link which collects the received RF emissions of the users and converts them to the optical domain through the analog modulation of a laser emitter (as shown in Fig. 2.1). The advantages of RoFSO for fronthaul are that it does not require complex sampling, quantization and recoding as is necessary with radio fronthaul links. Thus, the RoFSO fronthaul links act as amplify-and-forward (AF) nodes converting from RF to optical bands. Previous studies using RoFSO considered a fixed amplifier gain (Anees and Bhatnagar, 2015b; Lee *et al.*, 2011; Anees and Bhatnagar, 2014; Zedini *et al.*, 2015b; Petkovic, 2015; Park *et al.*, 2013; Ansari *et al.*, 2013c; Zedini *et al.*, 2014; Ansari *et al.*, 2013a; Anees and Bhatnagar,

2015a) in which case the signal is amplified with a constant value independent on the received signal power. Variable gain scenarios have also been studied in which the channel state information is needed to normalize the incoming signals to satisfy an output power constraint (Zedini *et al.*, 2015a; Ansari *et al.*, 2013b; Soleimani-Nasab and Uysal, 2016; Petkovic *et al.*, 2017). Recently and in parallel, a joint design of a hybrid RF/FSO fronthaul has been considered using digital FSO links (Najafi *et al.*, 2017). These digital FSO links are complex and the design procedure does not explicitly take into account the unique nature of the FSO channel, in particular issues of transmitter non-linearity. In all previous designs, however, the impact of the finite dynamic range of the RoFSO emitter was not considered and nonlinear clipping, inherent in such links, was ignored.

In this work, we present an optimization-based approach to the joint design of a C-RAN uplink fronthaul using both RF and RoFSO links. Unlike earlier work on RF/FSO fronthaul, this work develops the physical layer design of such networks to maximize user rates under a fairness criterion. Additionally, our design approach includes the gain, G_i, of the AF RoFSO links in the optimization formulation to balance the tradeoff between transmitted optical power and clipping distortion. Fronthaul networks for C-RAN uplink are designed in a number of scenarios with different numbers of RF and RoFSO fronthaul units. The cumulative distribution function (CDF) of user rates is computed for each design and using measured weather data from two locations to quantify the impact on the RoFSO fronthaul links.

The paper is organized as follows. In Sec. 2.2, a system model for the C-RAN with RF and RoFSO fronthaul is presented. In Sec. 2.3, an optimization problem is presented to design the uplink fronthaul of a C-RAN network considering a fixed RF fronthaul capacity and the RoFSO analog gain. Sec. 2.4 presents simulation results quantifying the rate gains

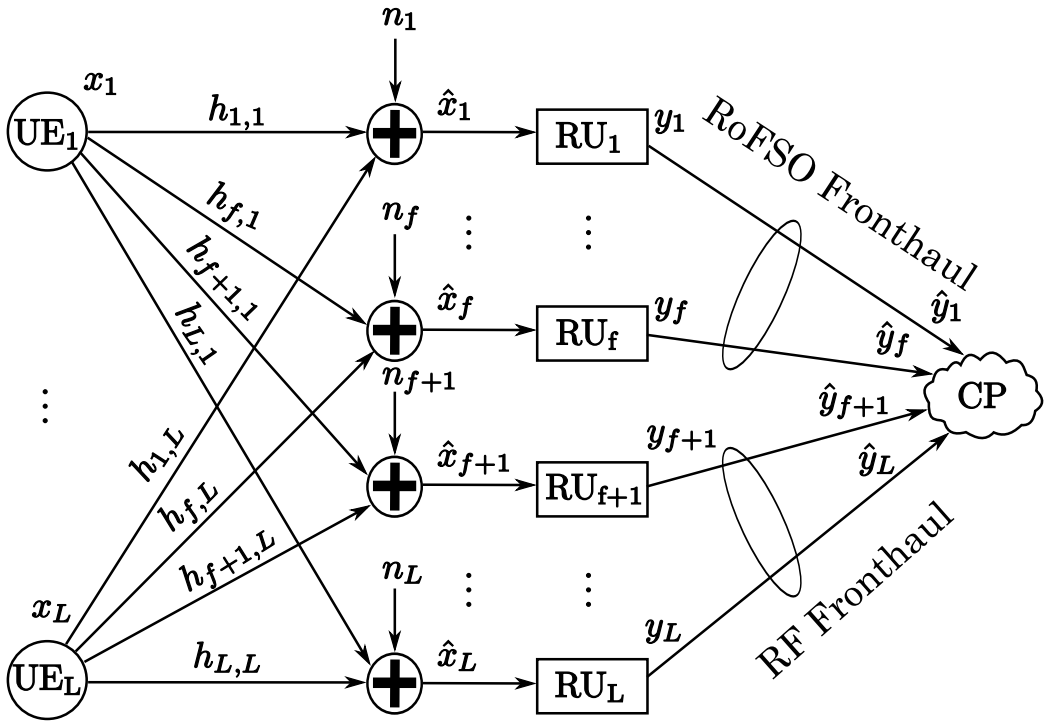

Figure 2.2: C-RAN System Model with RF and RoFSO fronthaul links.

for a variety of designs and the paper concludes in Sec. 2.5.

2.2 System Model

Fig. 2.2 shows a slice of the network consisting of L users in L cells transmitting to their RUs which forward signals to the CP over the fronthaul links. The C-RAN fronthaul in Fig. 2.2 consists of f RoFSO fronthaul links and $L - f$ RF fronthaul links. Assuming a frequency reuse of 1, then each slice of the network consists of L users from L cells transmitting signals to the corresponding RUs and interfering with each other. The complete network is formed using several such slices corresponding to independent user bands. In the following, the models of the access network and fronthaul are provided.

2.2.1 Radio Access Network

A set of L users from L cells transmit signals, x_i, with power P_i to the L RUs. The UE-to-RU radio channels, $h_{i,j}$, connecting users to RUs are assumed to have independent Rayleigh fading with pathloss dependent on their position. The noise, n_i, added at the RUs is assumed to be independent and identically distributed white Gaussian noise (AWGN) with zero mean and variance $\sigma^2_{n_i}$. The total received signal at the i^{th} RU, $\hat{x_i}$, is

$$\hat{x_i} = \sum_{j=1}^{L} x_j h_{i,j} + n_i \ , \qquad i = 1, 2, \ldots, L. \tag{2.1}$$

These received signals are forwarded to the CP over a mixed RF/RoFSO fronthaul links discussed in the following subsections.

2.2.2 Radio Frequency Fronthaul

The $L-f$ RUs with RF fronthaul quantize the received signals via Wyner-Ziv source coding and forward them to the CP over a shared radio fronthaul link. All RF fronthaul links are assumed to share a limited fronthaul capacity, C. The communication model from the users to the CP can be modelled as a *compress-and-forward* relaying system (Zhou and Yu, 2014).

The RUs employ a complex A/D to sample and quantize the received signal, $\hat{x_i}$, with acceptable resolution to yield

$$y_i = \hat{x_i} + z_i \ , \qquad i = f + 1, \ldots L \tag{2.2}$$

where z_i represents the quantization noise with a quantization noise power q_i^2. The quantizers for all RUs employing RF fronthaul are designed to ensure a sum fronthaul capacity constraint (defined in Sec. 2.3) is met. The quantization noise power terms can be collected into the following matrix

$$\Lambda_q = \begin{bmatrix} q_{f+1}^2 & 0 & \cdots & 0 \\ 0 & q_{f+2}^2 & & \vdots \\ \vdots & & \ddots & 0 \\ 0 & \cdots & 0 & q_L^2 \end{bmatrix}_{(L-f)\times(L-f)} .$$

Subject to the shared RF fronthaul capacity constraint, Λ_q is designed in Sec. 2.3 to maximize the weighted sum rate for each network slice.

In this work the RF fronthaul network is modelled as having a fixed and limited capacity, C, that can be shared between all RUs. This model has been used widely in the literature (e.g., (Zhou and Yu, 2014; Sanderovich *et al.*, 2008, 2009b,a)) to study the performance of the decode-and-forward relaying networks which also model the RF fronthaul in the proposed C-RAN structure. An implicit assumption of these models is that the total capacity of the fronthaul network is fixed, i.e. at C, and shared in a wireless medium using, for example, TDMA or FDMA orthogonal approaches. Specifically, the number of time or frequency slots for fronthaul can be allocated to different RUs as allocated in the design problem in Sec. 2.3. Though this RF fronthaul scenario does not model the instantaneous variation in the sum fronthaul capacity, it is used to model the key features of a shared fronthaul channel. This assumption is favorable for a simple system with fixed fronthaul rate in which a conservative design is adopted rather than a varying rate scheme.

It is assumed that the RUs employ powerful channel codes to approach the capacity of

the underlying RF fronthaul links. Thus, the received RF fronthaul signals at the CP are modelled as identical to the quantized user signals, i.e., $\hat{y}_i = y_i$.

2.2.3 Radio-over-Free-space Optics Fronthaul

RoFSO front end

For the f RUs with optical wireless fronthaul, as shown in Fig. 2.1, the RoFSO unit converts the received radio signals to optical domain for forwarding to the CP. The received RF signals from the access network are amplified and filtered at the receiver before being downconverted.

Given that the laser outputs an optical intensity, the input to the laser driver must be non-negative and the average optical power is constrained by eye-safety regulations. To ensure that both conditions are satisfied, an analog clipper is typically employed and a bias is added to ensure the input is non-negative. Define B as the clipping level for the signal as well as the added bias to ensure eye-safe operation, as shown in Fig. 2.1. Due to the random gain of the the wireless access channel, an amplifier with gain G_i is placed before the clipper to control the amount of clipping introduced.

Clipping Noise Analysis

In order to model the clipping noise in the RoFSO unit, a linear regression model based on Bussgang theory (Bussgang, 1952) is applied. As described in the appendix, for the i-th RU, the clipper is modelled as scaling the input by the correlation coefficient K_i and adding clipping noise n_{c_i}. Assuming the received $\hat{x}_i$ are zero mean and have variance $\sigma^2_{\hat{x}_i}$,

the overall model of the i^{th} RoFSO RU from radio input, $\hat{x}_i$, to optical output, y_i, is

$$y_i = K_i \, G_i \, \hat{x}_i + n_{c_i} \, , \qquad i = 1, \dots f \tag{2.3}$$

where

$$K_i = \text{erf} \left(\frac{B}{\sqrt{2G_i^2 \sigma_{\hat{x}_i}^2}} \right) \tag{2.4}$$

$$\sigma_{c_i}^2 = B^2 \left(1 - \frac{K_i^2 G_i^2 \sigma_{\hat{x}_i}^2}{B^2} - \sqrt{\frac{2G_i^2 \sigma_{\hat{x}_i}^2}{\pi B^2}} e^{-\frac{B^2}{2G_i^2 \sigma_{\hat{x}_i}^2}} + \left(\frac{G_i^2 \sigma_{\hat{x}_i}^2}{B^2} - 1 \right) \text{erf} \left(\frac{B}{\sqrt{2G_i^2 \sigma_{\hat{x}_i}^2}} \right) \right) \tag{2.5}$$

The clipping noise is in general non-Gaussian. In the remainder of this paper, however, n_{c_i} is modelled as an independent, Gaussian random variable per network slice with variance $\sigma_{c_i}^2$ which can be thought of as a worst case scenario given the maxentropic nature of the normal distribution. Additionally notice that that the gain G_i for each RU controls the amount of clipping introduced into the transmitted optical signal and is designed for each network slice in Sec. 2.3.

Unlike digital FSO links, there is no need to decode, quantize or modulate the optical signal which keeps the RoFSO node simple and cost-efficient with low power and low latency. Thus, the C-RAN model with the analog RoFSO node can be modelled as an analog amplify-and-forward relaying model.

Free-space optical propagation model

The received signal at the CP from the RoFSO link is

$$\hat{y}_i = \eta g_i y_i + v_i \ , \qquad i = 1, \ldots, f \tag{2.6}$$

where v_i is the received AWGN noise with variance σ^2_{FSO}, η is the responsivity of the photodiode and g_i represents the attenuation of the i^{th} FSO channel.

The FSO channel gain is typically factored into three components representing loss, scintillation and pointing errors, i.e., $g_i = g_{l_i} g_{a_i} g_{p_i}$ (Farid and Hranilovic, 2007). Since the fronthaul links are typically short (i.e., < 1 km), atmospheric intensity fluctuations are modeled by a log-normal distribution for the weak turbulence regime. Notice that for the range of distances given in Table 2.1, the resulting scintillation index is in the range of $[0 - 0.75]$ which makes the log-normal distribution a valid model for these cases (Kiasaleh, 2005). The log-normal distribution takes the form

$$f_{g_{a_i}}(g_{a_i}) = \frac{1}{2 g_{a_i} \sqrt{2\pi {\sigma_{d_i}}^2}} \exp\left(- \frac{(\ln g_{a_i} + 2{\sigma_{d_i}}^2)^2}{8{\sigma_{d_i}}^2} \right) \tag{2.7}$$

with ${\sigma_{d_i}}^2 = 0.30545 {C_n}^2 k^{7/6} {d_i}^{11/6}$ where C_n^2 is the index of refraction structure parameter, k is the optical wave number and d_i is the distance between the RU$_i$ and the CP.

The propagation loss is described by the Beers-Lambert law

$$g_{l_i} = \exp(-\gamma d_i) \tag{2.8}$$

where γ is the attenuation coefficient, in units of dB/km, which depends heavily on weather conditions.

The impact of the misalignment is not considered here, i.e. $g_{p_i} = 1$, since the lengths of the FSO fronthaul links are typically short, as shown in Table 2.1. For such short distances the effect of the pointing error can be largely mitigated using proper techniques at the transmitter and/or the receiver (Khalighi and Uysal, 2014). For example, at the transmitter, increasing the beam width and/or the beam divergence can allow acceptable power to be delivered at the receiver with little pointing error. Also, the receiver may employ active tracking to continuously point at the transmitter allowing for a better field of view.

2.2.4 Overall Fronthaul Model

The overall channel matrix describing the two stage UE-to-CP link is

$$H = \begin{bmatrix} K_1\, G_1\, \eta g_1 h_{1,1} & \dots & K_1\, G_1\, \eta g_1 h_{1,L} \\ \vdots & & \vdots \\ K_f\, G_f\, \eta g_f h_{f,1} & \cdots & K_f\, G_f\, \eta g_f h_{f,L} \\ h_{f+1,1} & \cdots & h_{f+1,L} \\ \vdots & & \vdots \\ h_{L,1} & \cdots & h_{L,L} \end{bmatrix}_{L \times L} \tag{2.9}$$

To simplify the formulation, define a diagonal matrix Ω that includes all noise powers received at the CP excluding the quantization noise power Λ_q. Each of the noise powers is

scaled according to gains along the path from its source to the CP as follows

$$\Omega = \begin{bmatrix} O_1 & 0 & \cdots & 0 \\ 0 & O_2 & & \vdots \\ \vdots & & \ddots & 0 \\ 0 & \cdots & 0 & O_L \end{bmatrix}_{L\times L}.$$

where

$$O_i = \begin{cases} \eta^2 g_i^2 \left(K_i^2 G_i^2 \sigma_{n_i}^2 + \sigma_{c_i}^2\right) + \sigma_{FSO}^2 & i = 1, \dots f \\ \sigma_{n_i}^2 & i = f+1, \dots L \end{cases} \tag{2.10}$$

Although the system model for the RF fronthaul links given in (Zhou and Yu, 2014) is employed, it is noteworthy that the RF fronthaul links in this model are compress-and-forward links that share a limited sum fronthaul capacity constraint and require powerful and complex quantization and coding techniques to be realized. On the contrary, the RoFSO links are simple *amplify-and-forward* links which have limited signal processing. Thus, it is necessary to account for the impacts of noise, attenuation, clipping, and range-dependent loss over weather conditions in order to model the RoFSO fronthaul link.

2.3 Optimization Problem Formulation

In order to model the C-RAN with the hybrid RF/RoFSO fronthaul, define the *pseudo identity matrix*, $\widehat{I}$, having $L - f$ rows and L columns as

$$\widehat{I} = \begin{bmatrix} \underbrace{0 & \cdots & 0}_{f} & \underbrace{1 & \dots & 0 \\ \vdots & \ddots & \vdots & \vdots & \ddots & \vdots \\ 0 & \cdots & 0 & 0 & \cdots & 1}_{I_{(L-f)\times(L-f)}} \end{bmatrix}_{(L-f)\times L}.$$

For a square $L \times L$ matrix, A, it is clear that $\widehat{I}A$ is an $L - f \times L$ matrix which is similar to A except that the top f Rows are deleted. Also for a square $L - f \times L - f$ matrix B, $\widehat{I}^T B \widehat{I}$ is the same as B but with f rows and f columns of all zeros concatenated at the top and the left of the matrix respectively.

Let the users $1 \dots L$ be ordered in terms of their long-term average rates from best to worst. Those rates are calculated over all previous assigned rates from previous channel instants and up to the current instant. While this order may not be optimum for maximizing the rates, it motivates more fairness. Since UEs with lower long-term rates are decoded the last after removing previous UEs' interference, this improves their SINR and increases their rates. If successive decoding is applied in the same order, and the received signals at the CP from both the RoFSO and the RF fronthaul links are jointly decoded, then the i^{th} user rate, R_i, is

$$R_i = \log \frac{\left| \sum_{j=i}^{L} P_j h_j h_j^H + \widehat{I}^T \Lambda_q \widehat{I} + \Omega \right|}{\left| \sum_{j>i}^{L} P_j h_j h_j^H + \widehat{I}^T \Lambda_q \widehat{I} + \Omega \right|} \tag{2.11}$$

where h_j is the i^{th}column of the channel matrix H. The user rate is limited by the interference from the successive users that are not yet decoded as well as the noise from the channel, the quantizers, and clipping. The sum of user rates arises directly from (2.11) as

$$\sum_{i=1}^{L} R_i = \log \frac{\left| H V_x H^H + \widehat{I}^T \Lambda_q \widehat{I} + \Omega \right|}{\left| \widehat{I}^T \Lambda_q \widehat{I} + \Omega \right|} \tag{2.12}$$

where V_x is a diagonal matrix with transmitted users' powers. The sum of the users' rates follows from (2.11) as the denominator of R_i is the same as the numerator of R_{i+1}. After cancellation, only the numerator of R_1 and the denominator of R_L remain and appear

in (2.12). Notice that the rate equation in (2.11) is quite similar to the rates obtained in NOMA, Sec. 1.1, since both are multiple access techniques that assume successive interference cancellation at the detector (Saito *et al.*, 2013).

The selection of the RoFSO gain, G_i, and the quantizer used for the RF fronthaul can be determined by considering the following joint optimization of the weighted sum rate as,

$$\max_{\Lambda_q, G_r} \sum_{i=1}^{L} \mu_i \log \frac{\left| \sum_{j=i}^{L} P_j h_j h_j^H + \widehat{I}^T \Lambda_q \widehat{I} + \Omega \right|}{\left| \sum_{j>i}^{L} P_j h_j h_j^H + \widehat{I}^T \Lambda_q \widehat{I} + \Omega \right|} \tag{2.13}$$

$$s.t. \quad \log \frac{\left| \sum_{j=1}^{L} P_j \widehat{I} h_j \left(\widehat{I} h_j \right)^H + \Lambda_q + \widehat{I} \Omega \widehat{I}^T \right|}{|\Lambda_q|} \leq C \tag{2.14}$$

$$\Lambda_q (i,j) = 0 \text{ for } i \neq j$$

$$\Lambda_q (i,i) \geq 0$$

$$G_r > 0, r = 1 \ldots f$$

where C is the total shared RF fronthaul capacity. Notice that $\widehat{I}$ eliminates the contribution of the FSO links in the RF fronthaul capacity such that the constraint (2.14) is applied to the RF fronthaul links only. Also, since C limits the fronthaul RF capacity, only Λ_q is considered as noise for the CP so it appears at the denominator while other noise terms in Ω are treated as signal powers transmitted from the RUs. Notice that the RoFSO gain G_i impacts the objective through K_r, the clipping noise $\sigma_{c_r}^2$ in Ω as well as scaling signal and noise powers depending on their path to the CP. Also notice that the obtained quantization noise variances can be used to design different parameters of the quantizers such as the number of levels, number of bits, and the voltage range.

The weights, $\mu_L > \cdots > \mu_1$, are chosen to approach a long term fairness among different users. At every new channel realization, the weight of each user is updated in inverse proportional to the long term average rates (Yu *et al.*, 2011). For each instance of the problem, the users are ordered according to their average rates, i.e., user 1 has the highest average rate and μ_1 is the lowest. After this reordering, decoding is assumed to progress starting form user 1 and proceeding to L.

Since the optimization problem (2.13) and constraints (2.14) over Λ_q and G_i are not convex, finding an analytical solution can be challenging. Additionally, the complex expressions in the modelling of the clipper in (2.4) and (2.5), lead to the numerical solution of the problem using Matlab toolbox (MATLAB, 2016). In spite of the fact that an optimum solution is not guaranteed with this approach, the results in Section 4.4 demonstrate that the optimizer was able to produce results which behave as expected when relaxing the constraints and which converge to analytical upper bounds.

2.4 Simulations

2.4.1 Simulation Setup

Figure 2.3 shows the simulation environment which consists of $L = 7$ cells spaced at 500 m, with 60 users per cell. This gives a total of 420 users which are assumed to be uniformly distributed over the cells. Table 2.1 lists the locations of all RUs as well as their distance from the CP which is located in the center cell. Full spectrum reuse is assumed in each cell incurring unavoidable interference at the RUs.

For each group of 7 users employing the same band and representing a slice of the network as in Fig. 2.2, the optimization problem (2.13) is solved using Matlab `fmincon`

Table 2.1: RU Locations and Distances from the CP

RU Number	RU Location [m]	Distance from CP [m]
CP	$[1000, 1100]$	–
RU_1	$[1100, 1100]$	100
RU_2	$[667, 1350]$	416.4
RU_3	$[667, 850]$	416.4
RU_4	$[1100, 1600]$	509.9
RU_5	$[1100, 600]$	509.9
RU_6	$[1533, 1350]$	588.7
RU_7	$[1533, 850]$	588.7

(MATLAB, 2016). The optimization problem is solved repeatedly over all 60 slices of the network. User locations are assumed to be fixed while solving the optimization problem over 40 channel realizations. The Matlab function, `fmincon`, obtains the solutions of this problem by converging to local minimums at which the objective function does not decrease to up to a tolerance value of 10^{-6} (MATLAB, 2016). This tolerance value is acceptable as a stopping criteria since it is much smaller than the objective function..

The radio access network is modelled as a Rayleigh fading channel with pathloss dependent on the distance between the users and the RUs using the expression in Table 2.3 (Zhou and Yu, 2014). Users as assumed to be stationary and channel realizations of the radio access are drawn independently with the computed pathlosses. For simplicity, both the UE transmit power and the RF frontend noise are assumed to have the same power for all users, i.e, $P_i = P$ and $\sigma_{n_i}^2 = \sigma_n^2$. Simulations were carried out under eight fronthauling scenarios representing the use of $f = 0, \ldots, L$ RoFSO links.

For FSO fronthaul links, the optical channel realizations for each link are drawn independently and log-normally distributed as in (4.10) where the fading strength depends on the link range. The parameters of the FSO fronthaul links are listed in Table 2.2. The transmitted optical power, responsivity and receiver noise variance are taken as identical in

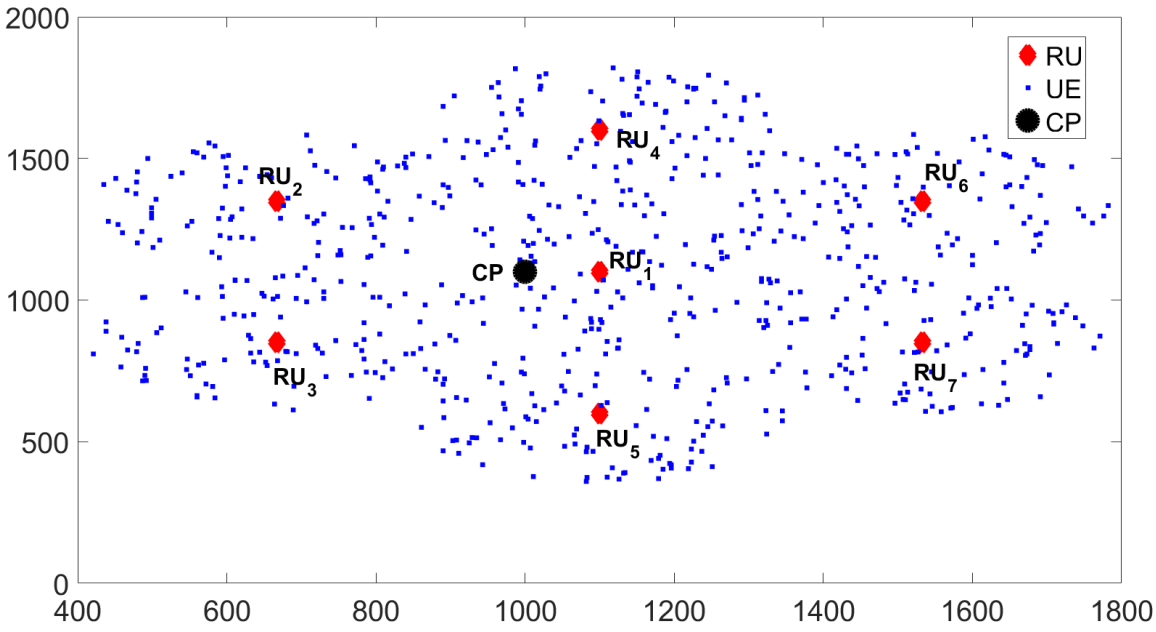

Figure 2.3: Simulation Setup. Seven cells with RUs, CP in central cell, and 420 uniformly distributed UEs.

all FSO links are are listed in the table. The optical path loss, g_{l_i}, is computed for a variety of weather scenarios described in Sec. 2.4.2.

The parameters of the shared RF fronthaul channel are given in Table 2.3. As discussed in Sec. 2.2.2, the RF fronthaul channel has a sum capacity constraint which transmits quantized signals from each RU. The total fronthaul capacity of the network is 1.26 Gbps with 21 Mbps fronthaul per network slice. Similar parameters are used in the literature, (e.g., Zhou and Yu, 2014), and are adopted in this work as a frame of reference. Higher rates are possible using a different technology. For example, rates in the range of Gbps are achievable when millimeter wave is assumed at the access network as discussed in **Chapter 3**.

As shown in Fig. 2.3, the CP is placed in the central cell with an RU in each cell. For the case of $f = 1, \ldots, L$, the RoFSO fronthaul links were allocated in order of increasing RU-CP distance as calculated in Table 2.1, i.e., closest RU-to-CP first. This allocation of

Table 2.2: Simulation Parameters for the FSO links (Farid and Hranilovic, 2007)

Wavelength (λ)	1550 nm
Bandwidth	1 GHz
Optical Transmitted Power	16 dBm
Responsivity (η)	0.5
Optical Noise Standard Deviation (σ_{FSO})	10^{-7}

Table 2.3: Simulation Parameters for the RF links

Cellular Layout	7cells, 60 UE per cell
BS-to-BS Distance	500m
Frequency Reuse	1
RF User Transmit Power (Zhou and Yu, 2014)	23dBm
Background Noise, σ_n^2 (Zhou and Yu, 2014)	-169dBm/Hz
Distance-dependent Path Loss (Zhou and Yu, 2014)	$128.1 + 37.6 \log_{10}(d)$
Log-normal Shadowing	8dB
Capacity (per network slice), C	21Mbps
Scheduling Strategy	Round-robin

RoFSO fronthaul links was done under the intuition that the closest links would provide the largest increases in end user rate. Though this may not necessarily be the optimal placement of the RoFSO links, it is a reasonable starting point given the sensitivity of FSO links to range and weather conditions.

2.4.2 Weather Models

FSO channels are highly dependent on weather conditions. The modelling of atmospheric attenuation in different conditions has been an active area of study for some time. In this work, in order to have tractable simulations, weather conditions were quantized into four cases: clear, rain, snow and fog. In each case, the value of attenuation coefficient γ in (4.8) is presented.

To make the simulations concrete, yearly weather data for 2016 at Pearson International

Airport, near Toronto, ON and Gander International Airport, Newfoundland & Labrador Canada (Weathercanada, 2017) were employed. For clear weather, a nominal attenuation coefficient of $\gamma_{\text{clear}} = 0.44$ dB/km is adopted (Farid and Hranilovic, 2007). A typical value of $\gamma_{\text{fog}} = 50$ dB/km was taken for a fog event in Toronto while more severe attenuation of $\gamma_{\text{fog}} = 100$ dB/km for Gander. Notice that in practice fog attenuation can reach as high as 250 dB/km (Awan *et al.*, 2009).

A popular optical attenuation models for rain is (M. Naboulsi and Fornel, 2005)

$$\gamma_{\text{rain}} = 1.076R^{0.67} \tag{2.15}$$

where R is the rate of rain fall in units of mm/hr.

An empirical model of snow attenuation is (M. Naboulsi and Fornel, 2005)

$$\gamma_{\text{snow}} = aS^b \tag{2.16}$$

where S is the rate of rain fall and a and b are coefficients depending on the composition of the snow. In this work, we consider the worst case of dry snow for which $a = 0.0000542\lambda + 5.4958776$ and $b = 1.38$.

Over the entire year, the average rates of rain and snow are computed to obtain R and S by averaging the rain and snow rates over rainy and snowy days (Weathercanada, 2017) respectively and substituted in (2.15) and (2.16). Furthermore, the relative frequency of the weather conditions over the year (α_c, α_r, α_s, α_f) are also computed using the same yearly weather data by evaluating the percentage of occurrences of these weather conditions over the year. Table 2.4 summarizes the weather statistics and parameters used for both locations.

Table 2.4: Weather Statistics: Toronto, ON and Gander, NL, Canada 2016

Province	Ontario	Newfoundland & Labrador
Station Name	Toronto Intl. Airport	Gander Intl. Airport
Latitude, Longitude	$43.68, -79.63$	$48.94, -54.57$
Elevation [m]	173.4	151.2
Relative Frequency (α_c, α_r, α_s, α_f)	$0.61, 0.174, 0.142, 0.072$	$0.3234, 0.2488, 0.2, 0.23$
Yearly Average Rain/Snow Rates R, S	$0.34, 0.86$ mm/hr	$0.48, 2.46$ mm/hr
Clear Attenuation γ_{clear}	0.44 dB/km	0.44 dB/km
Rain Attenuation γ_{rain}	0.523 dB/km	0.66 dB/km
Snow Attenuation γ_{snow}	4.53 dB/km	19.34 dB/km
Fog Attenuation γ_{fog}	50 dB/km	100 dB/km

For simplicity, C_n^2 is assumed to be the same for clear, rainy, and snowy weather $C_n^2 = 5 \times 10^{-14}$ and $C_n^2 = 0.5 \times 10^{-14}$ for the foggy weather.

2.4.3 Performance RoFSO Fronthaul

Figure 2.4 plots the the CDFs of end user rates, R_i (2.11) for clear weather when Λ_q and G_i are designed from problem (2.13). The parameters obtained by solving the optimization problem are substituted in (2.11) to evaluate the end user rate. Then, the CDF in Fig. 2.4 is generated empirically over all users and channel realizations. As expected, the addition of RoFSO fronthaul improves user rates, however, the improvement is not linear with the number of RoFSO units and depends on many factors most notably the distance between the added RoFSO unit and the CP. By adding a single RoFSO fronthauling unit at RU_1, the 50^{th} percentile end user rate is increased from 0.5 Mbps to 3.6 Mbps under clear weather conditions. The enhancement in system performance by adding RoFSO fronthaul is due both to the increase in the total fronthaul capacity of the network and to the redistribution of the existing RF fronthaul capacity over the remaining RUs.

Fig. 2.5 shows how the 50th percentile of end user rates changes with the number of

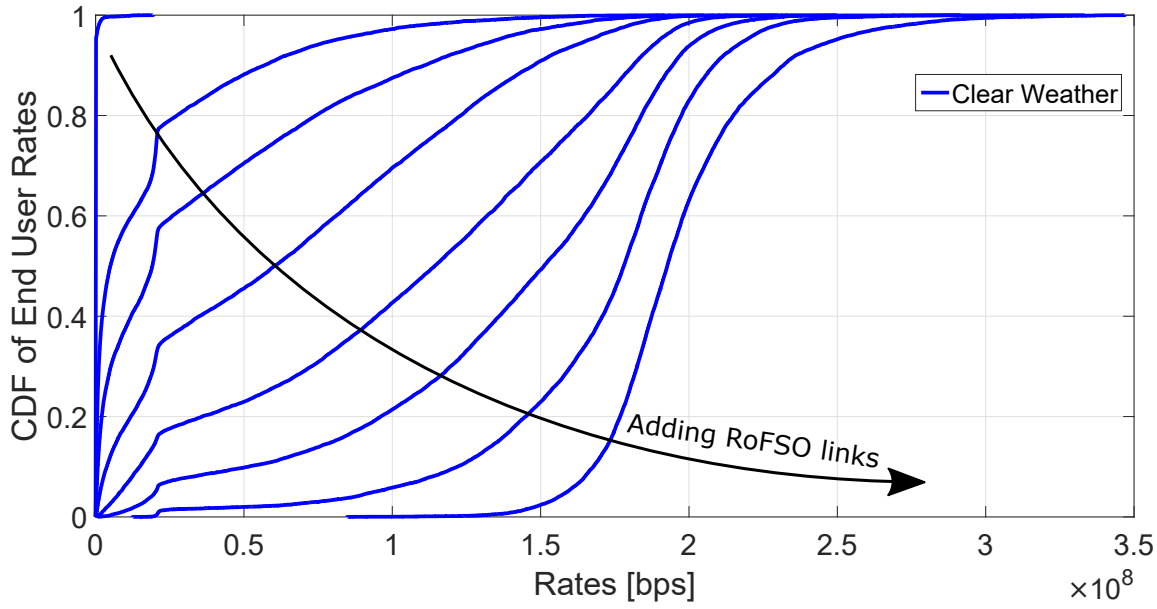

Figure 2.4: CDF of user rates for $0, 1, 2, \ldots 7$ RoFSO links, for clear weather.

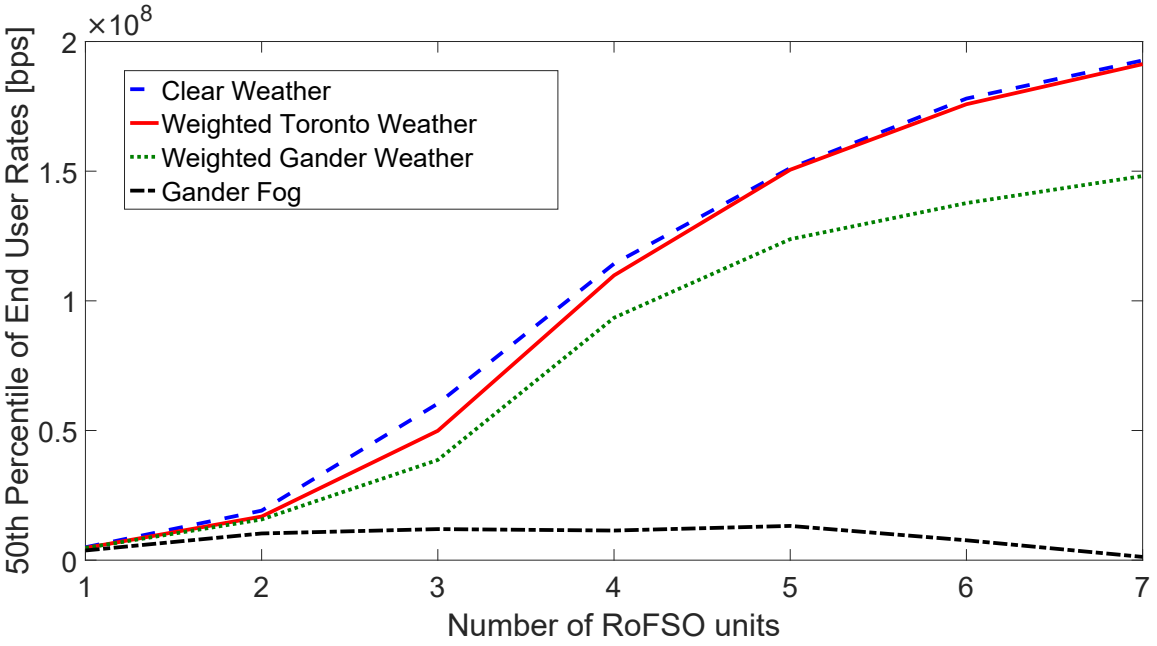

Figure 2.5: 50th percentile of user rates for $0, 1, 2, \ldots 7$ RoFSO links, for clear weather, different weather conditions weighted by weather data for Toronto, ON and Gander NL, Canada 2016, and severe fog of 100 dB/km as in Newfoundland.

RoFSO units under different weather conditions. The simulation is repeated for a clear weather, severe fog, and also the weighted weather conditions in Toronto and Gander using annual weather data data collected from two stations in 2016. Using the hourly and daily data measured at Toronto and Gander international airports, user statistics are obtained and used to model the variation of the parameters of the FSO links. The average rates of rain and snow are evaluated and substituted in 2.15 and 2.16 to obtain the corresponding attenuation. The weather data was also used to compute statistics for the different weather conditions which are quantized to four main conditions (clear/rain/snow/fog) and then used to weight the performance under each case. The average weighted CDF of end user rates over different weather conditions was computed as

$$\mathrm{CDF}_{\mathrm{avg}} = \alpha_c \mathrm{CDF}_c + \alpha_r \mathrm{CDF}_r + \alpha_s \mathrm{CDF}_s + \alpha_f \mathrm{CDF}_f. \tag{2.17}$$

All details about the weather stations and the weather statistics are shown in Table 2.4.

Newfoundland is known to be among the foggiest Canadian provinces which is evident from the relative frequency of fog in Gander as compared to Toronto in Table 2.4. Since fog has a dramatic effect on the quality of the FSO link, the weighted performance at Gander is lower than that at Toronto. Under severe fog of 100 dB/km attenuation, adding more RoFSO units can degrade performance. As shown in Fig. 2.5, the weighted performance for both locations improves with additional RoFSO units while at a slower rate for Gander.

End user rates improve with the addition of fronthaul capacity, whether from RF or RoFSO fronthaul. For a given average sum user rate, Fig. 2.6 presents the required RF-only fronthaul capacity required to achieve the same performance as the mixed RF/RoFSO system.

In the figure, the average of the sum user rates over all cells in a given network slice,

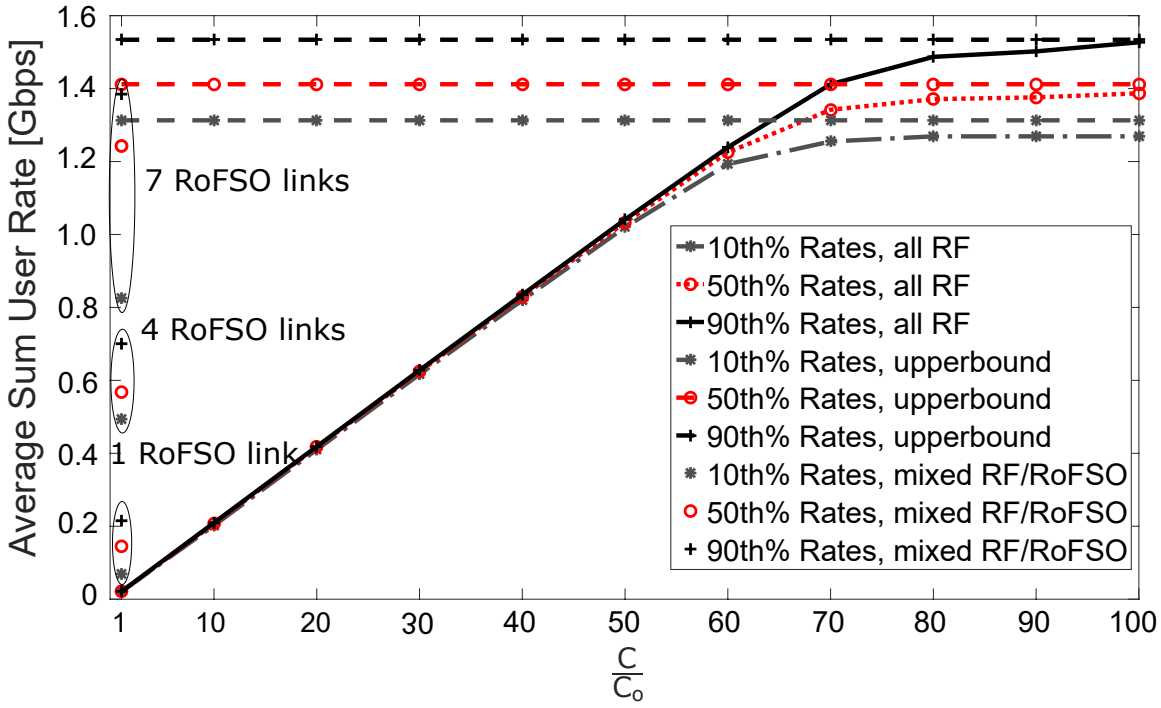

Figure 2.6: Average end user rates versus RF fronthaul capacity per network slice, C, from 21 Mbps–2.1 Gbps. All-RF and mixed RF/RoFSO fronthaul (clear weather).

$\sum_{i=1}^{L} R_i$ in (2.12), is considered. Considering all-RF fronthaul, increasing the C relaxes the constraint (2.14) leading to a larger feasible region of the possible solutions which in return allows for a better solution of the problem. As the fronthaul capacity tends to infinity, i.e. eliminating the constraint (2.14), the sum of the rates at the CP will approach a maximum which is limited by sum of the rates of the radio access network. This upperbound can be found from (2.12) and takes the form

$$\sum_{I=1}^{L} R_i \leq \log \frac{\left|HV_x H^H + \Gamma\right|}{|\Gamma|}$$

where Γ is the a diagonal matrix of AWGN variances added at the RUs. Notice that in Fig. 2.6 as C is relaxed, the average sum user rates of the all-RF fronthaul network approach the upperbound. The graph shows the 10^{th}, 50^{th}, and 90^{th} percentile of average sum rate and the corresponding upperbounds.

For comparison, the performance of a mixed RF/RoFSO fronthaul with 1, 4, and 7 RoFSO units designed following (2.13) is also plotted under a fixed RF fronthaul capacity of $C = C_o$. Notice that for the 50^{th} percentile of average sum rate, adding 1, 4, or 7 RoFSO units with $C = C_o$ is equivalent to increasing the fronthaul capacity of the all-RF fronthaul system from C_o to $7.1 \times C_o$, $27.6 \times C_o$, and $59.5 \times C_o$ respectively. This comparison is especially useful when designing the C-RAN and deciding, with the increasing rate demand, whether to add more RF fronthaul capacity or to add one or more RoFSO units.

It is also remarkable to mention that, although the numerical solver for the optimization problem does not guarantee an optimum, the results in Fig. 2.6 show the expected behavior by closely approaching the analytical upperbounds while relaxing the constraints.

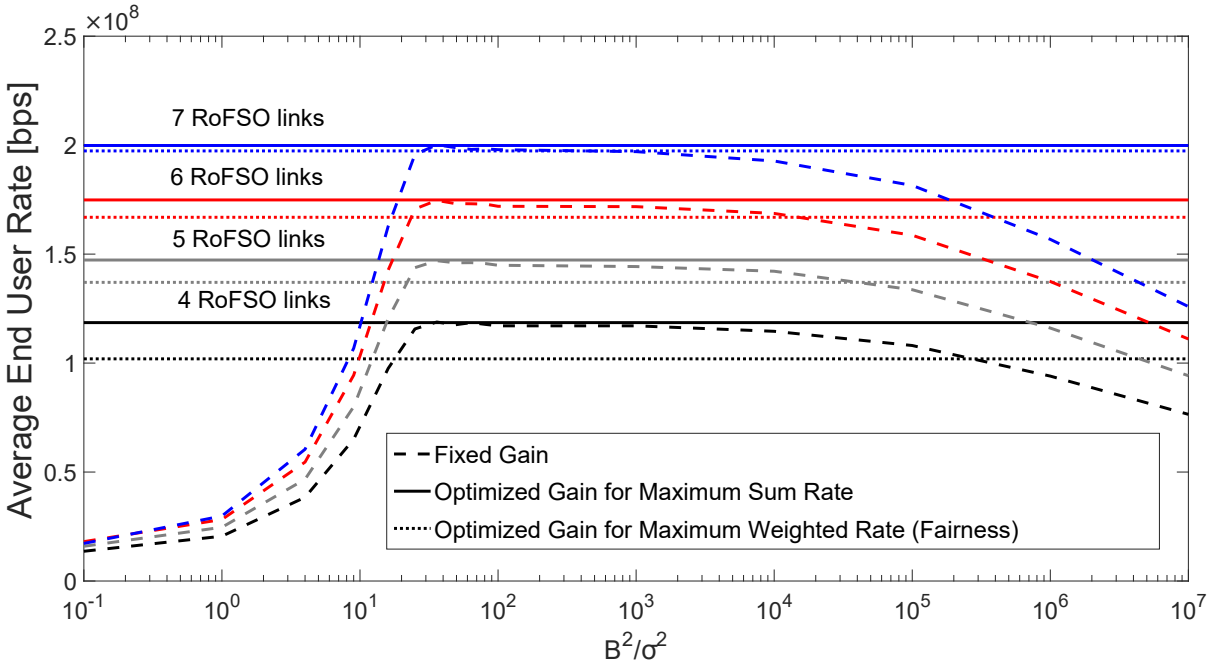

Figure 2.7: The effect of gain G_i on average end user rates (clear weather).

2.4.4 Impact of RoFSO Gain

The gains G_i of the amplifiers in the RoFSO nodes Fig. 2.1 play an important role not only in amplifying the transmitted signal but also in controlling the resulting clipping noise. Consider setting the clipping level and bias, B, to satisfy the average optical power constraint of the RoFSO unit. Notice from (2.4) and (2.5), that K and σ_c^2 depend on the ratio B/σ_i, where $\sigma_i^2 = G_i^2\sigma_{\hat{x}_i}^2$ is the input variance to the clipper. Increasing G_i, or equivalently decreasing B^2/σ_i^2, increases the signal power but also increases the clipping noise and vice versa. Thus, there is a trade-off between increasing the signal power and decreasing the clipping distortion.

In order to quantify this trade-off, Fig. 2.7 plots the average user rate in (2.11) versus B^2/σ^2 for two scenarios: fixed-gain and optimized-gain. The *fixed-gain* case (dashed curves) corresponds to a fixed G, i.e., fixed B^2/σ_i^2, over all RUs and the optimization in

(2.13) and (2.14) is done over the quantization noise only. In addition, $\mu_i = 1$ and the optimizer maximizes the sum of the rates in a greedy fashion. For the *optimized-gain* case, G_i and Λ_q are chosen for each RU via the joint optimization problem (2.13). Furthermore, the simulations are repeated for a greedy case ($\mu_i = 1$), and also while maintaining a fairness criteria (μ_i selected as in (Yu *et al.*, 2011)).

As shown in Fig. 2.7, the optimized-gain case is superior to the fixed-gain system when both are maximizing the sum rate (without fairness). On the other hand, when the optimized-gain system considers the fairness among users, the performance is slightly degraded. The reason for this degradation is that in order to maintain fairness, a sub-optimal allocation of resources must be done to ensure even users with especially poor channels have a level of service. Notice also that increasing the number of RoFSO units from 4–7 not only improves the performance of the system, but also decreases the gap between the fair and the greedy optimizers. This is because adding more RoFSO adds more fronthaul resources improves the channels for all users making the impact of fairness in the optimization problem less important. Also, for the fixed-gain system, at low B^2/σ^2 (i.e., high G) clipping noise dominates performance while at high B^2/σ^2 the reduction in signal power limits performance.

In clear weather, the performance of the fixed-gain system is not overly sensitive to the value of G, that is , as shown in Fig. 2.7 the average user rate is nearly flat over a wide range of B^2/σ^2. In Fig. 2.8 the simulation is repeated under light and severe fog conditions (50 dB/km and 100 dB/km attenuation). The all-RoFSO case (7 RoFSO units) is considered in which all the fronthaul links will be most sensitive to the weather and is compared with the same structure under a clear weather.

As the fog becomes more severe, the performance of both fixed-gain and optimized

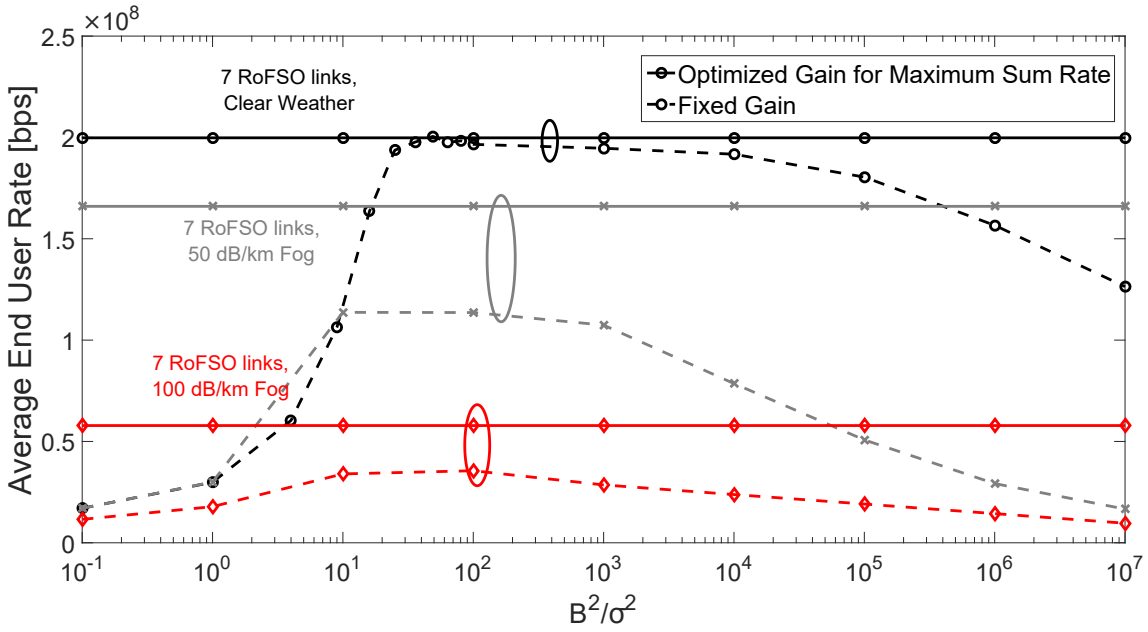

Figure 2.8: The effect of gain G_i on average end user rates (clear and foggy weather, no fairness).

systems degrades dramatically. Notice that as fog becomes more severe, the fixed gain performance is no longer flat over a wide range, but instead is more sensitive to the choice of G. This is because for severe fog attenuation the clipping noise is no longer the dominant impairment. Additionally, the relative gap in user rates between fixed-gain and optimized gain grows as fog attenuation increases. For 50 dB/km fog the relative rate degradation for fixed-gain over optimized gain is 1.46 while for 100 dB/km fog the degradation is 1.63. Thus, selecting an optimized gain, G_i, for each RU is essential in dense fog given the sensitivity of the RoFSO fronthaul links to the fog loss.

2.5 Conclusion

In this paper we develop a joint optimization problem to design a mixed RF/RoFSO fronthaul for a C-RAN by selecting the quantizers for the RF links and the gain of the RoFSO units to maximize the weighted sum rate of users. Adding the RoFSO fronthaul nodes improves user rates as well as makes the RUs simpler and more cost-efficient. Though impacted by weather conditions, RUs with RoFSO fronthaul were able to provide a substantial increase in end user rates due to the short ranges of the links. This work shows that it is essential to select the gain of RoFSO nodes to balance clipping noise and transmit power. Future directions include the study of network provisioning with RoFSO, the use of more comprehensive models for RF fronthaul links to quantify rates in a variety of weather/range as well as experimental studies of these C-RAN topologies. Other extensions for this work will include the impacts of pointing errors as well as analytical solutions for the proposed optimization problem in a distributed way at the RUs rather than the centralized problem considered here.

2.A Clipping Noise Power

In this appendix, the Bussgang model (Bussgang, 1952) is applied to derive the impact of clipping noise in this work. In particular, consider a Gaussian input $s \sim \mathcal{N}(m, \sigma_s^2)$, the clipped signal s_c can be written as

$$s_c = \begin{cases} -B & s < -B \\ s & -B \leq s \leq B \\ B & s > B \end{cases} \tag{2.18}$$

The Bussgang model allows for a linear representation for S_c as

$$s_c = Ks + w.$$

where

$$K = \frac{E\{ss_c\}}{E\{s^2\}} \tag{2.19}$$

and w is an additive noise term with variance σ_w^2.

The value of K can be found by computing the correlation as

$$E\{ss_c\} = \frac{1}{\sqrt{2\,\pi\sigma_s^2}}\left(-B\int_{-\infty}^{-B} s\, e^{-\frac{(s-m)^2}{2\sigma_s^2}} ds + \int_{-B}^{B} s^2 e^{-\frac{(s-m)^2}{2\sigma_s^2}} ds + B\int_{B}^{\infty} s e^{-\frac{(s-m)^2}{2\sigma_s^2}} ds\right) \tag{2.20}$$

to yield

$$K = \frac{1}{2m^2+2\sigma_s^2}\left(\left(m^2+mB+\sigma_s^2\right)\operatorname{erf}\left(\frac{B+m}{\sqrt{2\sigma_s^2}}\right) + \left(m^2-mB+\sigma_s^2\right)\operatorname{erf}\left(\frac{B-m}{\sqrt{2\sigma_s^2}}\right) + \sqrt{\frac{2m^2\sigma_s^2}{\pi}}\left(e^{-\frac{(B+m)^2}{2\sigma_s^2}} - e^{-\frac{(B-m)^2}{2\sigma_s^2}}\right)\right) \tag{2.21}$$

The mean of the clipping noise w can similarly be found to be

$$E\{w\} = \sqrt{\frac{\sigma_s^2}{2\pi}}\left(e^{-\frac{(m+B)^2}{2\,\sigma_s^2}} - e^{-\frac{(B-m)^2}{2\,\sigma_s^2}}\right) - m\,K + \left(\frac{m+B}{2}\right)\operatorname{erf}\left(\frac{m+B}{\sqrt{2\sigma_s^2}}\right) + \left(\frac{m-B}{2}\right)\operatorname{erf}\left(\frac{B-m}{\sqrt{2\sigma_s^2}}\right) \tag{2.22}$$

Finally the clipping noise power, $E\{w^2\} = E\{(s_c - Ks)^2\}$ can be written as

$$E\{w^2\} = \frac{1}{\sqrt{2\pi\sigma_s^2}} \left(B^2 \int_{-\infty}^{B} e^{-\frac{(s-m)^2}{2\sigma_s^2}} ds + \int_{-B}^{B} s^2 \, e^{-\frac{(s-m)^2}{2\sigma_s^2}} ds + B^2 \int_{B}^{\infty} e^{-\frac{(s-m)^2}{2\sigma_s^2}} ds \right) - K^2 \left(m^2 + \sigma_s^2 \right) \quad (2.23)$$

to give

$$E\{w^2\} = B^2 - K^2 \left(m^2 + \sigma_s^2 \right) + \left(\frac{m^2 + \sigma_s^2 - B^2}{2} \right) \left(\operatorname{erf} \left(\frac{B+m}{\sqrt{2\sigma_s^2}} \right) + \operatorname{erf} \left(\frac{B-m}{\sqrt{2\sigma_s^2}} \right) \right) - \sqrt{\frac{\sigma_s^2}{2\pi}} \left((B-m) \, e^{-\frac{(m+B)^2}{2\,\sigma_s^2}} + (B+m) \, e^{-\frac{(B-m)^2}{2\,\sigma_s^2}} \right) \quad (2.24)$$

The variance of the clipping noise can be computed from (2.22) and (2.24). Substituting $m = 0$ yields (2.4) and (2.5).

Chapter 3

Impact of Fiber Nonlinearity on 5G Backhauling via Mixed FSO/Fiber Network

In **Chapter** 2, a CRAN with mixed RF/RoFSO fronthaul was considered and a joint optimization tool was introduced to maximize the sum of weighted user rates. The results showed that RoFSO links outperform the RF links except at harsh weather conditions. Those results, along with the advantages of optical fronthaul links, Sec. 1.2, motivate the work towards a CRAN with all-optical fronthaul links. The work in this chapter extends the CRAN structure in **Chapter** 2 from a single-hop mixed RF/RoFSO fronthauling to dual-hop hybrid RoFSO/RoF fronthauling. Furthermore, this chapter's main focus is the effect of RoF impairments on the performance. While **Chapter** 2 quantified the performance in terms of UE data rates, the outage probability, Sec. 1.4, is considered in this chapter which reflects the reliability of the CRAN. The reliability analyses are then extended to derive analytical expressions for the average BER and the CDF of user capacities.

Further contributions to this work that did not appear in the final publication are added in **Appendix** A and **Appendix** B. Analysis and simulation that reflect the effect of clipping distortion on the performance of the system at different RoFSO and RoF gains are presented in **Appendix** A. Rate equations and Monte-Carlo simulation of the case with SIC decoding is provided in **Appendix** B.

The work in this chapter was published in *IEEE Access* (Volume: 5, Pages: 19942 – 19950, 2017) (Morra *et al.*, 2017). Minor modifications have been made to improve the clarity of this work. IEEE owns the copyright of the material in this chapter and it is permitted to be re-used in the thesis.

Abstract The inherently high bandwidth of fiber and free-space optical (FSO) links makes them ideally suited to provide broadband backhaul in fifth-generation (5G) mobile networks. However, both fiber and FSO systems suffer from a variety of impairments which must be properly modelled in order to design the network. In this paper, we present analytical results for mixed FSO/fiber amplify-and-forward (AF) backhauling systems where the impacts of radio-frequency (RF) co-channel interference, FSO pointing errors, and both fiber and FSO modulator nonlinearity are modelled and taken into consideration. Closed-form and asymptotic expressions are derived for the outage probability, the average bit-error rate (BER), and the cumulative distribution function (CDF) of the channel capacity for mixed FSO/fiber backhauling systems. Our results reveal an optimal average launched power for the fiber which balances the impact of fiber nonlinear distortion with the receiver noise. In particular, when using the optimal fiber average launched power, our estimated user capacity CDF results show that the 50-th percentile user rates using mm-wave RF access can reach over 1.5 Gbits/sec in ideal conditions. However, user rates are more sensitive to the FSO backhaul channel characteristics.

3.1 Introduction

Fifth-generation (5G) networks have promised impressive improvements in network performance at the cost of extreme cell densification (Ge *et al.*, 2016; Dehos *et al.*, 2014; Al-Dabbagh and Al-Raweshidy, 2017). Given the ultra-dense and widespread deployment of radio units in 5G, energy and cost effective backhaul networks are essential to realize the potential of 5G systems. Though fiber backhaul is preferred, it is often not available or expensive to install. Backhaul using free-space optical (FSO) links, though sensitive to weather conditions, provides inexpensive, huge bandwidth links and serves as an efficient

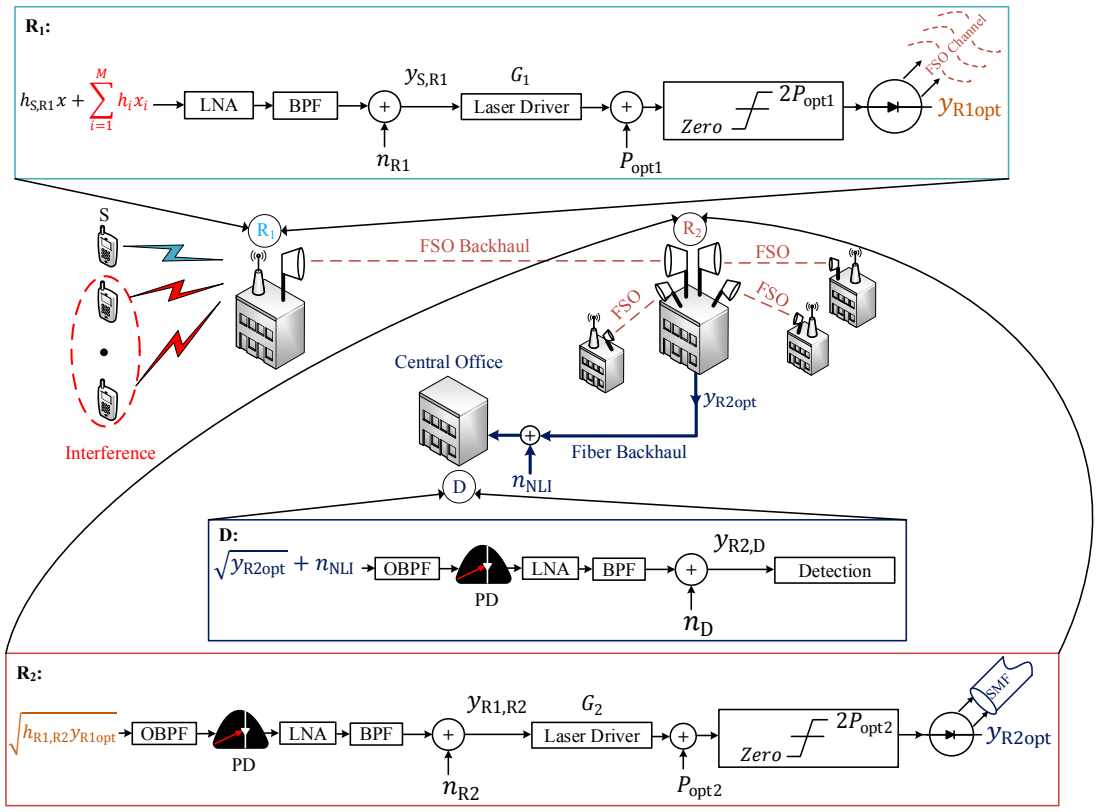

Figure 3.1: RF/FSO/Fiber hybrid architecture for 5G access and backhaul networks.

backhauling bridge between radio-frequency (RF) access and central fiber backhaul nodes (Trinh *et al.*, 2017; Soleimani-Nasab and Uysal, 2016). This paper considers the design of 5G networks with mixed FSO and fiber backhaul by considering the unique impairments inherent to both media. In particular, low complexity amplify-and-forward (AF) backhaul links are considered due to their low cost and energy requirements.

Free-space optics as a backhauling medium for radio systems has recently received increasing attention in the literature. Most studies consider outage performance, bit error rate (BER), and ergodic capacity results under a variety of statistical channel models for RF and FSO channels (Lee *et al.*, 2011; Ansari *et al.*, 2013a; Petkovic *et al.*, 2015; Petkovic, 2015; Petkovic *et al.*, 2017; Soleimani-Nasab and Uysal, 2016; Samimi and Uysal, 2013; Zedini

et al., 2015a; Anees and Bhatnagar, 2015b; Kong *et al.*, 2015; Zhang *et al.*, 2015; Zedini *et al.*, 2016; Trinh *et al.*, 2017). Lee *et al.* (Lee *et al.*, 2011) presented the first analysis of outage performance of a dual-hop AF relay system consisting of RF and FSO links with Rayleigh and gamma-gamma distributed channel gains respectively. As an extension to (Lee *et al.*, 2011), the impact of pointing errors on the BER performance and the ergodic capacity of a mixed AF RF/FSO systems was then carried out in (Ansari *et al.*, 2013a). Based on outdated channel state information (CSI), Petkovic *et al.* (Petkovic *et al.*, 2015) studied dual-hop AF with relay selection RF/FSO multiple relay systems. In (Petkovic, 2015; Petkovic *et al.*, 2017), an outage probability expression was derived for a fixed AF RF/FSO system which is corrupted by both noise and co-channel interference while assuming that the relay gain is selected based on outdated CSI. Soleimani-Nasab and Uysal present a comprehensive survey and analysis of AF RF/FSO systems which includes the impact of co-channel interference and pointing errors, where the RF and FSO links were distributed according to Nakagami-m and double generalized gamma distributions, respectively (Soleimani-Nasab and Uysal, 2016).

In this paper, we extend earlier work on FSO backhauling by including a fiber optical link to aggregate the backhaul from multiple FSO units in a 5G network. As shown in Fig. 3.1, received signals from a radio access network are AF-relayed over an FSO link and multiple such backhaul channels are AF-relayed over a fiber trunk. Like earlier work, co-channel interference, pointing errors, and scintillation of the FSO links are considered explicitly. The multipath fading in the RF links is assumed to follow a Rayleigh fading distribution and the FSO link is assumed to have a gamma-gamma atmospheric turbulence fading distribution. Additionally, the effect of the nonlinearity of the FSO and fiber relay nodes is taken into consideration here by selecting the gain to ensure negligible clipping

likelihood. For AF relaying over the fiber, the impact of nonlinear propagation on the performance of the system can be significant. Here we employ the Gaussian noise (GN) model (Poggiolini *et al.*, 2011) to quantify the impact of fiber nonlinearities which is tractable and widely used for system design and analysis (El-Fiqi *et al.*, 2016; Shieh and Chen, 2011; Poggiolini *et al.*, 2012, 2014; Bosco *et al.*, 2012). Under the assumption of AF relaying, closed-form expressions are derived for the outage probability, the average bit-error rate (BER), and the cumulative distribution function (CDF) of user capacities of the network using a mixed FSO/fiber backhaul system. In addition, asymptotic expressions at high FSO and fiber signal-to-noise ratios (SNRs) are derived to provide useful physical insights. The optimal average launched fiber power is derived, in the case of high SNR at both the FSO and fiber links, and shown to provide good performance over a variety of practical scenarios.

The balance of the paper is organized as follows. In Section 3.2, system and the channels model are presented. Outage probability, capacity-CDF, and the average BER expressions are derived in Sections 3.3 and 3.4, while asymptotic results are given in Section 3.5. Section 3.6 provides numerical results on the performance evaluation using a mm-wave radio access network and mixed FSO/fiber backhaul. Finally, the conclusions are summarized in Section 3.7.

3.2 System and Channel Models

As shown in Fig. 3.1, the system consists of an RF access medium corrupted by interference and a mixed FSO/fiber backhaul. Two AF relays, R_1 and R_2, forward received signals from the source node, S, to the destination node, D, using FSO and fiber respectively.

3.2.1 Radio Access

The received RF signal at the relay node, R_1, can be expressed as

$$y_{\mathrm{S,R1}} = h_{\mathrm{S,R1}} x + \sum_{i=1}^{M} h_i x_i + n_{\mathrm{R1}} \tag{3.1}$$

where $h_{\mathrm{S,R1}}$ is the fading RF channel coefficient, x is the modulation symbol, h_i is the fading RF channel coefficient for the i^{th} interferer, x_i is the modulation symbol of the i^{th} interferer, and n_{R1} is an additive white Gaussian noise (AWGN) with variance σ^2_{R1} at the relay node, R_1. Both $h_{\mathrm{S,R1}}$ and h_i are assumed to be Rayleigh distributed (Simon and Alouini, 2000) and there are M RF co-channel interferers. We assume that $E\{y_{\mathrm{S,R1}}\} = 0$ which is consistent with an ac-coupled RF channel.

3.2.2 FSO Relay

To ensure that the received RF signal is unipolar in order to be able to drive the laser, a DC bias is added to the received signal after amplifying it at the first relay with a fixed gain G_1. Let P_{opt1} denote the emitted average optical power of the FSO relay node which is limited by eye-safety regulations. Since the radio signal is zero mean, the output signal will have an average optical power P_{opt1} as required. To consider the finite dynamic range of the laser driver, G_1 is selected to ensure that $\mid G_1 y_{\mathrm{S,R1}} \mid \leq P_{\mathrm{opt1}}$ with high probability to avoid over modulation induced clipping (Song *et al.*, 2013; Petkovic *et al.*, 2015). Consider selecting G_1 to normalize the variance of the modulating signal. In particular, define G_1 as

$$G_1 = \frac{P_{\mathrm{opt1}}}{K_1 \sqrt{E\left[\mid h_{\mathrm{S,R1}} \mid^2\right] P_{\mathrm{RF}} + \sum_{i=1}^{M} E\left[\mid h_i \mid^2\right] P_{\mathrm{Ri}} + \sigma^2_{\mathrm{R_1}}}} \tag{3.2}$$

where P_{RF} and P_{Ri} are the average powers of the RF signal and the i^{th} RF interferer. The parameter K_1 is selected so that $2K_1$ standard deviations of the modulating signal are within the dynamic range of the modulator. Assuming Gaussian statistics, for $K_1 = 4$ the likelihood of clipping is on the order of 10^{-5}. Thus, when K_1 is chosen large enough, the impact of clipping in the laser driver of R_1 can be ignored.

Assuming direct analog modulation of the laser intensity at the relay node, R_1 and assuming that the electrical-to-optical conversion coefficient $\eta_1 = 1$, the retransmitted optical signal is

$$y_{R1\mathrm{opt}} = P_{\mathrm{opt1}} + G_1 y_{\mathrm{S,R1}}. \tag{3.3}$$

3.2.3 Fiber Backhaul Link

The received electrical signal at the relay node, R_2, after removing the DC bias is given by

$$y_{\mathrm{R1,R2}} = \mathcal{R}_1 h_{\mathrm{R1,R2}} G_1 y_{\mathrm{S,R1}} + n_{\mathrm{R2}} \tag{3.4}$$

where $\mathcal{R}_1$ is the responsivity of the photodiode (PD) at the relay node, R_2, $h_{\mathrm{R1,R2}}$ is the fading FSO irradiance fluctuations and n_{R_2} is AWGN added at relay node R_2 with variance σ^2_{R2}.

After amplifying the received signal at the second relay with a fixed gain G_2, a DC bias is added to be able to drive the laser. Similar to the case in relay R_1,

$$G_2 = \frac{P_{\mathrm{opt2}}}{K_2 \sqrt{\frac{\mathcal{R}_1^2 E\left[|h_{\mathrm{R1,R2}}|^2\right] P_{\mathrm{opt1}}^2}{K_1^2} + \sigma^2_{\mathrm{R2}}}} \tag{3.5}$$

where P_{opt2} is the average launched optical power in the single-mode fiber (SMF) per channel and K_2 is selected to control the likelihood of clipping by the laser driver. Considering an electrical-to-optical conversion coefficient $\eta_2 = 1$ and K_2 large enough, the optical signal forwarded into the fiber is

$$y_{\text{R2opt}} = P_{\text{opt2}} + G_2 y_{\text{R1,R2}}. \tag{3.6}$$

Following the GN model (Poggiolini *et al.*, 2011), the impairments caused by the fiber nonlinear interference can be considered as an additive Gaussian noise n_{NLI} of power P_{NLI} that is statistically independent from the transmitted signal (El-Fiqi *et al.*, 2016; Poggiolini *et al.*, 2011, 2012, 2014). Since a photodetector responds to the optical intensity, at node D, and assuming that the fiber loss is compensated by an electrical amplifier, the received electrical signal is

$$\begin{aligned} y_{\text{R2,D}} =& \mathcal{R}_2 \left| \sqrt{y_{\text{R2opt}}} + n_{\text{NLI}} \right|^2 + n_{\text{D}} \\ =& \mathcal{R}_2 \left(y_{\text{R2opt}} + n_{\text{NLI}}^2 + 2 n_{\text{NLI}} \sqrt{y_{\text{R2opt}}} \right) + n_{\text{D}} \end{aligned} \tag{3.7}$$

where $\mathcal{R}_2$ is the responsivity of the photodiode and n_{D} is AWGN with variance σ_{D}^2 added in electrical domain at D. After removing the DC bias, the received electrical signal can be written as

$$y_{\text{R2,D}} = \mathcal{R}_2 \left(G_2 y_{\text{R1,R2}} + n_{\text{NLI}}^2 + 2 n_{\text{NLI}} \sqrt{y_{\text{R2opt}}} \right) + n_{\text{D}}. \tag{3.8}$$

Under a worst case assumption, P_{NLI} is set according to the maximum allowed launched optical power ($2P_{\text{opt2}}$). In this case, the nonlinear interference variance is given by (El-Fiqi *et al.*, 2016; Poggiolini *et al.*, 2011; Shieh and Chen, 2011; Poggiolini *et al.*, 2012, 2014;

Bosco *et al.*, 2012)

$$P_{\mathrm{NLI}} = \frac{\gamma_{\mathrm{nl}}^2}{\pi|\beta_2|}\frac{L_{\mathrm{eff}}^2}{L_{\mathrm{eff,a}}}\frac{(2P_{\mathrm{opt2}})^3}{B_{\mathrm{ch}}^2}\mathrm{arcsinh}\left(\frac{3}{8}\pi^2 L_{\mathrm{eff,a}}|\beta_2|B_\omega^2\right) \tag{3.9}$$

where $L_{\mathrm{eff}} = (1 - e^{-2\alpha_f L})/2\alpha_f$ and $L_{\mathrm{eff,a}} = 1/2\alpha_f$ are the effective and asymptomatic-effective fiber lengths, respectively, for a fiber with a physical fiber length L and a SMF attenuation coefficient α_f. The total wavelength-division multiplexing (WDM) bandwidth is denoted $B_\omega = B_{\mathrm{ch}}N_{\mathrm{ch}}$, where N_{ch} is the number of WDM channels and B_{ch} is the fiber channel bandwidth. The group-velocity dispersion (GVD) is denoted β_2, and $\gamma_{\mathrm{nl}} = 2\pi n_2/\lambda A_{\mathrm{eff}}$ is the fiber nonlinearity coefficient, where A_{eff} is the core effective area, λ is the propagated wavelength, and n_2 is the nonlinear-index coefficient.

Notice from (3.8) that the noise term n_{NLI}^2 has variance $(2P_{\mathrm{NLI}}^2)$ while the beating noise term $\left(2n_{\mathrm{NLI}}\sqrt{y_{\mathrm{R2opt}}}\right)$ has variance $(4P_{\mathrm{opt2}}P_{\mathrm{NLI}})$. In practice the impact of the beating noise term dominates and, using the parameters in Sec. 3.6, its power is at least about 3 orders of magnitude larger than the power of n_{NLI}^2. Thus, in the following the impact of n_{NLI}^2 is removed from the channel model in (3.8) yielding

$$y_{\mathrm{R2,D}} = \mathcal{R}_2\left(G_2 y_{\mathrm{R1,R2}} + 2n_{\mathrm{NLI}}\sqrt{y_{\mathrm{R2opt}}}\right) + n_{\mathrm{D}}. \tag{3.10}$$

The beating noise term is also modelled as having a Gaussian distribution which can be shown to be a good fit for the power ranges considered in this work.

3.2.4 Overall Signal-to-Interference-plus-Noise Ratio

The overall signal-to-interference-plus-noise ratio (SINR) of the radio access link and the FSO/fiber backhaul at node D, γ_{T}, can be written in terms of the SNRs of each portion of

the relay network as

$$\gamma_{\mathrm{T}} = \frac{\gamma_1 \gamma_2}{\gamma_2 + \gamma_2 \gamma_{\mathrm{R}} + C_1^2 (1 + C_2^2/\gamma_3)} \tag{3.11}$$

where

$$\begin{aligned}
\gamma_1 &= \frac{\mid h_{\mathrm{S,R1}} \mid^2 P_{\mathrm{RF}}}{\sigma_{\mathrm{R1}}^2} \\
\gamma_{\mathrm{R}} &= \sum_{i=1}^{M} \gamma_{\mathrm{Ri}} = \frac{\sum_{i=1}^{M} \mid h_i \mid^2 P_{\mathrm{Ri}}}{\sigma_{\mathrm{R1}}^2} \\
\gamma_2 &= \frac{\mathcal{R}_1^2 \mid h_{\mathrm{R1,R2}} \mid^2 P_{\mathrm{opt1}}^2}{\sigma_{\mathrm{R2}}^2} \\
\gamma_3 &= \frac{\mathcal{R}_2^2 P_{\mathrm{opt2}}^2}{4\mathcal{R}_2^2 P_{\mathrm{opt2}} P_{\mathrm{NLI}} + \sigma_{\mathrm{D}}^2} \\
C_1 &= K_1 \sqrt{\overline{\gamma_1} + \sum_{i=1}^{M} \overline{\gamma_{\mathrm{Ri}}} + 1} \\
C_2 &= K_2 \sqrt{\frac{\overline{\gamma_2}}{K_1^2} + 1}
\end{aligned} \tag{3.12}$$

and where γ_1, γ_{R}, γ_2, and γ_3 are the instantaneous SNR of the RF link, the instantaneous overall interference-to-noise ratio (INR) of the RF link, the instantaneous electrical SNR of the FSO link, and the electrical SNR of the fiber link, respectively. Notice that γ_3 is deterministic under the condition of the worst case fiber nonlinear interference. The notation $\overline{\gamma_k}$ denotes the expected value of SNR, i.e, $E\{\gamma_k\}$.

3.2.5 Channel Statistics

The RF link (i.e. S-R_1 link) is assumed to experience Rayleigh fading and hence γ_1 is exponentially distributed (Simon and Alouini, 2000)

$$f_{\gamma_1}(\gamma_1) = \frac{1}{\overline{\gamma_1}} \exp\left(\frac{-\gamma_1}{\overline{\gamma_1}}\right). \tag{3.13}$$

It is known that the distribution of the sum of M independent and identically distributed equal power exponential random variables (RVs) is gamma distribution (Evans *et al.*, 2000). Then, $\gamma_{\mathrm{R}} = \sum_{i=1}^{M} \gamma_{\mathrm{Ri}}$ follows gamma distribution, where γ_{Ri} is the instantaneous INR of the i^{th} interferer, with distribution

$$f_{\gamma_{\mathrm{R}}}(\gamma_{\mathrm{R}}) = \frac{\gamma_{\mathrm{R}}^{M-1}}{\overline{\gamma_{\mathrm{Ri}}}^{M}\Gamma(M)} \exp\left(\frac{-\gamma_{\mathrm{R}}}{\overline{\gamma_{\mathrm{Ri}}}}\right) \tag{3.14}$$

where $\Gamma(.)$ is the gamma function.

The FSO link (i.e. R_1-R_2 link) is assumed to have gamma-gamma fading with pointing error impairments. The distribution of γ_2 is (Zedini *et al.*, 2015b; Zhang *et al.*, 2015)

$$f_{\gamma_2}(\gamma_2) = \frac{\zeta^2}{2\Gamma(\alpha)\Gamma(\beta)\gamma_2} G_{1,3}^{3,0}\left(E\alpha\beta\sqrt{\frac{\gamma_2}{\mu_2}} \middle| \begin{matrix} \zeta^2+1 \\ \zeta^2, \alpha, \beta \end{matrix} \right) \tag{3.15}$$

where $\mu_2 = \frac{\overline{\gamma_2}\alpha\beta\zeta^2(\zeta^2+2)}{(\alpha+1)(\beta+1)(\zeta^2+1)^2}$, $E = \frac{\zeta^2}{\zeta^2+1}$, ζ is the ratio between the equivalent beam radius at the receiver and the pointing error displacement standard deviation at the destination node (Farid and Hranilovic, 2007), $G(\cdot)$ is the Meijer G function (Gradshteyn and Ryzhik,

2007), and α and β are the scintillation parameters (Al-Habash *et al.*, 2001)

$$\alpha = \left(\exp \left[\frac{0.49\sigma_{\mathrm{R}}^2}{\left(1 + 1.11\sigma_{\mathrm{R}}^{\frac{12}{5}}\right)^{\frac{7}{6}}} \right] - 1 \right)^{-1} \tag{3.16}$$

$$\beta = \left(\exp \left[\frac{0.51\sigma_{\mathrm{R}}^2}{\left(1 + 0.69\sigma_{\mathrm{R}}^{\frac{12}{5}}\right)^{\frac{5}{6}}} \right] - 1 \right)^{-1} \tag{3.17}$$

where $\sigma_{\mathrm{R}}^2 = 1.23 C_{\mathrm{n}}^2 (2\pi/\lambda)^{\frac{7}{6}} L_{\mathrm{FSO}}^{\frac{11}{6}}$ is unitless Rytov variance, C_{n}^2 is the refractive-index structure parameter, and L_{FSO} is the FSO propagation distance.

3.3 Outage Probability and Capacity-CDF Analysis

The outage probability of the AF relayed FSO/fiber backhauled system is defined as

$$\begin{aligned} P_{\mathrm{out}}(\gamma_{\mathrm{th}}) &= Pr[\gamma_{\mathrm{T}} < \gamma_{\mathrm{th}}] \\ &= Pr\left[\frac{\gamma_1 \gamma_2}{\gamma_2 + \gamma_2 \gamma_R + C_1^2 (1 + C_2^2/\gamma_3)} < \gamma_{\mathrm{th}} \right] \end{aligned} \tag{3.18}$$

where $\gamma_{\rm th}$ is the threshold on overall SINR that guarantees a minimum level of link quality. Substituting distributions from Sec. 3.2.5 yields

$$\begin{aligned} P_{\rm out}(\gamma_{\rm th}) = & \\ & \int_0^\infty \int_0^\infty Pr\left[\gamma_1 < \gamma_{\rm th}\frac{\gamma_2+\gamma_2\gamma_R+C_1^2(1+C_2^2/\gamma_3)}{\gamma_2}\right] \\ & \quad \times f_{\gamma_{\rm R}}(\gamma_{\rm R}) f_{\gamma_2}(\gamma_2) d\gamma_{\rm R} d\gamma_2 \\ = 1 - & \int_0^\infty \int_0^\infty \exp\left(-\gamma_{\rm th}\frac{\gamma_2+\gamma_2\gamma_{\rm R}+C_1^2(1+C_2^2/\gamma_3)}{\overline{\gamma_1}\gamma_2}\right) \\ & \quad \times f_{\gamma_{\rm R}}(\gamma_{\rm R}) f_{\gamma_2}(\gamma_2) d\gamma_{\rm R} d\gamma_2. \end{aligned} \tag{3.19}$$

Using (Gradshteyn and Ryzhik, 2007, Eq. (3.351.3)), the last integration can be written as

$$\begin{aligned} P_{\rm out}(\gamma_{\rm th}) = & 1 - \left(1+\frac{\gamma_{\rm th}\overline{\gamma_{\rm Ri}}}{\overline{\gamma_1}}\right)^{-M} \exp\left(\frac{-\gamma_{\rm th}}{\overline{\gamma_1}}\right) \\ & \times \int_0^\infty \exp\left(\frac{-\gamma_{\rm th}C_1^2(1+C_2^2/\gamma_3)}{\overline{\gamma_1}\gamma_2}\right) f_{\gamma_2}(\gamma_2) d\gamma_2. \end{aligned} \tag{3.20}$$

By expressing $\exp\left(\frac{-\gamma_{\rm th}C_1^2(1+C_2^2/\gamma_3)}{\overline{\gamma_1}\gamma_2}\right)$ in terms of the Meijer G function using (Wolfram Research, 2017, Eq. (07.34.03.0046.01)), the last integration can be written as

$$\begin{aligned} P_{\rm out}(\gamma_{\rm th}) = & 1 - \left(1+\frac{\gamma_{\rm th}\overline{\gamma_{\rm Ri}}}{\overline{\gamma_1}}\right)^{-M} \exp\left(\frac{-\gamma_{\rm th}}{\overline{\gamma_1}}\right) \frac{\zeta^2}{2\Gamma(\alpha)\Gamma(\beta)} \\ & \times \int_0^\infty \gamma_2^{-1} G_{1,0}^{0,1}\left(\frac{\overline{\gamma_1}\gamma_2}{\gamma_{\rm th}C_1^2(1+C_2^2/\gamma_3)}\middle|\begin{matrix}1\\ \_\end{matrix}\right) \\ & \times G_{1,3}^{3,0}\left(E\alpha\beta\sqrt{\frac{\gamma_2}{\mu_2}}\middle|\begin{matrix}\zeta^2+1\\ \zeta^2,\alpha,\beta\end{matrix}\right) d\gamma_2. \end{aligned} \tag{3.21}$$

Using (Adamchik and Marichev, 1990, Eq. (21)) and (Wolfram Research, 2017, Eqs. (07.34.04.0003.01), (07.34.04.0004.01), (07.34.03.0002.01)), $P_{\rm out}$ can be written more compactly as

$$\begin{aligned} P_{\rm out}(\gamma_{\rm th}) =& 1 - \frac{2^{\alpha+\beta}\zeta^2}{8\pi\Gamma(\alpha)\Gamma(\beta)} \left(1 + \frac{\gamma_{\rm th}\overline{\gamma_{\rm Ri}}}{\overline{\gamma_1}}\right)^{-M} \exp\left(\frac{-\gamma_{\rm th}}{\overline{\gamma_1}}\right) \\ & \times G_{1,6}^{6,0}\left(\frac{(E\alpha\beta)^2\gamma_{\rm th}C_1^2(1+C_2^2/\gamma_3)}{16\overline{\gamma_1}\mu_2}\middle|\begin{matrix} a \\ b \end{matrix}\right) \end{aligned} \tag{3.22}$$

where $a \stackrel{\rm def}{=} \left\{\frac{\zeta^2}{2}+1\right\}$ and $b \stackrel{\rm def}{=} \left\{\frac{\zeta^2}{2}, \frac{\alpha}{2}, \frac{\alpha+1}{2}, \frac{\beta}{2}, \frac{\beta+1}{2}, 0\right\}$.

As another performance metric, the CDF of end user capacity using mixed FSO/fiber backhaul system can be computed in a similar manner. The capacity of the overall system in bits per second can be estimated as (Essiambre *et al.*, 2010)

$$C = R_{\rm s}\log_2\left(1+\gamma_{\rm T}\right) \tag{3.23}$$

where $R_{\rm s}$ is the symbol rate. The CDF of user capacity takes the form

$$\begin{aligned} F_{\rm C}(C_0) &= Pr\left[R_{\rm s}\log_2\left(1+\gamma_{\rm T}\right) < C_0\right] \\ &= Pr\left[\gamma_{\rm T} < 2^{(C_0/R_{\rm s})} - 1\right] \end{aligned} \tag{3.24}$$

for some target capacity C_0. Using (3.22) and replacing $\gamma_{\rm th}$ with $\left(2^{(C_0/R_{\rm s})}-1\right)$ yields $F_{\rm C}(C_0)$.

3.4 Average BER Analysis

Using (Ansari *et al.*, 2011, Eq. (12)), the average user BER using mixed FSO/fiber backhaul systems for a variety of binary modulations can be obtained as

$$\overline{BER} = \frac{q^p}{2\Gamma(p)} \int_0^\infty \exp\left(-q\gamma_{\rm th}\right)\gamma_{\rm th}^{p-1} P_{\rm out}(\gamma_{\rm th}) d\gamma_{\rm th} \tag{3.25}$$

where p and q account for different modulation techniques. Expressing $\left(1+\frac{\gamma_{\rm th}\overline{\gamma_{\rm Ri}}}{\overline{\gamma_1}}\right)^{-M}$ in terms of Meijer G function (Wolfram Research, 2017, Eq. (07.34.03.0271.01)), and substituting (3.22) into (3.25) gives

$$\begin{aligned}\overline{BER} =& \frac{1}{2} - \frac{2^{\alpha+\beta}\zeta^2 q^p}{16\pi\Gamma(\alpha)\Gamma(\beta)\Gamma(p)\Gamma(M)} \int_0^\infty \gamma_{\rm th}^{p-1} \\ & \times \exp\left(-\left(q+\frac{1}{\overline{\gamma_1}}\right)\gamma_{\rm th}\right) G_{1,1}^{1,1}\left(\frac{\overline{\gamma_{\rm Ri}}}{\overline{\gamma_1}}\gamma_{\rm th}\middle|\begin{matrix}1-M\\0\end{matrix}\right) \\ & \times G_{1,6}^{6,0}\left(\frac{(E\alpha\beta)^2\gamma_{\rm th}C_1^2(1+C_2^2/\gamma_3)}{16\overline{\gamma_1}\mu_2}\middle|\begin{matrix}a\\b\end{matrix}\right) d\gamma_{\rm th}.\end{aligned} \tag{3.26}$$

Using (Ansari *et al.*, 2011, Eqs. (14 and 20) and Table I), the last integration can be written as

$$\begin{aligned}\overline{BER} =& \frac{1}{2} - \frac{2^{\alpha+\beta}\zeta^2 q^p}{16\pi\Gamma(\alpha)\Gamma(\beta)\Gamma(p)\Gamma(M)\left(q+\frac{1}{\overline{\gamma_1}}\right)^p} \\ & \times G_{1,0:1,1:6,0}^{1,0:1,1:6,0}\left(\begin{matrix}p\\-\end{matrix}\middle|\begin{matrix}1-M\\0\end{matrix}\middle|\begin{matrix}a\\b\end{matrix}\middle|\frac{\overline{\gamma_{\rm Ri}}}{(1+q\overline{\gamma_1})}, \frac{(E\alpha\beta)^2C_1^2(1+C_2^2/\gamma_3)}{16\mu_2(1+q\overline{\gamma_1})}\right)\end{aligned} \tag{3.27}$$

where $G^{\cdot,\cdot,\cdot,\cdot,\cdot,\cdot}_{\cdot,\cdot,\cdot,\cdot,\cdot,\cdot}\left(\begin{array}{c|c|c|c} \cdot & \cdot & \cdot & \\ \cdot & \cdot & \cdot & \end{array}.,.\right)$ is the extended generalized bivariate Meijer G function (EGBMGF) (Ansari *et al.*, 2011). The EGBMGF is efficiently implemented in a variety of commercial mathematics software (e.g., (Ansari *et al.*, 2011; Chergui *et al.*, 2016)).

For the interference free case $(M = 0)$, a simpler expression for $\overline{BER}$ is (following a similar approach as (Ansari *et al.*, 2013a, Eq. (14)))

$$\begin{aligned}\overline{BER_0} =& \frac{1}{2} - \frac{2^{\alpha+\beta}\zeta^2 q^p}{16\pi\Gamma(\alpha)\Gamma(\beta)\Gamma(p)\left(q+\frac{1}{\overline{\gamma_1}}\right)^p} \\ & \times G_{2,6}^{6,1}\left(\frac{(E\alpha\beta)^2 C_1^2(1+C_2^2/\gamma_3)}{16\mu_2(q\overline{\gamma_1}+1)}\middle| \begin{matrix} 1-p, a \\ b \end{matrix}\right).\end{aligned} \tag{3.28}$$

3.5 Asymptotic Analysis

In order to provide greater physical insights, in this section the asymptotic outage probability and average BER expressions at high SNR regime are derived and used to compute the optimum fiber average launched power.

3.5.1 Asymptotic Outage and BER

In (3.22), the Meijer G function makes additional analytical derivations difficult. In the case of large $\overline{\gamma_2}$ and γ_3 the following approximation can be applied (Wolfram Research,

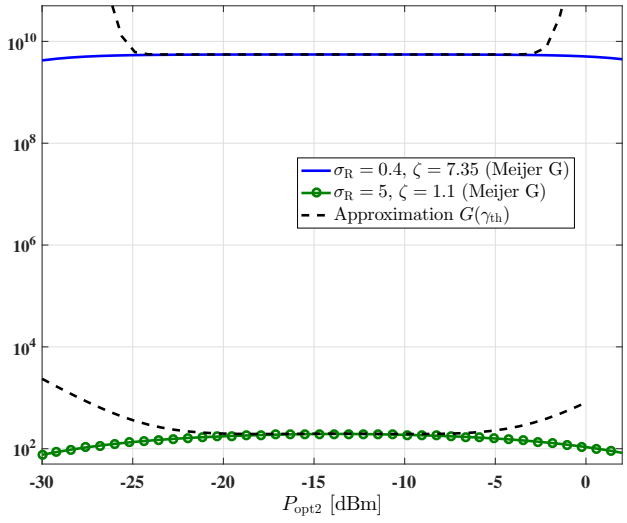

Figure 3.2: Approximation $G(\gamma_{\text{th}})$ versus P_{opt2} ($M = 0, \gamma_{\text{th}} = 0$ dB, and $\overline{\gamma_2} = 70$ dB).

2017, Eq. (07.34.06.0006.01))

$$G_{1,6}^{6,0}\left(\frac{(E\alpha\beta)^2\gamma_{\text{th}}C_1^2(1+C_2^2/\gamma_3)}{16\overline{\gamma_1}\mu_2}\middle|\begin{matrix}a\\b\end{matrix}\right) \approx G(\gamma_{\text{th}}) = \sum_{k=1}^{6}\frac{\prod_{j=1,j\neq k}^{6}\Gamma(b_j-b_k)}{\Gamma(a-b_k)}\left(\frac{(E\alpha\beta)^2\gamma_{\text{th}}C_1^2(1+C_2^2/\gamma_3)}{16\overline{\gamma_1}\mu_2}\right)^{b_k}. \tag{3.29}$$

In Fig. 3.2, the Meijer G function in (3.29) and its approximation, $G(\gamma_{\text{th}})$, are plotted versus P_{opt2} at high $\overline{\gamma_2}$ for different turbulence and pointing error conditions levels. Initially as P_{opt2} increases, γ_3 becomes high and so the approximation is tight. This is true as long as the fiber nonlinearity noise is low and not dominant. However, at high values of P_{opt2}, γ_3 is reduced due to fiber nonlinearity noise. Thus there is a range of P_{opt2} values over which this fit is tight as will be discussed in Sec. 3.6.

For a fixed and finite $\overline{\gamma_1}$, the asymptotic outage probability at high $\overline{\gamma_2}$ and γ_3 is

$$\begin{aligned} P_{\text{out}}^{\text{asym}}(\gamma_{\text{th}}) = \\ 1 - \frac{2^{\alpha+\beta}\zeta^2}{8\pi\Gamma(\alpha)\Gamma(\beta)} \left(1 + \frac{\gamma_{\text{th}}\overline{\gamma_{\text{Ri}}}}{\overline{\gamma_1}}\right)^{-M} \exp\left(\frac{-\gamma_{\text{th}}}{\overline{\gamma_1}}\right) \\ \times \sum_{k=1}^{6} \frac{\prod_{j=1, j\neq k}^{6} \Gamma(b_j - b_k)}{\Gamma(a - b_k)} \left(\frac{(E\alpha\beta)^2 \gamma_{\text{th}} C_1^2 (1 + C_2^2/\gamma_3)}{16\overline{\gamma_1}\mu_2}\right)^{b_k}. \end{aligned} \tag{3.30}$$

The asymptotic CDF of user capacity can be similarly derived.

Substituting (3.30) into (3.25) yields,

$$\begin{aligned} \overline{BER}^{\text{asym}} = \frac{1}{2} - \frac{2^{\alpha+\beta}\zeta^2 q^p}{16\pi\Gamma(\alpha)\Gamma(\beta)\Gamma(p)} \sum_{k=1}^{6} \frac{\prod_{j=1, j\neq k}^{6} \Gamma(b_j - b_k)}{\Gamma(a - b_k)} \\ \times \left(\frac{(E\alpha\beta)^2 C_1^2 (1 + C_2^2/\gamma_3)}{16\overline{\gamma_1}\mu_2}\right)^{b_k} \int_0^{\infty} \gamma_{\text{th}}^{b_k + p - 1} \\ \times \exp\left(-\gamma_{\text{th}}\left(q + \frac{1}{\overline{\gamma_1}}\right)\right) \left(1 + \frac{\gamma_{\text{th}}\overline{\gamma_{\text{Ri}}}}{\overline{\gamma_1}}\right)^{-M} d\gamma_{\text{th}}. \end{aligned} \tag{3.31}$$

Simplifying using (Soleimani-Nasab *et al.*, 2013, Eq. (27)) gives

$$\begin{aligned} \overline{BER}^{\text{asym}} = \frac{1}{2} - \frac{2^{\alpha+\beta}\zeta^2 q^p}{16\pi\Gamma(\alpha)\Gamma(\beta)\Gamma(p)} \sum_{k=1}^{6} \frac{\prod_{j=1, j\neq k}^{6} \Gamma(b_j - b_k)}{\Gamma(a - b_k)} \\ \times \left(\frac{(E\alpha\beta)^2 C_1^2 (1 + C_2^2/\gamma_3)}{16\overline{\gamma_1}\mu_2}\right)^{b_k} \Gamma(b_k + p) \left(\frac{\overline{\gamma_1}}{\overline{\gamma_{Ri}}}\right)^{b_k + p} \\ \times \Psi\left(b_k + p, b_k + p - M + 1; \frac{(q\overline{\gamma_1} + 1)}{\overline{\gamma_{\text{Ri}}}}\right) \end{aligned} \tag{3.32}$$

where $\Psi(.,.;.)$ is the Tricomi confluent hypergeometric function (Gradshteyn and Ryzhik,

Table 3.1: Parameters of Fiber Backhaul Link

Parameter	Symbol	Value
Physical SMF length	L	10 km
SMF attenuation coefficient	α_f	0.22 dB/km
SMF dispersion coefficient	D	16.7 ps/km.nm
SMF nonlinearity coefficient	$\gamma_{\rm nl}$	1.3 $\mathrm{W}^{-1}\mathrm{km}^{-1}$
SMF channel bandwidth	$B_{\rm ch}$	32 GHz
The number of WDM channels	$N_{\rm ch}$	1
Detector Noise	$\sigma_{\rm D}^2$	10^{-14} A^2

2007, Eq. (9.210.2)).

For the interference free case (i.e., $M = 0$), a simpler expression can be obtained for $\overline{BER}^{\rm asym}$ using $G(\gamma_{\rm th})$ as

$$\begin{aligned}\overline{BER_0}^{\rm asym} =& \frac{1}{2} - \frac{2^{\alpha+\beta}\zeta^2 q^p}{16\pi\Gamma(\alpha)\Gamma(\beta)\Gamma(p)\left(q+\frac{1}{\overline{\gamma_1}}\right)^p} \\ &\times \sum_{k=1}^{6} \frac{\prod_{j=1,j\neq k}^{6}\Gamma(b_j-b_k)\Gamma(p+b_k)}{\Gamma(a-b_k)} \\ &\times \left(\frac{(E\alpha\beta)^2 C_1^2(1+C_2^2/\gamma_3)}{16\mu_2\left(q\overline{\gamma_1}+1\right)}\right)^{b_k}.\end{aligned} \tag{3.33}$$

3.5.2 Optimum Fiber Average Launched Power $P^*_{\rm opt2}$

Due to the fiber channel, the average launched power must be carefully selected to balance the impacts of receiver noise and the inherent nonlinearity of the channel.

Let $P^*_{\rm opt2}$ denote the optimum average launched fiber optical power which minimizes

outage. Consider setting the first derivative of $P_{\text{out}}^{\text{asym}}$ in (3.30) with respect to P_{opt2} to zero,

$$\begin{aligned}\frac{\partial P_{\text{out}}^{\text{asym}}}{\partial P_{\text{opt2}}} =& -\frac{2^{\alpha+\beta}\zeta^2 C_2^2}{8\pi\Gamma(\alpha)\Gamma(\beta)}\left(1+\frac{\gamma_{\text{th}}\overline{\gamma_{\text{Ri}}}}{\overline{\gamma_1}}\right)^{-M}\exp\left(\frac{-\gamma_{\text{th}}}{\overline{\gamma_1}}\right)\\ &\times\sum_{k=1}^{6}\frac{\prod_{j=1,j\neq k}^{6}\Gamma(b_j-b_k)}{\Gamma(a-b_k)}\left(\frac{(E\alpha\beta)^2\gamma_{\text{th}}C_1^2}{16\overline{\gamma_1}\mu_2}\right)^{b_k}\\ &\times b_k\left(1+\frac{C_2^2\sigma_D^2}{\mathcal{R}_2^2P_{\text{opt2}}^2}+4C_2^2C_{\text{NLI}}P_{\text{opt2}}^2\right)^{b_k-1}\\ &\times\left(\frac{-2\sigma_{\text{D}}^2}{\mathcal{R}_2^2P_{\text{opt2}}^3}+8C_{\text{NLI}}P_{\text{opt2}}\right)=0\end{aligned} \tag{3.34}$$

where $C_{\text{NLI}} = P_{\text{NLI}}/P_{\text{opt2}}^3$. After some simplification, the optimal P_{opt2} can be written as

$$P_{\text{opt2}}^* = \left(\frac{\pi\sigma_{\text{D}}^2|\beta_2|L_{\text{eff,a}}B_{\text{ch}}^2}{32\mathcal{R}_2^2\gamma_{\text{nl}}^2L_{\text{eff}}^2\,\text{arcsinh}\left(\frac{3}{8}\pi^2L_{\text{eff,a}}|\beta_2|B_\omega^2\right)}\right)^{\frac{1}{4}}. \tag{3.35}$$

Note that P_{opt2}^* does not depend on $\overline{\gamma_1}$, $\overline{\gamma_{\text{Ri}}}$ nor $\overline{\gamma_2}$ under the condition of the worst case fiber nonlinearity interference scenario. It worth mentioning that P_{opt2}^* in (3.35) can also be obtained using the first derivative of (3.32) or (3.33).

3.6 Numerical Results

The analytic expressions for the performance of the mixed FSO/fiber backhaul system are studied in this section to quantify the tightness of the asymptotic results and to reveal approaches for the design of such systems. The parameters for the SMF used in the backhaul network are given in Table 3.1 (El-Fiqi *et al.*, 2016). Though in this study we consider a single WDM channel, in practice multiple FSO receptions can be multiplexed on a single or over multiple WDM channels. Without loss of generality, the responsivities $\mathcal{R}_1 = \mathcal{R}_2 = 1$

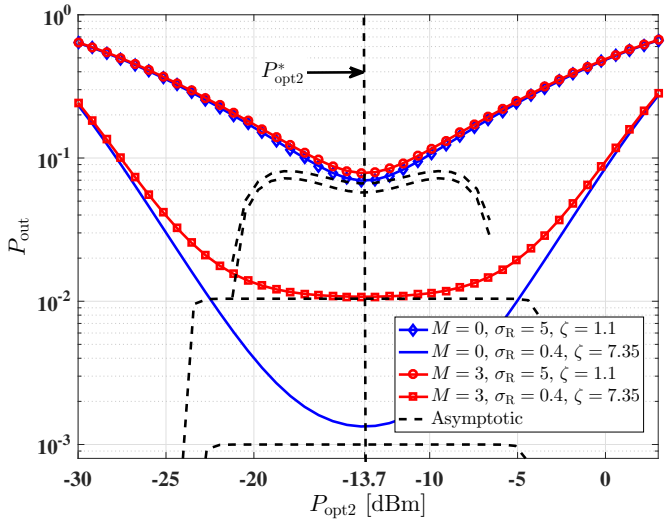

Figure 3.3: P_{out} versus P_{opt2} ($\gamma_{\text{th}} = 0$ dB, $\overline{\gamma_1} = 30$ dB, $\overline{\gamma_2} = 70$ dB, and $\overline{\gamma_{\text{Ri}}} = 5$ dB).

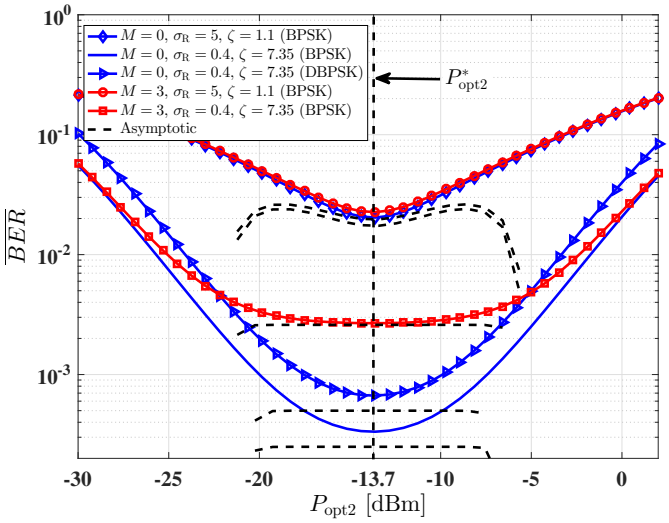

Figure 3.4: $\overline{BER}$ versus P_{opt2} for different modulation techniques ($\gamma_{\text{th}} = 0$ dB, $\overline{\gamma_1} = 30$ dB, $\overline{\gamma_2} = 70$ dB, and $\overline{\gamma_{\text{Ri}}} = 5$ dB) ($p = 0.5$ and $q = 1$ for BPSK and $p = 1$ and $q = 1$ for DBPSK (Ansari *et al.*, 2011)).

are assumed. Given the variability of the RF and FSO channels, performance will be studied for a variety of SNR values, turbulence strengths and pointing error severity.

Figures 3.3 and 3.4 show the outage probability (3.22) and the average BER, computed in (3.27) and (3.28), versus P_{opt2} with different values for the average overall RF access network INR, FSO pointing error, and turbulence strength levels. In all cases, there is an optimal value for the average launched fiber power which maximizes performance. If $P_{\text{opt2}} > P^*_{\text{opt2}} \approx -13.7$ dBm (computed via (3.35)), fiber nonlinearity dominates limiting the system performance. Notice also that the asymptotic results, from (3.30), (3.32) and (3.33), are only tight near P^*_{opt2} when γ_3 is large enough to make the approximation valid. Furthermore, the addition of RF co-channel interference in the access network degrades performance, as expected. An interesting feature is that in the presence of co-channel interference in the RF access network, the performance flattens near P^*_{opt2}. This phenomenon occurs because the RF co-channel interferers dominate over the backhaul impairments of both FSO and fiber links. However, in worse FSO channel conditions, optical fading and pointing errors dominate and the impact of co-channel interferers is not as significant. In the case of no co-channel interferers, the curves do not flatten near P^*_{opt2} and the system performance is greatly improved for good FSO channel conditions.

The minimum outage probability (P^*_{out}), computed at P^*_{opt2}, is plotted versus $\overline{\gamma_1}$ and $\overline{\gamma_2}$ in Figs. 3.5 and 3.6, respectively. As expected, by increasing $\overline{\gamma_1}$ or $\overline{\gamma_2}$, P^*_{out} improves. Similarly, as the number of interferers increase or the weather and the pointing error conditions become worse, P^*_{out} degrades. In addition, at high $\overline{\gamma_1}$ or $\overline{\gamma_2}$, P^*_{out} saturates. This saturation in performance is due to the selection of G_1 (3.2) and G_2 (3.5) to control the clipping distortion and to ensure non-negativity of the signal inputted to the optical intensity modulator. In this work $K_1 = K_2 = 4$ and are fixed to model a simple automatic gain control system

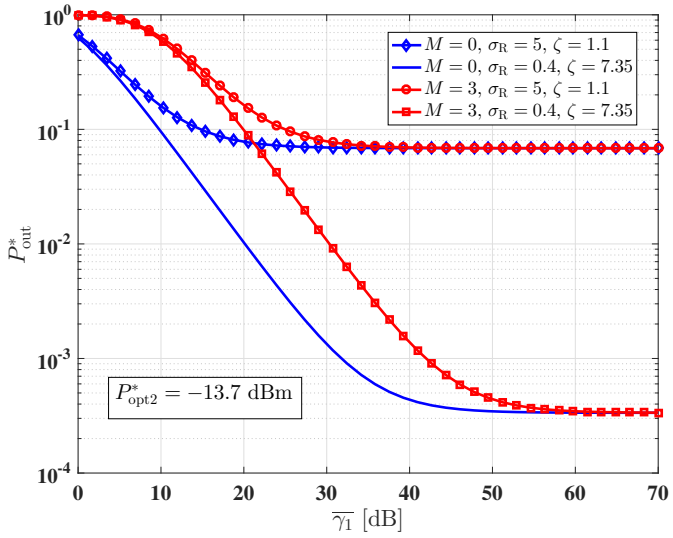

Figure 3.5: P^*_{out} versus $\overline{\gamma_1}$ for different FSO conditions and RF interferers ($\gamma_{\text{th}} = 0$ dB, $\overline{\gamma_2} = 70$ dB, and $\overline{\gamma_{\text{Ri}}} = 5$ dB, $P_{\text{opt2}} = P^*_{\text{opt2}}$).

which is already available in many commercial FSO systems (fSONA Corporation, 2017).

Notice in Fig. 3.5, that P^*_{out} saturates at a lower $\overline{\gamma_1}$ when FSO conditions are worse due to the dominance of the FSO impairments. Furthermore, in Fig. 3.6, for good FSO conditions, the system performance saturates at a lower $\overline{\gamma_2}$ after adding the RF co-channel interference due to the dominance of the RF impairments. However, for worse FSO channel conditions, the RF co-channel interference has little impact.

In Fig. 3.7, the CDF of the estimated user capacity is plotted at P^*_{opt2}, for different $\overline{\gamma_1}$ and $\overline{\gamma_2}$, using mm-wave RF access with $R_{\text{s}} = 220$ Msymbols/sec (Dehos *et al.*, 2014). The distribution of user rates is impacted by both RF and FSO channels, however, they are much more sensitive to the FSO backhaul conditions. When the FSO channel is poor, $\overline{\gamma_1}$ has little impact on system performance. However, in good FSO conditions, the RF SNR greatly impacts user rates. In particular, the 50-th percentile user rates can reach 1.5 Gbits/sec under favorable RF and FSO conditions.

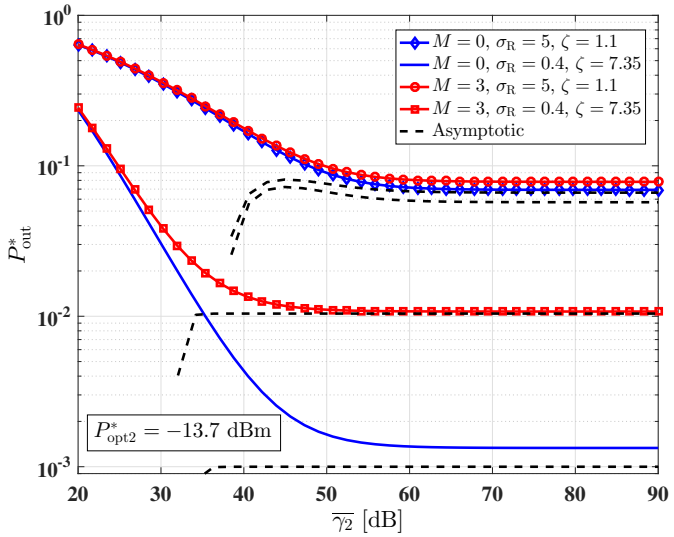

Figure 3.6: P^*_{out} versus $\overline{\gamma_2}$ for different FSO conditions and RF interferers ($\gamma_{\text{th}} = 0$ dB, $\overline{\gamma_1} = 30$ dB, and $\overline{\gamma_{\text{Ri}}} = 5$ dB, $P_{\text{opt2}} = P^*_{\text{opt2}}$).

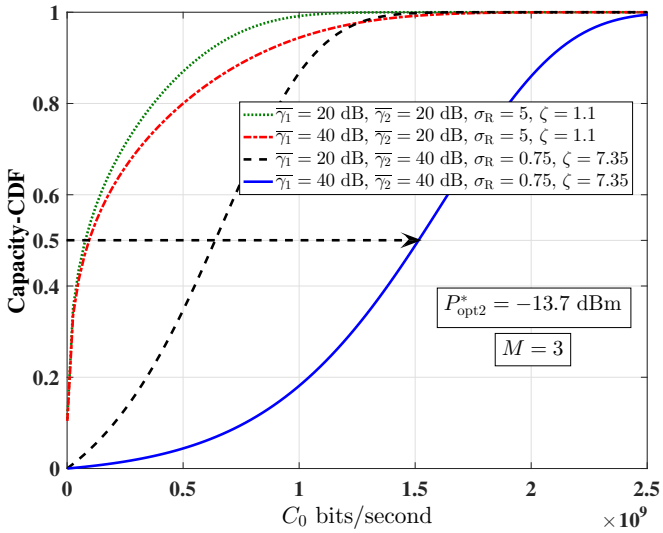

Figure 3.7: CDF of the estimated user capacity for different RF and FSO backhaul conditions ($\overline{\gamma_{\text{Ri}}} = 5$ dB and $R_s = 220$ Msymbols/sec, $P_{\text{opt2}} = P^*_{\text{opt2}}$).

3.7 Conclusion

In this paper, we present analytical results quantifying the performance of 5G RF access networks with a mixed AF FSO and fiber backhaul. In the access network, the impact of RF co-channel interferers is considered while in the backhaul the impact of FSO pointing errors, fiber nonlinearity as well as the limited dynamic range of optical emitters are modelled. Under fixed gain relaying, closed-form and asymptotic expressions for the outage probability, the average BER, and the CDF of end user capacity of the mixed FSO/fiber backhaul systems are derived. Our results reveal that there is an optimal average launched optical power into the fiber which balances the impact of improving received signal power with the distortion of fiber nonlinearity. In the region above the optimal fiber average launched power, increasing the optical average launched power yields more outage because of the dominance of the fiber nonlinearity. A key conclusion that is quantified in this work is that the quality of the variable FSO backhaul channel has a dominating impact on the user rates as compared to the RF access channel (when transmitting at optimum fiber average launched power P^{*}_{opt2}). This work thus serves as a tool to help in the planning and provisioning of the 5G networks with FSO and fiber backhaul components.

Chapter 4

Network Planning of Uplink All-Optical Passive FSO/OF C-RAN Fronthaul

A network planning framework for a C-RAN with all-optical passive RoFSO/RoF fronthauling is presented in this chapter. The coverage area, the RoF near-far problem, the RU density, the OF length, the optical power, and the RoFSO gain are all considered in the analyses to show their impacts on the fronthaul reliability. The design of the coverage area, i.e. range, is the third branch of the rate-reliability-range trade-offs discussed in Sec. 1.4 while the first two branches were investigated in **Chapter** 2 and **Chapter** 3 respectively. Although the RoFSO gain was designed numerically in **Chapter** 2 and conservatively in **Chapter** 3, an approximate analytical optimum gain is derived in this chapter which maximizes system reliability. Guidance on choosing and tuning each of those parameters is provided in this chapter for planning the network both on individual-RU scale and system-wide scale.

The material in this chapter has been submitted to *IEEE/OSA Journal of Optical Communications and Networking*(11 pages, May 2019) and is currently under review. Additional contribution to this work that was not submitted is provided in **Appendix** C. **Appendix** C presents the outage probability derivation for the case when the nonlinear interference in the OF dominates other noise sources. However the OF length and the optical power in this chapter would not trigger such a dominant nonlinearity, the analyses in **Appendix** C is particularly useful when long OF, e.g. hundreds of kilometers, is deployed and high optical power is transmitted. Thus, for completeness, the analysis is added in **Appendix** C.

Abstract

Though the cloud radio access network (C-RAN) architecture is a promising approach to enabling the necessary densification of radio networks in future systems, its utility relies on the availability of high bandwidth reliable fronthaul links. In this paper, we propose a new all-optical fronthaul architecture in which user signals are forwarded over radio-over-FSO (RoFSO) links which are passively coupled to an optical fiber (OF) for transport to a central office. We develop tools to plan such a network to optimize the outage probability while considering the coverage area, the density of the radio units (RUs), and the signal gain at the RUs. Each of these parameters can be designed to maintain an upperbound of the outage probability. Analytical expressions of the outage probability of the fronthaul network as well as the optimum RU gain are obtained. For a realistic design, clipping noise, atmospheric scintillation, the effect of different weather conditions are considered for the RoFSO links while non-linear interference is modelled in the OF link. Given a required outage probability and density of RUs, the tools developed here can give the coverage area as well as optimum values for transmitted optical power and gain which balance the impact of all impairments.

4.1 Introduction

To enable future radio networks, extreme cell densification is required together with a high degree of frequency reuse. These factors will result in interference becoming a dominating impairment limiting system performance. A promising solution to this issue is the cloud radio access network (C-RAN) architecture where a dense network of radio units (RUs) forward their received radio frequency (RF) signals from user equipment (UEs) to a central office (CO) for joint processing. While interference on UEs is unavoidable in the RF

access network, joint processing of the forwarded signals from RUs permits interference mitigation. However, the gains available from the C-RAN approach depend entirely on the availability of high-rate, reliable fronthaul links.

Fronthaul over optical fibre (OF) links is preferred, however, is also the most costly option. Optical wireless fronthaul via free-space optics (FSO) is easily deployable, high data rate and uses unlicensed spectrum. Unlike the RF links, FSO fronthaul is largely immune to interference due to its highly directional nature. However, the reliability of all FSO links are dependent on weather condtions (e.g., dense fog).

While it is possible to have digital fronthaul over FSO links, simpler and less expensive radio-over-FSO (RoFSO) fronthaul collects UE signals, scales them with a gain and analog modulates the intensity a laser to transmit the signals (Ahmed and Hranilovic, 2018). Such approaches simplify the fronthaul by eliminating the need for high speed samplers, quantizers and A-to-D converters and are essential to widespread RU deployments. However, non-linear clipping distortion is present in all RoFSO transmissions due to the limited dynamic range of the modulator and the design of the modulator gain is essential to balance signal power with clipping distortion. Initial work considered a fixed gain for the RoFSO fronthaul links (Anees and Bhatnagar, 2015b; Lee *et al.*, 2011; Anees and Bhatnagar, 2014; Zedini *et al.*, 2015b; Petkovic, 2015; Park *et al.*, 2013; Ansari *et al.*, 2013c; Zedini *et al.*, 2014; Ansari *et al.*, 2013a; Anees and Bhatnagar, 2015a) and clipping noise was neglected. A variable gain in the RoFSO fronthaul has also been considered (Zedini *et al.*, 2015a; Ansari *et al.*, 2013b; Soleimani-Nasab and Uysal, 2016; Petkovic *et al.*, 2017) to adapt to channel conditions, however, clipping noise was not considered. In (Morra *et al.*, 2017) the gain of the RoFSO link is set conservatively to justify ignoring the clipping distortion inherent in such links. In (Ahmed and Hranilovic, 2018) clipping noise was considered in

for an RoFSO/RF fronthaul links to maximize the weighted sum of user rates.

Analogously, radio-over-fibre (RoF) approaches have also been considered as a low-cost means to achieve fronthaul for C-RAN (Sauer *et al.*, 2007; Li *et al.*, 2019; Checko *et al.*, 2015; Wake *et al.*, 2010). Recent work on RoF (Li *et al.*, 2019) introduces an analogue beamforming technique based on fibre non-linearity which is one step towards an all-optical system. Though RoF based C-RANs provide improvement to the system performance, they lack the flexibility of RoFSO due to the last-mile problem of the OF which is exacerbated in the case of a large number of nodes forwarding the signals to a CP e.g. a distributed antenna system as in (Wake *et al.*, 2010).

While there has been some work in the design of individual RoFSO and RoF fronthaul links, there has been comparatively little work on the network planning of a C-RAN using such links. In (Douik *et al.*, 2016), the cost of deploying a fronthaul using either OF or RF/FSO is minimized subject to reliability and rate constraints. Earlier work (Smadi *et al.*, 2009) considered a network planning problem in which the positions of the FSO/RF gateways were selected to minimize the number of additional links needed to satisfy a capacity requirement.

This paper introduces a passive, all-optical fronthaul topology for C-RAN deployments (see Fig. 4.1) where UE signals are collected by multiple RUs and forwarded to an intermediate unit (IU) via RoFSO links. The IU in turn passively couples these optical signals into a short span fiber link which transmits them via RoF to the CO for joint processing. This topology is scalable and flexible as the locations and numbers of the RoFSO links can be chosen to improve overall system performance. Additionally, this approach is cost-effective since it is a passive optical network which minimizes the number of required fiber

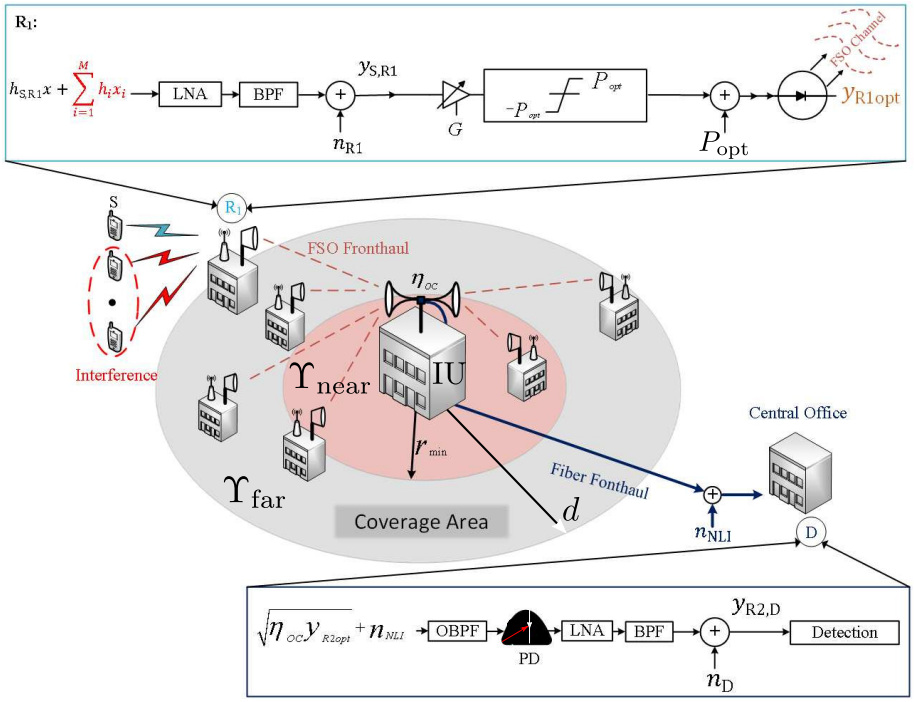

Figure 4.1: C-RAN system model with passive FSO/OF fronthaul links for uplink.

links. Passive opto-couplers are also simpler and less expensive than optical active amplifiers such as erbium-doped fiber amplifier (EDFA) (Cai *et al.*, 2019; Zheng *et al.*, 2016).

The design and performance of such multi-hop optical fronthaul is considered by optimizing the parameters of both RoFSO and RoF links to optimize both the density of RUs and coverage area. In our design problem, we include different channel impairments including FSO geometric loss, atmospheric scintillation, numerical simulations of pointing errors, clipping distortion at the RoFSO nodes and non-linear interference in the OF. Unlike earlier work in RoFSO for C-RAN that ignored the clipping noise, we derive an analytical expression for the optimum RU gain in the presence of clipping distortion to maximize system reliability. Furthermore, the impact of different weather conditions on system reliability using measured weather data.

In Sec. 4.2, the all-optical fronthaul topology is introduced along with modelling approaches and assumptions. Section 4.3 presents the formulation of the design problem in terms of the fronthaul outage probability and presents analytical results on the optimum RoFSO gain which considers clipping noise. Simulation results are presented in Sec. 4.4 which provide a network planning tool to design the C-RAN all-optical fronthaul considering the tradeoffs between the coverage area and density of RUs under impairments inherent to FSO channels as well as fiber nonlinearity. The paper concludes in Sec. 4.5 with suggestions for future work.

4.2 System Model

4.2.1 Overview

A diagram of the uplink fronthaul network is presented in Fig. 4.1. In the access network, UEs transmit radio frequency (RF) signals to the corresponding RUs. The received RF signal at each RU consists of the signal from users, interference, and the noise added at the receiver front-end.

In order for the RF signal to be converted to the optical domain, several practical constraints must be satisfied. The received signal is amplified and clipped to fit into the limited dynamic range of the laser diode. Additionally, the clipped signal must be biased to ensure non-negativity and to permit intensity modulation of the laser. Given that the input RF signals are AC coupled, the added bias also represents the average optical power which is limited by eye-safety regulations. Thus, the RU can be thought of as an RoFSO amplify-and-forward relay that converts the received RF signal into optical domain for forwarding

over an FSO link while adding clipping distortion. All RUs within the *coverage area* forward their signals via the RoFSO link to an intermediate unit (IU). The optical signals collected at the IU are coupled into an OF using a passive opto-coupler and forwarded to the CO.

In the following subsections, the modelling of each of the stages of the network are discussed in detail.

4.2.2 Coverage Area

Definition

The *coverage area*, Υ, is defined as a circular region in which RUs forward their signals to a given IU which is located at the center. The coverage area has a number of users transmitting RF signals to their corresponding RUs which each forwarding signals over RoFSO links to the IU. As shown in Fig. 4.1, the radius of the coverage area is denoted as d and is the maximum length of any RoFSO link connecting an RU to the IU. The selection of d critically impacts system performance and its impact and design are discussed in Sec. 4.4.3.

Near-far problem

Consider partitioning the coverage area as $\Upsilon = \Upsilon_{\text{near}} \cup \Upsilon_{\text{far}}$ as shown in Fig. 4.1. The region Υ_{near} is a disc of radius r_{min} centred on the IU. The RUs in Υ_{far} transmit at an optical power limited by eye-safety regulations. The RUs located in the Υ_{near} are near to the IU and have a high received power which risks incurring significant nonlinear distortion in the OF (see Sec. 4.2.5). Let P_r denote the average optical power received at the IU from an RU at distance r. In order to avoid this near-far problem, the transmitted optical power from

the RUs in the Υ_{near} is scaled so that $\forall r \leq r_{\text{min}}$, $P_r = P_{r_{\text{min}}}$.

The value of r_{min} is another parameter to be chosen when planning the network. The value of r_{min} must be selected by considering both the sensitivity of the receiver and the impact of OF nonlinearity as discussed in Sec. 4.4.3.

Continuous Approximation

Let Ω denote the set of coordinates of RU locations in the coverage area Υ. In order to simplify analysis and design for the network, consider approximating sums over the discrete elements of Ω by an integral over Υ. In particular, for an integrable function $f : \mathbb{R}^2 \to \mathbb{R}$, define the *continuous approximation*

$$\sum_{\mathbf{x}\in\Omega} f(\mathbf{x}) \approx R \int_{\Upsilon} f(\mathbf{x}) \mathrm{d}A \tag{4.1}$$

where R is the density of RUs in units of m^{-2}. This approximation has been first developed for the design of multi-dimensional constellations (Forney and Wei, 1989) and is tight for dense networks. The tightness of this approximation is verified in Sec 4.4.7 using both discrete RUs and the continuous model. Notice that if the number of users per RU is nearly constant, that R is linearly related to the density of users in the network.

4.2.3 Radio Access Network

As shown in Fig. 4.1 (top left), a UE sends a desired symbol x to the corresponding RU which is corrupted by multipath fading, $h_{S,R1}$, and additive white Gaussian noise AWGN n_{R1}. In addition, the signal received at the RU will experience interference from UEs in the M neighboring cells. The overall received RF signal at the RU can then be modelled as

$$y_{S,R1} = x h_{S,R1} + \sum_{i=1}^{M} x_j h_i + n_{R1}. \tag{4.2}$$

4.2.4 Free-space Optical Fronthaul

Electrical-to-Optical Conversion

Given that the laser outputs an optical intensity, the input to the laser driver must be non-negative and the average optical power is constrained by eye-safety regulations. To ensure that both conditions are satisfied, an analog clipper is employed and a bias is added to ensure the input is non-negative. Define P_{opt} as the clipping level for the signal as well as the added bias to ensure eye-safe operation, as shown in Fig. 4.1. Notice that this biasing swings the laser intensity through its entire linear range.

Due to the random gain of the the wireless access channel, an amplifier with gain G is placed before the clipper to control the signal power which in return controls the amount of clipping introduced. Finally, the signal is converted to optical domain by analog modulating the laser intensity.

Clipping Noise and Gain Design

Employing a Bussgang model (Bussgang, 1952), the clipped signal $y_{R1_{\text{opt}}}$ in Fig. 4.1 can be approximated as (Ahmed and Hranilovic, 2018)

$$y_{R1_{opt}} \approx K\, G\, y_{S,R1} + P_{\text{opt}} + n_c \tag{4.3}$$

where

$$K = \text{erf}\left(\frac{P_{\text{opt}}}{\sqrt{2G^2 P_{\text{RF}}}}\right) \tag{4.4}$$

and $P_{\text{RF}} = E\{y_{S,R1}^2\}$. The clipping noise, n_c, has a variance (Ahmed and Hranilovic, 2018)

$$\sigma_c^2 = P_{opt}^2 \left(1 - \frac{K^2 G^2 P_{\text{RF}}}{P_{opt}^2} - \sqrt{\frac{2G^2 P_{\text{RF}}}{\pi P_{opt}^2}} e^{-\frac{P_{opt}^2}{2G^2 P_{\text{RF}}}} + \left(\frac{G^2 P_{\text{RF}}}{P_{opt}^2} - 1\right) \text{erf}\left(\frac{P_{opt}}{\sqrt{2G^2 P_{\text{RF}}}}\right)\right). \quad (4.5)$$

Notice that the gain G affects both the optical signal and the clipping noise. Hence, a careful design of G is essential to balance the two effects to optimize system performance.

Free-space optical propagation model

The optical signal $y_{R1_{opt}}$ emitted from the RU travels through the FSO channel to the IU yielding the signal

$$y_{R2_{\text{opt}}} = y_{R1_{\text{opt}}} g_{\text{FSO}}(r) \quad (4.6)$$

where the FSO channel gain can be factored as (Farid and Hranilovic, 2007)

$$g_{\text{FSO}}(r) = g_l g_d g_a g_p(r). \quad (4.7)$$

for a range r between RU and the IU. The propagation loss due to absorption and scattering, g_l, follows the Beers-Lambert law

$$g_l(r) = \exp(-\gamma_{\text{FSO}} r) \quad (4.8)$$

where the attenuation coefficient γ_{FSO} depends on the weather conditions and r is the length of the FSO link. The geometric loss g_d caused by the beam divergence is

$$g_d(r) = \frac{D_{\text{rx}}^2}{\theta_{\text{tx}}^2 r^2} \tag{4.9}$$

where D_{rx} is the receiver diameter and θ_{tx} is the beam divergence angle. The turbulent atmosphere causes scintillation which is modelled by the random channel gain g_a. A log-normal distribution models g_a for a weak-to-moderate turbulence regime which typically happens with short links, when the scintillation index is in the range $[0, 0.75]$ (Kiasaleh, 2005), and has the form

$$f_{g_a}(g_a; r) = \frac{1}{2g_a\sqrt{2\pi\sigma_d^2}} \exp\left(-\frac{(\ln g_a + 2{\sigma_d}^2)^2}{8{\sigma_d}^2}\right) \tag{4.10}$$

with ${\sigma_d}^2 = 0.30545{C_n}^2 k^{7/6} r^{11/6}$ where C_n^2 is the index of refraction structure parameter, and k is the optical wave number. Notice that the mean atmospheric fading is $\bar{g}_a = 1$.

The pointing error, $g_p(r)$, results from the misalignment of the transmitter and the receiver due to dynamic building sway. The pointing error is random and is distributed as

$$f_{g_p}(g_p; r) = \frac{\Gamma^2}{A_o^{\Gamma^2}} g_p^{\Gamma^2 - 1} \quad 0 \leq g_p \leq A_o \tag{4.11}$$

where A_o is the fraction of collected power when there is no pointing error, $\Gamma = \frac{w_{\text{eq}}}{2\sigma_s}$ where w_{eq} is the equivalent beam width at the receiver, and σ_s is the standard deviation of the pointing error displacement (Farid and Hranilovic, 2007) . For the purposes of system design, $g_p = 1$ to ensure the model remains tractable. However, in Sec. 4.4.7 the impact of pointing errors is quantified on the design using the above FSO model.

4.2.5 Passive Optical Fiber Fronthaul Model

Opto-Coupler

All-optical FSO relays using free space opto-couplers have attracted attention recently due to their simplicity (Cai *et al.*, 2019; Zheng *et al.*, 2016). Unlike electrical relays, there is no need for high speed electronics and conversion between optical and electrical domains. Though erbium-doped fibre amplifiers (EDFAs) can provide a gain in an all-optical network, they also add noise and significant cost. In this work, we adopt a passive opto-coupler topology in which the IU collects the optical signals from all RUs within the coverage area and couples it to an optical fiber for transmission to the CO. The passive opto-coupler is modelled a a linear and passive device which attenuates the optical input signals by the factor $\eta_{\text{OC}} < 1$.

OF link

The propagation loss in the OF is modelled as

$$g_{OF} = \exp(-\gamma_{OF} L_{OF}) \tag{4.12}$$

where γ_{OF} is the attenuation coefficient, and L_{OF} is the length of the OF link.

Another impairment for OF links is distortion due to nonlinearity from the Kerr-effect. The impact of fibre non-linearity can be well modelled using the *GN-model* (Poggiolini *et al.*, 2011) which has been used extensively in the literature for both the design and analysis of OF systems (El-Fiqi *et al.*, 2016; Poggiolini *et al.*, 2014; Shieh and Chen, 2011; Poggiolini *et al.*, 2012; Bosco *et al.*, 2012; Morra and Hranilovic, 2019; Morra *et al.*, 2017).

The interference due to fiber non-linearily is modelled as a Gaussian noise term, n_{NLI},

whose statistics depend on the power input to the fiber (El-Fiqi *et al.*, 2016; Poggiolini *et al.*, 2011, 2014, 2012). The power spectral density of this noise term is nearly flat so it is assumed to be locally white per channel band (Poggiolini *et al.*, 2011), (Poggiolini *et al.*, 2014). Thus, the received optical signal at the front end of the CO is

$$y_{OF} = \sqrt{\eta_{OC} y_{\text{R2opt}} g_{OF}} + n_{\text{NLI}} \tag{4.13}$$

The non-linear interference term is generally complex $n_{\text{NLI}} = n_{\text{NLI,R}} + j n_{\text{NLI,I}}$. The real and imaginary components of the noise have equal variances of $P_{\text{NLI}}/2$ where P_{NLI} is given by (El-Fiqi *et al.*, 2016; Poggiolini *et al.*, 2011, 2014; Shieh and Chen, 2011; Poggiolini *et al.*, 2012; Bosco *et al.*, 2012)

$$P_{\text{NLI}} = \frac{\gamma_{\text{nl}}^2}{\pi \left|\beta\right|} \frac{L_{\text{eff}}^2}{L_{\text{eff,a}}} \frac{P_{\text{inOF}}^3}{B_{\text{ch}}^3} \text{arcsinh}\left(\frac{3}{8}\pi^2 L_{\text{eff,a}} \left|\beta\right| B_w^2\right) B_{\text{RU}} \tag{4.14}$$

where $L_{\text{eff}} = (1 - e^{-2\gamma_{\text{OF}} L_{\text{OF}}})/2\gamma_{\text{OF}}$ and $L_{\text{eff,a}} = 1/2\gamma_{\text{OF}}$ are the effective and asymptomatic-effective fiber lengths. P_{inOF} is the input power at the optical fiber's front end. $B_w = B_{\text{ch}} N_{\text{ch}}$ is the total bandwidth, where N_{ch} is the number of wavelength-division multiplexing (WDM) channels and B_{ch} is the WDM channel's bandwidth while B_{RU} is the bandwidth dedicated to each RU. β is the group velocity dispersion. $\gamma_{\text{nl}} = 2\pi n/\lambda A_{\text{eff}}$ denotes the fiber non-linearity coefficient, where n is the nonlinear index coefficient, λ is the laser wavelength, and A_{eff} is the core effective area.

Then, as shown in Fig. 4.1 (bottom), the optical signal from the fiber is detected and

converted into the electrical domain. The received electrical signal is

$$\begin{aligned} y_{\text{R2,D}} &= \eta_{\text{OF}} |y_{\text{OF}}|^2 + n_D \\ &= \eta_{\text{OC}} g_{\text{OF}} \eta_{\text{OF}} y_{\text{R2opt}} + n_{\text{beat}} + n^2_{\text{NLI,R}} + n^2_{\text{NLI,I}} + n_D \end{aligned} \tag{4.15}$$

where

$$n_{\text{beat}} = 2\sqrt{\eta_{\text{OC}} y_{\text{R2opt}} g_{\text{OF}}} n_{\text{NLI,R}} \tag{4.16}$$

and n_D is Gaussian noise at the receiver with variance σ^2_D. It can also be shown that the total variance of the non-linear interference terms $n^2_{\text{NLI,R}} + n^2_{\text{NLI,I}}$ is P^2_{NLI}.

Non-linear Interference Calculations

The term P_{inOF} in (4.14) depends on the number and locations of the RUs transmitting optical signals to the IU which are then coupled to the fiber. Each RU contributes to the total optical input power in the OF. Thus, the larger the coverage area, the more RUs are included resulting in higher received optical power at the IU and greater non-linear distortion in the fiber. Notice that

$$P_{\text{inOF}} = P_{\text{near}} + P_{\text{far}} \tag{4.17}$$

were P_{near} and P_{far} are the instantaneous optical powers collected by the IU from Υ_{near} and Υ_{far} respectively.

The continuous approximation defined in (4.1) can be used to estimate P_{near} and P_{far} by replacing sums over RUs with integrals over the the coverage area. In particular, P_{near} can

be computed as

$$P_{\text{near}} = R \int_0^{2\pi} \int_0^{r_{\min}} P_{\text{opt}} g_l(r) g_d(r) g_a(r) g_p(r) \eta_{\text{OC}} \, r \mathrm{d}r \mathrm{d}\theta \tag{4.18}$$

$$= \int_0^{r_{\min}} 2\pi r R P_{\text{opt}} \eta_{\text{OC}} \frac{D_{\text{rx}}^2}{\theta_{\text{tx}}^2 r_{\min}^2} e^{-\gamma_{\text{FSO}} r_{\min}} g_a(r) \mathrm{d}r \tag{4.19}$$

$$\approx \pi r_{\min}^2 R P_{\text{opt}} \eta_{\text{OC}} \frac{D_{\text{rx}}^2}{\theta_{\text{tx}}^2 r_{\min}^2} e^{-\gamma_{\text{FSO}} r_{\min}} g_a(d) \tag{4.20}$$

Equation (4.18) arises due to the application of the continuous approximation in (4.1) where the sum of received optical powers from RUs in Υ_{near}, i.e., $y_{R2_{\text{opt}}}$ in (4.6), is replaced by an integral over Υ_{near} (see Fig. 4.2). In (4.19), the outer integral over angle θ is easily computed due to the circular symmetry of the problem. As discussed in Sec. 4.2.2, the transmitted average optical power of all RUs in Υ_{near} are scaled so that the received power at the IU of each is the same, i.e., $P_r = P_{r_{\min}}$. Thus, for RUs in Υ_{near}, $g_d(r) = g_d(r_{\min})$ and $g_l(r) = g_l(r_{\min})$. Additionally, $g_p(r) = 1$ for tractability. The atmospheric scintillation, $g_a(r)$, is a lognormal random variable with mean 1 and variance increasing with the range r. The sum of many independent but not identically distributed log-normal random variables is difficult to handle in practice, and in (4.20) the integral is evaluated by assuming $g_a(r) = g_a(d)$, In other words, the g_a for all RUs in Υ_{near} is assumed to be the same as the one with the largest variance, i.e., the furthest RU in the network. This approximation is made to allow for a tractable network design. In the Appendix a comparison of outage of the fronthaul link with and without this assumption are shown to be nearly identical.

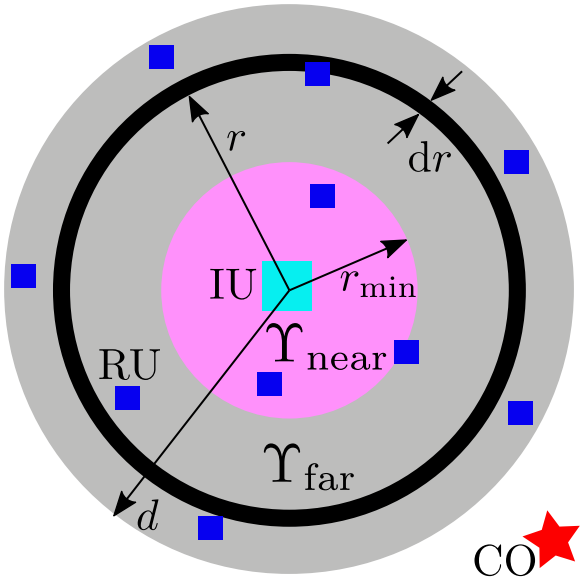

Figure 4.2: Power calculations over different regions.

Similarly, P_{far} can be computed using the continuous approximation as

$$\begin{aligned} P_{\text{far}} &= R \int_0^{2\pi} \int_{r_{\min}}^{d} P_{\text{opt}} g_l(r) g_d(r) g_a(r) g_p(r) \eta_{\text{OC}} \, r \mathrm{d}r \mathrm{d}\theta \\ &\approx 2\pi R P_{\text{opt}} \eta_{\text{OC}} g_a(d) \frac{D_{\text{rx}}^2}{\theta_{\text{tx}}^2} \left(\text{Ei}\left(-\gamma_{\text{FSO}} d\right) - \text{Ei}\left(-\gamma_{\text{FSO}} r_{\min}\right) \right) \end{aligned} \tag{4.21}$$

where (4.21) arises following the same assumptions taken in (4.19) and (4.20) and Ei is the exponential integral $\text{Ei}(x) = \int_{-\infty}^{x} \frac{e^t}{t} \mathrm{d}t$ (Gradshteyn and Ryzhik, 2007).

Substituting (4.20) and (4.21) into (4.17) and (4.14) yields

$$P_{\text{NLI}} = c_1 g_a(d)^3 \left(c_2 \left(\text{Ei}\left(-\gamma_{\text{FSO}} d\right) - \text{Ei}\left(-\gamma_{\text{FSO}} r_{\min}\right) \right) + c_3 \right)^3 \tag{4.22}$$

where $c_1 = \frac{\gamma_{nl}^2}{\pi |\beta|} \frac{L_{eff}^2}{L_{eff,a} B_{\text{ch}}^3} \text{arcsinh}\left(\frac{3}{8} \pi^2 L_{eff,a} |\beta| B_w^2 \right) B_{RU}$, $c_2 = 2\pi R P_{\text{opt}} \eta_{\text{OC}} \frac{D_{\text{rx}}^2}{\theta_{\text{tx}}^2}$, and $c_3 = \pi R P_{\text{opt}} \eta_{\text{OC}} \frac{D_{\text{rx}}^2}{\theta_{\text{tx}}^2} e^{-\gamma_{\text{FSO}} r_{\min}}$.

4.3 Problem Formulation

In this section, the outage probability for the RU which is furthest from the IU (i.e., at $r = d$) is taken as a metric of system performance. The RUs at $r = d$ are a worst case and have the highest FSO channel attenuation while other RUs that are closer to the IU (i.e., $r < d$) have a lower outage probability. Using the derived outage probability, a closed form expression of the RoFSO gain which minimizes the outage probability is derived.

4.3.1 SNR of the Fronthaul Network

Let $\text{SNR}_{\text{FH}}(d)$ denote the signal-to-noise ratio of fronthaul network for the furthest RU (i.e., at $r = d$) considering the impacts of clipping noise at the RoFSO unit, fiber-nonlinear interference terms in the OF link, and thermal noise at the receiver. Specifically, following Fig. 4.1, SNR_{FH} is the overall signal to noise ratio from the collected radio signal $y_{S,R1}$ (with power P_{RF}) to the received signal $y_{R2,D}$ defined in (4.15)

$$\text{SNR}_{\text{FH}}(d) = \frac{P_{\text{RF}} K^2 G^2 \eta_{\text{OC}}^2 \eta_{\text{OF}}^2 g_{\text{FSO}}^2(d) g_{\text{OF}}^2}{\sigma_c^2 \eta_{\text{OC}}^2 \eta_{\text{OF}}^2 g_{\text{FSO}}^2(d) g_{\text{OF}}^2 + P_{\text{NLI}}^2 + P_{\text{beat}} + \sigma_D^2} \tag{4.23}$$

where P_{NLI}^2 and P_{beat} represent the variance of the interference terms due to OF nonlinearity defined in (4.15). In most practical cases of interest to the CRAN scenario considered here (i.e., moderate to short fibre length), $P_{\text{NLI}}^2 \ll P_{\text{beat}}$. As discussed in (Morra and Hranilovic, 2019; Morra *et al.*, 2017), in these scenarios P_{NLI}^2 can be several orders of magnitude smaller than P_{beat} and is omitted in the following analysis. From (4.16), P_{beat} will depend on the instantaneous optical power in the fiber. As an upper bound, a worst case for P_{beat} is used by fixing y_{R2opt} at its maximum amplitude amplitude of $2P_{\text{opt}} g_{\text{FSO}}(d)$. From

(Morra *et al.*, 2017), the power of the beating interference can be written as

$$P_{\text{beat}} \leq 4\eta_{\text{OF}}^2 \eta_{\text{OC}} P_{\text{opt}} c_1 g_l(d) g_d(d) g_a(d)^4 c_d^3 \tag{4.24}$$

where $c_d = c_2 \left(\text{Ei}\left(-\gamma_{\text{FSO}} d\right) - \text{Ei}\left(-\gamma_{\text{FSO}} r_{\min}\right)\right) + c_3$.

4.3.2 Fronthaul Outage Probability

An outage occurs when the $\text{SNR}_{\text{FH}}(d)$ drops below a threshold denoted γ_{th}, that is, the probability of outage is

$$P_{\text{out}}\left(\gamma_{\text{th}}\right) = \Pr\left(\text{SNR}_{\text{FH}}(d) < \gamma_{\text{th}}\right) \tag{4.25}$$

Applying the assumptions described above, the randomness in $\text{SNR}_{\text{FH}}(d)$ is due to $g_{\text{FSO}}(d)$ which scales the signal and clipping noise for the RU at d as well as P_{beat} for the network.

Simplifying (4.23) yields,

$$\text{SNR}_{\text{FH}}(d) = \frac{P_{\text{RF}} K^2 G^2}{\sigma_c^2 + \frac{P_{\text{beat}} + \sigma_D^2}{\eta_{\text{OC}}^2 \eta_{\text{OF}}^2 g_{\text{FSO}}^2 g_{\text{OF}}^2}} \tag{4.26}$$

and the outage probability

$$P_{\text{out}}\left(\gamma_{\text{th}}\right) = \Pr\left(\frac{P_{\text{RF}} K^2 G^2}{\sigma_c^2 + \frac{P_{\text{beat}} + \sigma_D^2}{\eta_{\text{OC}}^2 \eta_{\text{OF}}^2 g_{\text{FSO}}^2 g_{\text{OF}}^2}} < \gamma_{\text{th}}\right). \tag{4.27}$$

Rearranging gives

$$P_{\text{out}}\left(\gamma_{\text{th}}\right) = \Pr\left(\hat{g}_a^2 - \frac{c_4}{\alpha_B}\hat{g}_a + \sigma_D^2 > 0\right) \tag{4.28}$$

where

$$c_4 = \eta_{\text{OC}}^2 \eta_{\text{OF}}^2 g_{\text{OF}}^2 g_l^2 g_d^2 \left(\frac{P_{\text{RF}} K^2 G^2}{\gamma_{\text{th}}} - \sigma_c^2\right) \tag{4.29}$$

$\alpha_B = 8\eta_{\text{OF}}^2 \eta_{\text{OC}} P_{\text{opt}} c_1 g_l g_d c_d^3$ and $\hat{g}_a = g_a^2$.

Given that $g_a(d)$ is lognormal as defined in (4.10),

$$f_{\hat{g}_a}(\hat{g}_a) = \frac{1}{4\hat{g}_a\sqrt{2\pi{\sigma_d}^2}} \exp\left(-\frac{(\ln \hat{g}_a + 4{\sigma_d}^2)^2}{32{\sigma_d}^2}\right) \tag{4.30}$$

Further, the roots of the quadratic expression in (4.28) are defined as

$$r_{1,2} = \frac{1}{2}\left(\frac{c_4}{\alpha_B} \mp \sqrt{\frac{c_4^2}{\alpha_B^2} - 4\sigma_D^2}\right) \tag{4.31}$$

where $r_1 < r_2$. Notice that quadratic is less than zero in the interval $[r_1, r_2]$. Thus,

$$P_{\text{out}}(\gamma_{\text{th}}) = 1 - \int_{r_1}^{r_2} f_{\hat{g}_a}(\hat{g}_a)\, \mathrm{d}\hat{g}_a. \tag{4.32}$$

After change of variables and applying (Gradshteyn and Ryzhik, 2007, Eq. (3.322.1)),

$$P_{\text{out}}(\gamma_{\text{th}}) = 1 - \overbrace{\frac{1}{2}\text{erfc}\left(\frac{\sigma_d}{\sqrt{2}} + \frac{\ln r_1}{4\sqrt{2}\sigma_d}\right)}^{e_1} + \underbrace{\frac{1}{2}\text{erfc}\left(\frac{\sigma_d}{\sqrt{2}} + \frac{\ln r_2}{4\sqrt{2}\sigma_d}\right)}_{e_2} \tag{4.33}$$

where $\text{erfc}(\cdot)$ is the complementary error function.

4.3.3 Gain Optimization

The gain of the amplifier in the RoFSO unit, G, has an impact on both the signal and noise of the fronthaul network as seen in the SNR expression (4.23). Not only does G scale $y_{S,R1}$ but also to determines the amount of clipping noise power σ_c^2 as shown (4.4) and (4.5). Thus, G must be designed carefully to minimize $P_{\text{out}}(\gamma_{\text{th}})$ in (4.33).

The outage probability expression in (4.33) is a function of the roots r_1, r_2 which are in turn a function of G from (4.31) and (4.29). Notice that G gain appears explicitly in (4.29) as well as implicitly in the definitions of K and σ_c^2. To clarify the discussion, define $F(G)$ as

$$F(G) = \frac{P_{\text{RF}} K^2 G^2}{\gamma_{\text{th}}} - \sigma_c^2. \tag{4.34}$$

From (4.33), $P_{\text{out}}(\gamma_{\text{th}}) = 1 - e_1 + e_2$. Thus, minimizing $P_{\text{out}}(\gamma_{\text{th}})$ is equivalent to maximizing e_1 while minimizing e_2. Notice that both e_1 and e_2 are functions of r_1 and r_2 respectively which are additionally functions of $F(G)$. From (4.29) and (4.31), increasing $F(G)$ increases c_4 which monotonically decreases r_1 and increases r_2. Since erfc$(\cdot)$ is monotonically decreasing, maximizing $F(G)$ minimizes e_1 and maximizes e_2. Therefore, minimizing $P_{\text{out}}(\gamma_{\text{th}})$ is achieved by maximizing $F(G)$.

In order to maximize $F(G)$, substitute the definition of K (4.4) and σ_c^2 (4.5) into (4.34) to yield

$$F\left(q\frac{P_{\text{opt}}}{\sqrt{2P_{\text{RF}}}}\right) \quad = \quad P_{\text{opt}}^2\left(\frac{(2-\gamma_{\text{th}})q^2}{2\gamma_{\text{th}}}\epsilon^2(q) - 1 + \frac{qe^{-1/q^2}}{\sqrt{\pi}} + \epsilon(q)\left(1 - \frac{q^2}{2}\right)\right) \tag{4.35}$$

where $q = G\sqrt{2P_{\text{RF}}}/P_{\text{opt}}$ and $\epsilon(q) = \text{erf}\,(1/q)$. Differentiating with respect to q, equating to zero, and simplifying yields the expression

$$v\left(q\epsilon^2(q) + q^2\epsilon(q)\dot{\epsilon}(q)\right) + \frac{e^{-1/q^2}}{\sqrt{\pi}}\left(1 + \frac{2}{q^2}\right) + \dot{\epsilon}(q)\left(1 - \frac{q^2}{2}\right) - \epsilon(q)q \;=\; 0 \tag{4.36}$$

where $v = 1 + \frac{1}{\gamma_{\text{th}}}$ and $\dot{\epsilon}(q) = \frac{-2}{\sqrt{\pi}q^2}e^{-1/q^2}$.

In practice solving (4.36) is is difficult and approximate solutions can be obtained.

Consider the upper bound on erf$(\cdot)$ (Chiani *et al.*, 2003)

$$\text{erf}\left(\frac{1}{q}\right) \leq 1 - e^{-1/q^2} \tag{4.37}$$

which is tight for small q. In typical operation where severe clipping distortion is avoided, the value q will be small as P_{opt} (i.e., the clipping level) is larger than $G\sqrt{2P_{\text{RF}}}$ which is the standard deviation at the input of the clipper. This approximation is justified in the simulations in Sec. 4.4.4.

Substituting (4.37) into (4.36) gives

$$ve^{-2/q^2}\left(q + \frac{2}{\sqrt{\pi}}\right) + e^{-1/q^2}\left(q + 2 - 2v\left(q + \frac{4}{\sqrt{\pi}}\right)\right) + q\left(v - 1\right) = 0 \tag{4.38}$$

As discussed, in typical operation clipping is small and a reasonable assumption is $q \ll 1$. In this case, $e^{-2/q^2} \ll 1$ and the first term may be ignored. Also q in the second term may be ignored w.r.t. 2 and $\frac{4}{\sqrt{\pi}}$.

Simplifying (4.38) yields,

$$qe^{1/q^2} - \gamma_{\text{th}}\left(\frac{8}{\sqrt{\pi}}\left(1 + \frac{1}{\gamma_{\text{th}}}\right) - 2\right) = 0 \tag{4.39}$$

Notice that (4.39) can be written as

$$qe^{1/q^2} = u \tag{4.40}$$

where $u = \frac{8}{\sqrt{\pi}}\left(1 + \gamma_{\text{th}}\right) - 2\gamma_{\text{th}}$. Squaring both sides and rearranging the terms allows (4.40)

to be written in terms of the Lambert-W function (Corless *et al.*, 1996) $W(\cdot)$ as,

$$\frac{-2}{q^2} = W\left(\frac{-2}{u^2}\right). \tag{4.41}$$

Thus, using the approximations above, the solution of (4.39) is

$$q \approx i\sqrt{\frac{2}{W\left(-2/u^2\right)}} \tag{4.42}$$

Finally the optimum gain follows

$$G^* \approx \frac{iP_{\text{opt}}}{\sqrt{P_{\text{RF}}W\left(-2/u^2\right)}} \tag{4.43}$$

In the range of interest, the Lambert-W function is not one-to-one and has two values corresponding to its 2 "branches" conventionally termed W_0 and W_{-1} (Corless *et al.*, 1996). Thus, there are two approximate values for the optimum gain in (4.43) termed G_1^* and G_2^*. From the numerical simulations in Sec. 4.4, G_1^* and G_2^* are shown to approach the optimum gain but do not coincide due to the approximations made to make the problem tractable. The geometric mean

$$\hat{G}^* \approx \sqrt{G_1^* G_2^*} \tag{4.44}$$

is adopted as an approximation for the optimum gain and shown to be close in practice. A thorough comparison between G_1^*, G_2^*, and $\hat{G}^*$ is presented in Sec. 4.4. Furthermore, the heuristic solution obtained by (4.44) can be used as a starting point to numerically solve (4.38) using Newton's method. Such an approach is promising since the function in (4.38) is smooth and differentiable.

4.4 Simulation Results

This section applies the analytical results of Secs. 4.2 and 4.3 to illustrate a design framework for the all-optical fronthaul network shown in Fig. 4.1. Given the parameters of the network such as fibre span, density of users, reliability (i.e., P_{out}), the maximum coverage area is computed by optimizing the choice of transmitted optical power, P_{opt} and the RoFSO gain, G. Next, the sensitivity of the design to each of the parameters is investigated to provide guidance on how to choose and tune them. Simulation results for different weather conditions based on a year of weather measurements from two locations are provided to show how the outage probability and coverage area are impacted. The accuracy of the continuous approximation used in our analytical results is verified via simulations with discrete RUs with pointing error.

4.4.1 Simulation Setup

Table 4.1 contains the parameters used in subsequent simulations. In all cases, it is assumed that each RU serves 100 UEs in the access network with each UE experiences interference from 6 neighbors. The average received RF power at each RU is assumed to be identical. Nominal values for the parameters are given in the table, however, in subsequent sections these parameters will varied to determine the sensitivity of the design to their variation. The radius of the near area has a nominal value of $r_{\text{min}} = 50$ m, as described in Sec. 4.4.3, and the nominal density of RUs is set so that there is a single RU in Υ_{near}, i.e. $R = 1/\pi r_{\text{min}}^2$. Without loss of generality, $\gamma_{\text{th}} = 1$ for the results computed in this section. Unless stated otherwise, the nominal values listed in Table 4.1 are used in all subsequent simulations.

Table 4.1: Simulation Parameters

RF Parameters	
Number of UEs per RU	100
Number of interfering UEs	6
UE RF Power	23 dBm
RF Antenna Gain	20 dB
RoFSO Parameters	
Wavelength (λ)	1550 nm
Bandwidth (B_{RU})	1 GHz
Optical Transmitted Power (P_{opt})	25 dBm (nominal)
Near area radius (r_{min})	50 m (nominal)
RU density (R)	127.3 km^{-2}(nominal)
Opto-coupler Loss (η_{OC})	0.5
OF Parameters (Morra *et al.*, 2017)	
OF length (L_{OF})	5 km (nominal)
Thermal Noise Standard Deviation (σ_D)	10^{-7} A
Channel Bandwidth (B_{ch})	32 GHz
OF Attenuation Coefficient (γ_{OF})	0.22 dB/km
Nonlinearity Coefficient (γ_{nl})	1.3 W^{-1}km^{-1}
Weather Parameters (Clear, Rain, Snow, Fog) (Ahmed and Hranilovic, 2018)	
Toronto, FSO attenuation	$0.44, 0.523, 4.53, 50$ dB/km
Toronto, Weather Probability	$0.61, 0.174, 0.142, 0.072$
Newfoundland, FSO attenuation	$0.44, 0.66, 19.34, 100$ dB/km
Newfoundland, Weather Probability	$0.3234, 0.2488, 0.2, 0.23$

4.4.2 Network Planning Procedure

Fig. 4.3 shows the minimum P_{out} versus the density of RUs, R, and the coverage area radius, d. The colour map corresponds to the optimum optical power, P^*_{opt}, chosen for each combination of R and d which minimizes P_{out}. For each pair of R and d, a grid search over P_{opt} is performed to minimize P_{out}. Notice that for each value of P_{opt} considered, the optimum gain $\hat{G}^*$ is computed via (4.44) and (4.43).

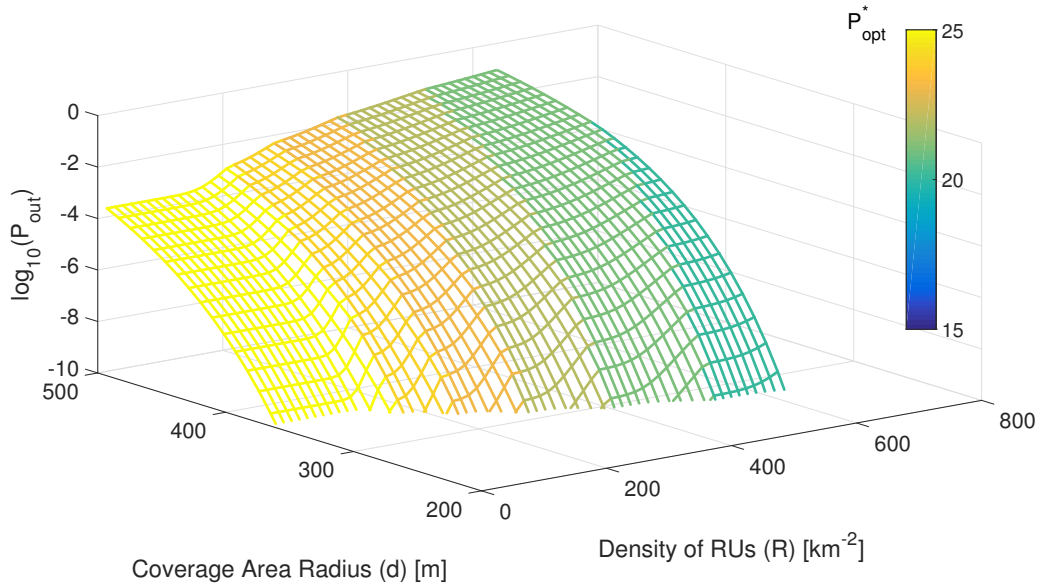

Figure 4.3: Minimum outage probability versus coverage area and RU density. The corresponding optimum optical power P^*_{opt} is indicated by the colour of the surface.

As shown in Fig. 4.3, for a given d increasing R increases P_{out} since more RUs contribute to the total collected optical power at the IU which triggers more severe fiber nonlinearity. Also, increasing d for a given R has a similar effect for the same reason and additionally suffers from increased RoFSO channel attenuation due to longer propagation distances. Notice that for a given d, P^*_{opt} decreases with R. This arises to balance the increase in nonlinear interference as the number of RUs increases. Sections 4.4.3 and 4.4.5 present more detailed discussions on the impact of changing d and R.

Figure 4.3 serves as a useful tool to aid in the design of a fronthaul network to provide coverage in a certain region. The maximum allowable outage probability is assumed to be provided as a design specification. Additionally, the density of UEs in a region will vary (e.g., urban versus sub-urban areas) and is also provided as an input to the design problem. Since each RU can serve a certain number of UEs, R is assumed to be directly proportional

to the density of users. From Fig. 4.3, for a given R and P_{out}, the size of the coverage area d can be found along with P^*_{opt} for each FSO fronthaul unit. Furthermore, the optimum gain can also evaluated using (4.43) as a function of the optical power P_{opt}, the received RF power P_{RF}, and the SNR threshold γ_{th}. Thus, results in this section provide guidance on choosing the overall parameters for the network while the following sections provide more insights on the tradeoffs inherent in selecting each of those parameters.

4.4.3 Near-Far Problem and Fibre Length

In this subsection, the impact of increasing the coverage area, d, on the outage probability (4.33) is investigated for a fixed R. In general, as d increases more RUs are included in the network and hence more optical power is received and coupled into the optical fiber increasing the non-linear interference. In addition, increasing d increases the length of the furthest RoFSO link further degrading performance.

Figure 4.4 presents the variation of P_{out} with d for a variety of P_{opt} values and $r_{\text{min}} \to 0$. Notice that P_{out} is not monotonic in P_{opt}. For small P_{opt}, increasing the optical power decreases clipping noise which in return allows for higher levels of signal power to be transmitted without significant clipping distortion. As P_{opt} increases, fiber non-linearity dominates resulting in a degradation in P_{out} with increasing P_{opt}. The nonlinear distortion in the fiber is dominated by the optical powers transmitted by RUs near the IU. In Fig. 4.5, the same scenario is considered with $r_{\text{min}} = 50$ m. Notice that P_{out} improves with P_{opt} for the range of powers considered. Furthermore, for a given P_{opt}, a larger coverage area d is attainable for $r_{\text{min}} = 50$ m rather than $r_{\text{min}} \to 0$. The scaling of the powers for RUs inside Υ_{near} decreases the overall impact of non-linearity in the fiber and results in a lower overall fronthaul outage probability.

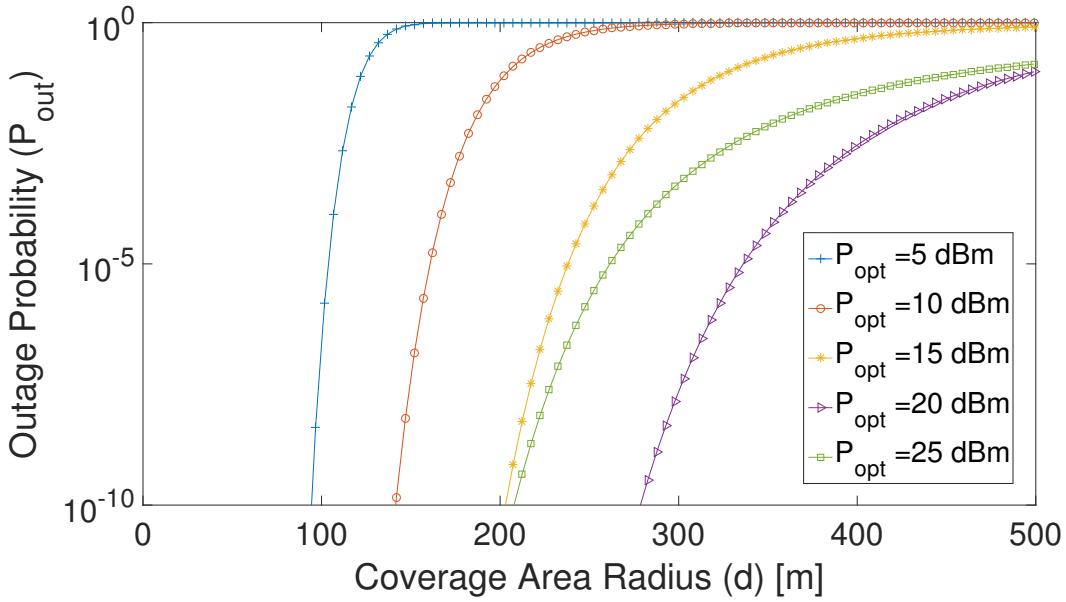

Figure 4.4: Outage probability versus coverage area with $r_{\text{min}} \to 0$.

Thus, r_{min} must be selected to carefully balance the opposing constraints of nonlinear distortion and high P_{opt}. One method to select r_{min} is to ensure that $P_{r_{\text{min}}}$ equals the receiver sensitivity even under severe weather conditions. Another method is to consider a maximum allowable total received power under clear weather conditions which in return limits the interference inside the OF.

A similar analysis is performed in Fig. 4.6, where the effect of increasing the optical fiber length, L_{OF} is explored. Notice that the effect of fiber non-linearity becomes more severe as the length of the OF increases (as apparent from (4.14)). The performance is particularly impacted when $L_{\text{OF}} > 5$ km. Thus, when planning the network, the location of the CO and hence the length of the optical fiber also constrains the maximum coverage area for a given P_{out}.

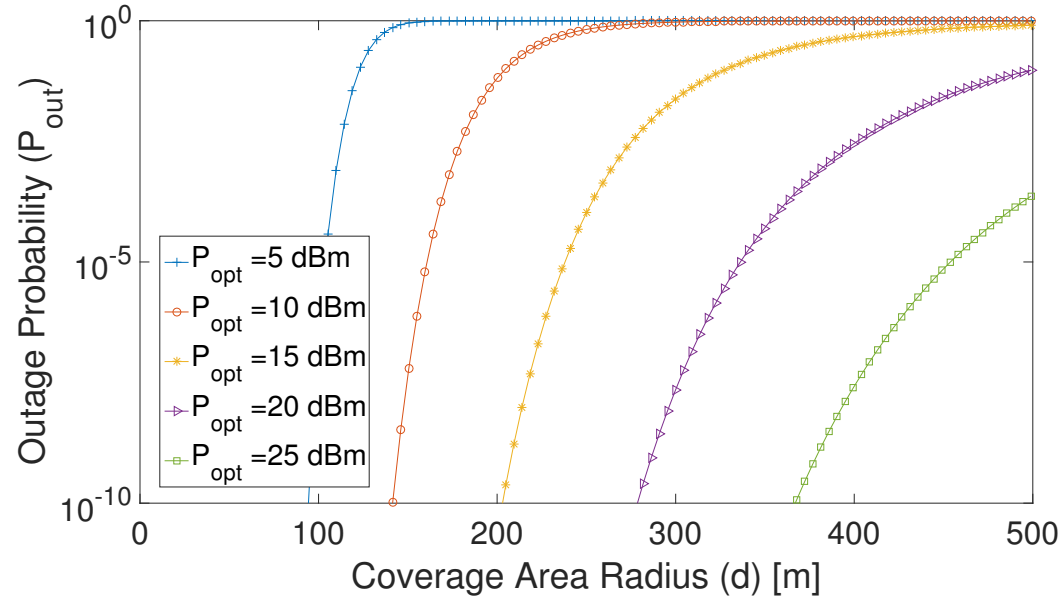

Figure 4.5: Outage probability versus coverage area with $r_{\min} = 50$ m.

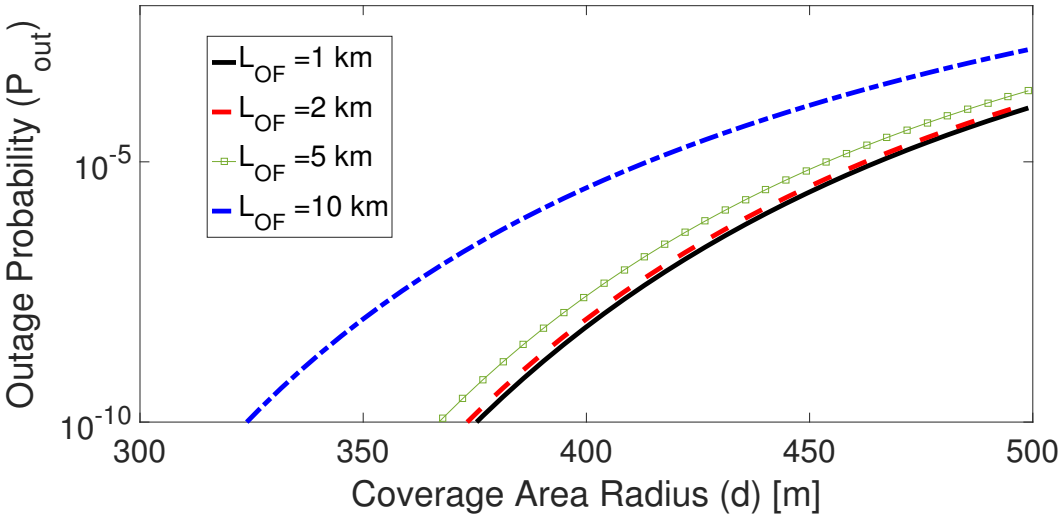

Figure 4.6: Outage probability versus coverage area, $r_{\min} = 50$ m and $R = 1/\pi r_{\min}^2$.

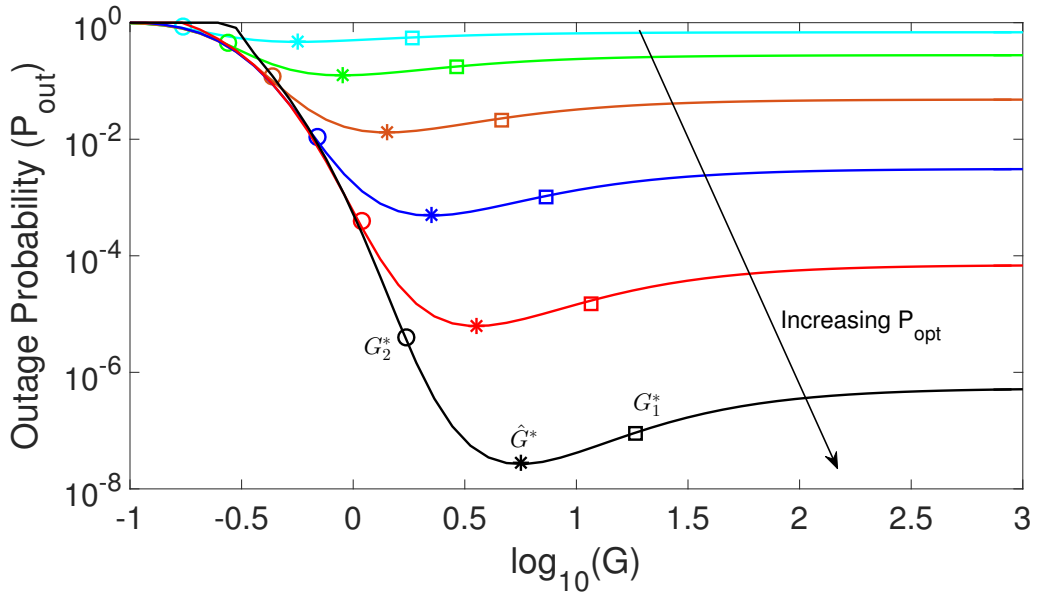

Figure 4.7: Outage probability versus RoFSO gain G for $d = 400$ m and $P_{\text{opt}} \in \{15, 17, 19, 21, 23, 25\}$ dBm. (all other values nominal)

4.4.4 Gain Optimization

Figure 4.7 plots P_{out}, computed via (4.33), versus the selection of G for a fixed d and R and a variety of P_{opt} values. Additionally, the estimates for optimum gain (4.44) and (4.43) are also plotted for each case.

Notice that P_{out} is sensitive to the selection of G. For example, for $P_{\text{opt}} = 25$ dBm, in Fig. 4.7, P_{out} varies up to six orders of magnitude with G. The analytical approximation for the optimum gain obtained by (4.43), denoted G_1^* and G_2^*, approach the optimum point found via grid search, while $\hat{G}^*$ (4.44) is close to the optimum gain. In the case of $P_{\text{opt}} = 25$ dBm, in Fig. 4.7, the analytical approximation $\hat{G}^*$ is only 0.2 dB away from the optimal gain found via grid search. Notice that increasing P_{opt} allows for less clipping of the forwarded RoFSO signal. Thus, the optimum gain increases with P_{opt} leading to more signal amplification, higher SNR, and hence lower outage P_{out}.

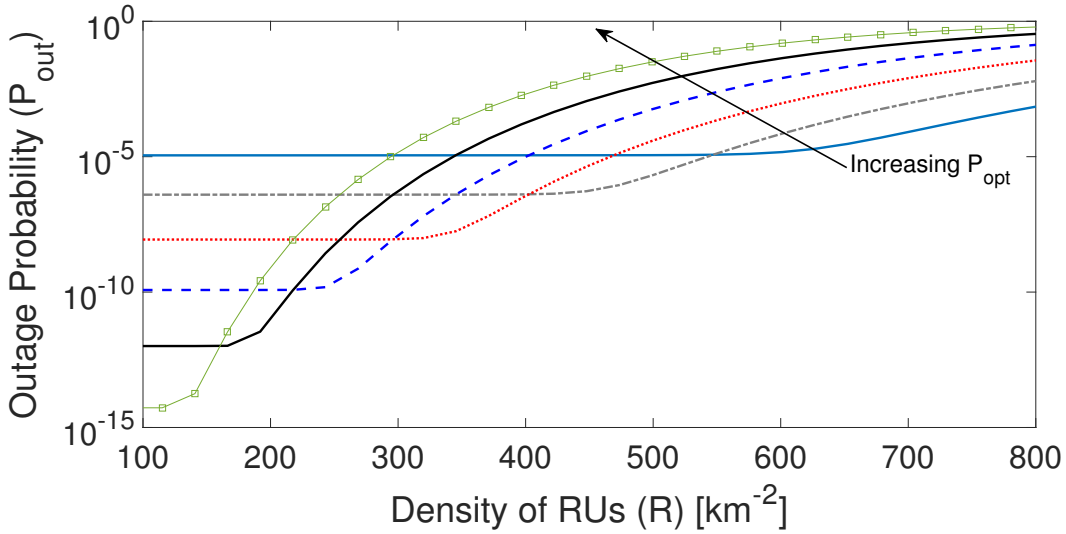

Figure 4.8: Outage probability versus density of RUs for $d = 300$ m and $P_{\text{opt}} \in \{20, 21, 22, 23, 24, 25\}$ dBm. (all other values nominal)

4.4.5 Density of RUs

As shown in Sec. 4.4.2, increasing the density of RUs results in the inclusion of more RUs which in turn increases the input optical power to the fiber and triggers more non-linear interference. In this subsection, P_{out} peformance is investigated with varying R for a given d and several values of P_{opt} .

While P_{out} is monotonically increasing in R, it may increase or decrease with P_{opt} depending on R and whether the clipping noise or the non-linear interference is dominant. Qualitatively, at low RU density, the amount of collected optical power at the IU is relatively small and does not trigger severe non-linear interference. Thus, increasing P_{opt} leads to less clipping, higher transmitted signal powers, and hence lower outage. This can be seen on the left part of Fig. 4.8, i.e. at low R. On the other hand, at high R, there is more optical power at the IU and thus high the non-linear interference becomes dominant. Thus at high values of R, counterintuitively, lower values of P_{opt} result in lower P_{out} and better overall

performance as seen in the right part of Fig. 4.8.

Notice also that the optimum optical power P^*_{opt} which minimizes P_{out}, can be obtained from the lower envelope of the set of curves in Fig. 4.8. As shown in Fig. 4.8, the optimum optical power P^*_{opt} decreases as R increases. This is also shown in Fig. 4.3 since, at fixed d, as R increases the colormap changes indicating a lower P^*_{opt}.

4.4.6 Impact of Weather

The impact of weather is of critical importance to any free-space optical system. In particular, the reliability of a fronthaul network will also be determined by the likelihood of severe atmospheric attention due to a fog event.

Following a similar approach to (Ahmed and Hranilovic, 2018), weather conditions for two locations are quantized into four main cases: clear, rain, snow, and fog. The relative frequency for each weather condition is obtained from a year of hourly weather data measured at the airports in Toronto and Newfoundland, Canada. For each weather condition, the FSO parameters g_l (4.8) and C_n^2 in (4.10) are selected using different modelling approaches which depend on weather conditions (e.g., rates of rain and snow fall) as described in (Ahmed and Hranilovic, 2018). The overall outage probability over weather conditions can be expressed as

$$\begin{aligned} P_{\text{out}}\left(\gamma_{\text{th}}\right) = &\Pr\left(\text{SNR}_{\text{FH}} < \gamma_{\text{th}} | \text{clear}\right) \cdot \Pr\left(\text{clear}\right) + \Pr\left(\text{SNR}_{\text{FH}} < \gamma_{\text{th}} | \text{rain}\right) \cdot \Pr\left(\text{rain}\right) \\ &+ \Pr\left(\text{SNR}_{\text{FH}} < \gamma_{\text{th}} | \text{snow}\right) \cdot \Pr\left(\text{snow}\right) + \Pr\left(\text{SNR}_{\text{FH}} < \gamma_{\text{th}} | \text{fog}\right) \cdot \Pr\left(\text{fog}\right). \quad (4.45) \end{aligned}$$

Figures 4.9 and 4.10 present the outage probability versus d with other parameters fixed at nominal values. The P_{out} for each weather condition is plotted as well as the results for

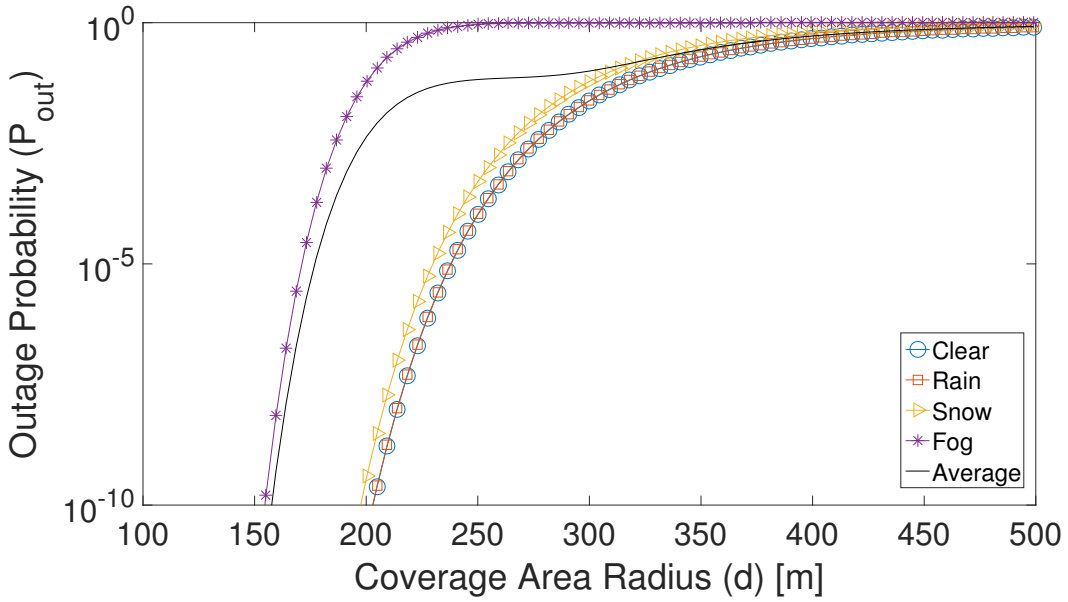

Figure 4.9: Outage probability over different weather conditions, Toronto, Canada.

the overall outage computed in (4.45). Newfoundland is known to be one of the foggiest locations in Canada, while Toronto has less fog events and has a continental weather pattern. From a network planning perspective, the main conclusion from Figs. 4.9 and 4.10 is that regardless of the frequency of fog events, the outage probability is dominated by the performance of the fronthaul network during a fog event. The figures clear show that asymptotically for low P_{out}, that the P_{out} averaged over weather conditions (4.45) approaches $\Pr\left(\text{SNR}_{\text{FH}} < \gamma_{\text{th}} | \text{fog}\right)$. This applies both to cases when the fog is frequent, e.g. 23% of the year in Newfoundland , and also when it not as frequent, e.g. 7% of the year in Toronto. Thus, for a conservative fronthaul design, fog weather conditions should be considered as a worst case scenario since this scenario dominates the average performance over the year.

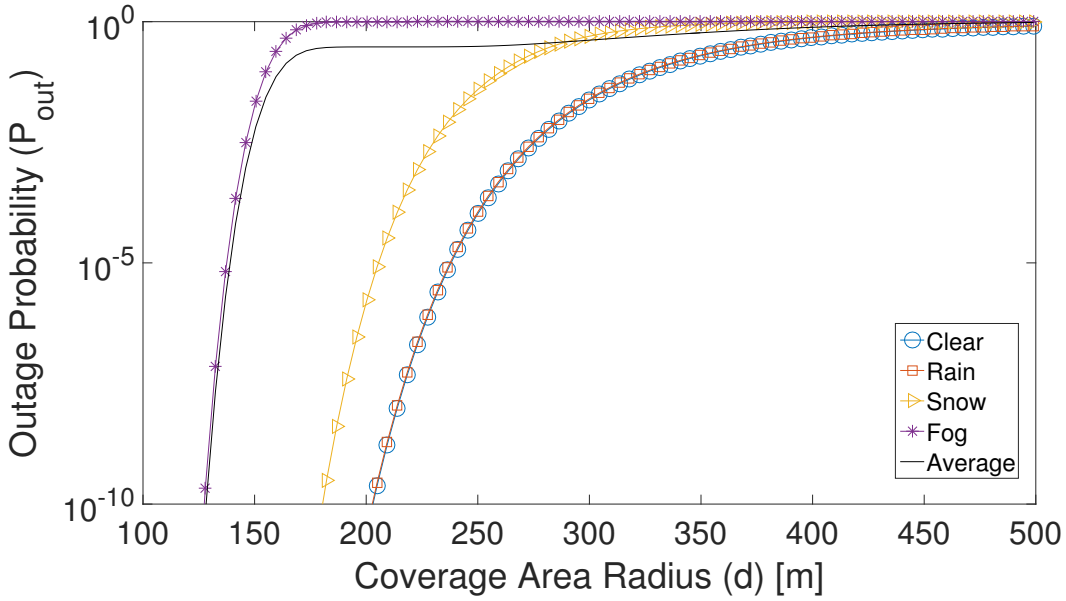

Figure 4.10: Outage probability over different weather conditions, Newfoundland, Canada.

4.4.7 Numerical Simulation: Discrete RUs, Pointing Errors, n^2_{NLI}

In this part, numerical simulations are performed to validate the performance of the designed fronthaul network under more exhaustive and realistic conditions.

Rather than assuming a sea of RUs spread over the coverage area, discrete RUs at specific locations are considered while maintaining a nominal RU density of $R = 127.3\,\text{km}^{-2}$. The received optical power from each RU is calculated, the total optical power input to the OF is obtained and the resulting non-linear interference terms are computed. The beating term, the n^2_{NLI} term and the detector thermal noise are all considered. In addition, although not considered explicitly in the design, the impact of pointing error considered in cases of low, moderate ($\Gamma = 7$), and severe pointing error ($\Gamma = 3$).

Fig. 4.11 plots P_{out} versus the coverage area radius d to compare to the analytical results which were derived using the continuous approximation, no pointing error and ignoring

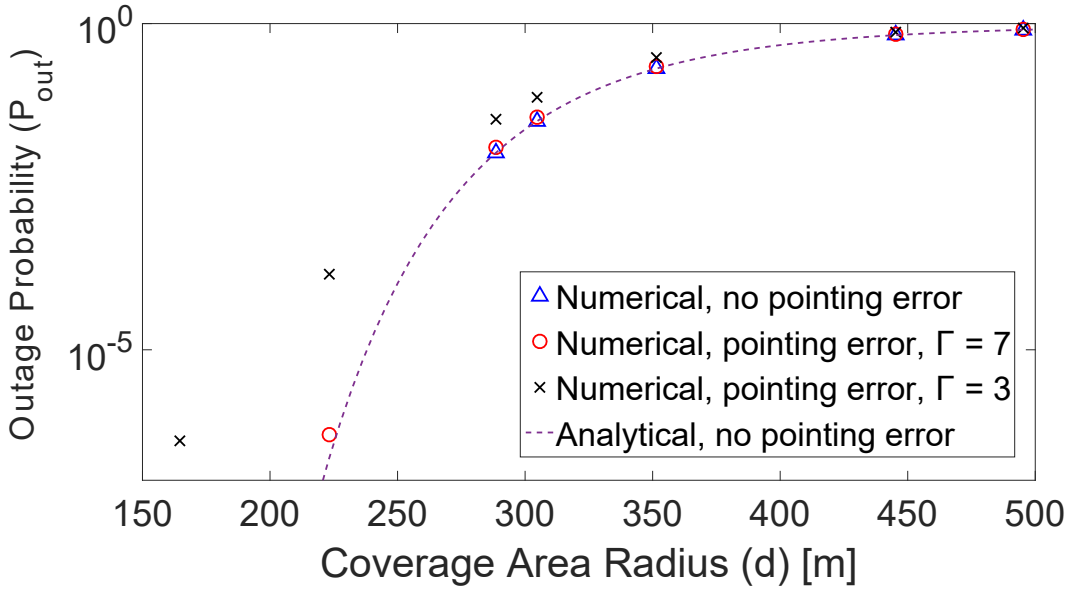

Figure 4.11: Numerical results of the outage probability with and without pointing errors, $P_{\text{opt}} = 15$ dBm.

n^2_{NLI}. The outage probability is estimated by generating 10^7 random realizations of the channel which includes FSO fading, misalignment as fibre nonlinear distortion.

Figure 4.11 shows that both analytical and numerical results are nearly identical for the case with no pointing error. This validates the use of the continuous approximation and also demonstrates that the impact of the n^2_{NLI} term is insignificant for the fronthaul design for the given scenario. The performance of the designed fronthaul network does not change greatly under moderate misalignment due to the short ranges of the RoFSO links. However, at higher misalignment values, the outage probability performance is significantly degraded.

4.5 Conclusion

In this paper, a novel passive all-optical fronthaul topology for C-RAN is presented along with tools to plan an uplink network. Design parameters such as the radius of the coverage area, the RU density, the optical fiber length, the optimum gain, and the optimum FSO power were investigated showing their effect on the performance of the system. An analytical expression for the optimum gain was obtained that balances the effect of the signal amplification versus clipping noise distortion leading to the minimization of the outage probability. Different channel impairments were considered including the clipping distortion, the effect of weather conditions, and fiber non-linearity, and the pointing error. Simulation results show that the outage probability increases with the the radius of the coverage area and the density of RUs. The results also shows that a careful design of the gain and the optical power values should be done to maximize the system reliability.

Future work includes extending our analytical work to more explicitly include the impact of pointing errors which may be important in scenarios with severe misalignment.

4.A Appendix

In Sec. 4.2.5 in order to make the non-linear power calculations tractable the fading value of $g_a(d)$ for the furthest RU was used for all RUs to calculate the nonlinear interference. In this appendix, the distribution of SNR_{FH} is plotted for nominal network values given in Table 4.1 using (4.26) as well as using a Monte Carlo simulation considering discrete RUs with independent $g_a(r)$ distributed as in (4.10).

The value of P_{out} is estimated from (4.26) using 10^8 random samples for 3 different levels of optical power. Notice that P_{inOF} relies on the approximation in (4.20) and (4.21)

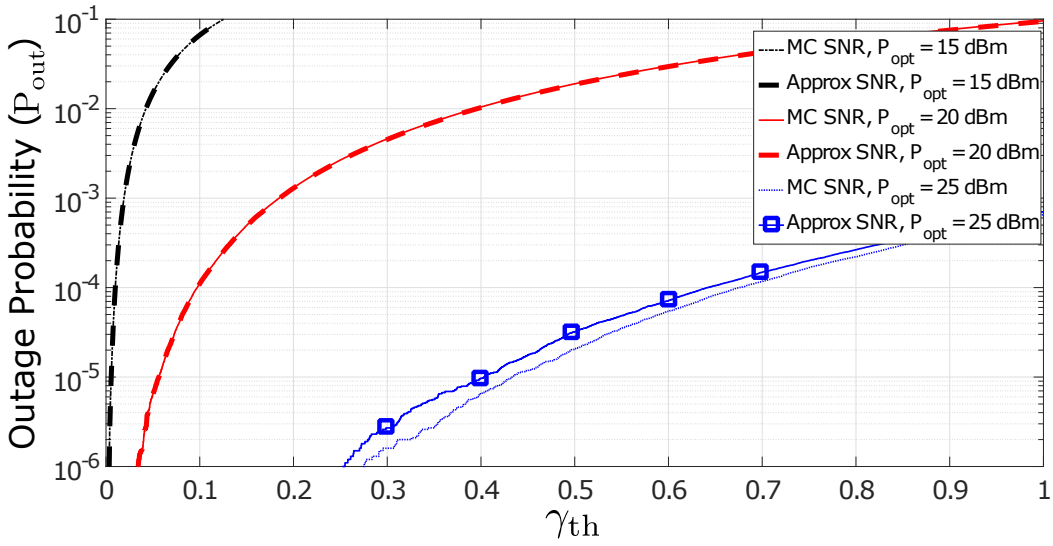

Figure 4.12: Outage probability computed using (4.26) ('Approx SNR') as well as a Monte Carlo simulation using complete SNR ('MC SNR').

as well as the continuous approximation. In another numerical simulation, discrete RUs are randomly placed inside the coverage area at the nominal density and 10^8 random realizations of P_{near} and P_{far} are computed without the simplifying assumption nor the continuous approximation as

$$P_{\text{inOF}} = \sum_{\Omega \in \Upsilon_{\text{near}}} P_{\text{opt}} g_l(r_{\min}) g_d(r_{\min}) g_a(r) \eta_{\text{OC}} + \sum_{\Omega \in \Upsilon_{\text{far}}} P_{\text{opt}} g_l(r) g_d(r) g_a(r) \eta_{\text{OC}}$$

Figure 4.12 shows P_{out} from (4.26) and from Monte Carlo (MC) simulation. For all P_{opt} the two CDFs nearly coincide even at low SNRs. Notice that the approximation is conservative as it uses the fading with the highest variance for all RUs. In all cases, P_{out} from (4.26) is an upper bound on the MC results.

Chapter 5

Conclusions

5.1 Summary

For the first time, this thesis considered RoFSO in conjunction with both RF and RoF fronthaul links in a CRAN. Unlike previous work, the work in this thesis modelled and designed the clipping distortion caused by the finite dynamic range of the laser devices in analog RoFSO and RoF links. Novel performance optimization tools were provided for various CRAN architectures to maximize the sum of weighted UE rates in RF/RoFSO CRAN and minimize the fronthaul outage in RoFSO/RoF CRAN. The work in this thesis not only considered the design of the links, but also introduced a network planning framework that provides design tools and guidance on choosing a set of network parameters. Additionally, for a cost-efficient CRAN architecture, the work in this thesis considered analog radio units which do not require digitization hardware. Furthermore, a passive analog all-optical fronthaul link was considered in this work for further simplification and cost and energy-consumption reduction. A detailed description of the work is as follows:

Chapter 2 included a joint optimization tool for mixed RF/RoFSO fronthaul links.

The objective of the optimization problem is to maximize a weighted sum of UE rates. Maximizing UE rates is the first part of the rate-range-reliability trade-off discussed in Sec. 1.4. The problem was solved by designing the quantization noise of the digital decode-and-forward RF links and the amplifier gains of the amplify-and-forward RoFSO links. The clipping distortion in the analog RoFSO links was included using a Bussgang model of the clipper. Despite those distortions, significant gains can still be obtained by a careful design of the RoFSO fronthaul links. This design tool is particularly useful for rate maximization while maintaining a long-term fairness between UEs. It provides guidance on designing different CRAN architectures with all-RF fronthul links, mixed RF/RoFSO fronthaul links, or all-RoFSO fronthaul links.

The advantages of the RoFSO links, in favorable weather conditions as illustrated in **Chapter** 2, motivated the work in **Chapter** 3 in which an all-optical fronthaul C-RAN was considered. While the work in **Chapter** 2 studied a single-hop fronthaul network, **Chapter** 3 looked at a CRAN with two-hop RoFSO/RoF fronthaul links. The nonlinearities of both the RoFSO and RoF links were included in the analyses and the design. The reliability, Sec. 1.4, was addressed by evaluating and optimizing the outage probability by designing the average optical power in the OF. Furthermore, analytical derivations of the average bit-error rate and the CDF of user rates were derived.

In **Chapter** 4, the outage probability of a passive all-optical fronthaul network was investigated from a network planning perspective. Both the nonlinearities of the RoFSO and RoF links were included in the analyses. Different system parameters such as the coverage area, the RU density, RoFSO gain, and the optical power were included in the fronthaul outage derivation. An analytical approximation of the optimum gain was derived and various network planning tools were provided. The results in **Chapter** 4 provide guidance on

network planning from reliability perspective.

5.2 Conclusions

The work in this thesis included various architectures of C-RAN fronthaul links and considered different metrics to evaluate their performance. Several observations and insights are obtained from each scenario. Firstly, for mixed RF/RoFSO fronthauling, the RoFSO links are shown to improve the data rates significantly. For example, replacing one RF link by a RoFSO link increases the 50th percentile of the CDF of end user rates by 7 times. Furthermore, for an all-RF fronthaul network with capacity $C_o = 21$ Mbps, replacing 4 RF links by RoFSO links achieves the same 50th percentile rates as if the RF capacity is increased by 27.6 times. Replacing more RF links by RoFSO links improves the average user rates except under severe weather conditions of dense fog where the RoFSO links are highly degraded and the average rates may decrease accordingly.

Secondly, for an all-optical active RoFSO/RoF fronthauling with fixed gain, the nonlinear interference in the RoF link can impact the reliability of the system severely. Thus, a careful design of the average transmitted optical power is required to balance the effect of fiber nonlinearity. The optimal average RoF optical power is shown to improve both the reliability and the CDF of user rates. For example, under favorable weather conditions, the 50th percentile of UE rates using mm-wave access network exceeds 1.5 Gbps.

Thirdly, for an all-optical passive fronthauling, tuning different system parameters affects the fronthaul outage probability in various ways. Increasing the radius of the coverage area, i.e. the maximum length of the FSO link, degrades the RoFSO channel which degrades the reliability of the link. Also, increasing the density of RUs increases the amount of received optical power which in turn triggers more nonlinear interference in the fiber.

Furthermore, the RoFSO gain must be selected in a way that balances the clipping distortion with signal amplification.

5.3 Future work

The work in this thesis covered different problems in several scenarios with various architectures, however, there are other directions for extending this work. The suggested extensions are categorized as follows:

1. **Architecture:** This work considered different architectures of CRANs with a variety of fronthaul links. **Chapter** 2 looked at the joint design of a CRAN with single-hop mixed RF/RoFSO fronthaul links. **Chapter** 3 and **Chapter** 4 considered a CRAN with two-hop hybrid RoFSO/RoF fronthauling. The next step of this hierarchy is to investigate multi-hop RoFSO fornthauling. This architecture triggers many research problems. Firstly, the network planning becomes more challenging with the added relaying nodes in the fronthaul network. Secondly, choosing the optimum signal path through different relaying nodes is another interesting problem. Thirdly, the clipping distortion has to be designed at each of the relaying nodes which increases the dimensions of the design problem. Fourthly, the evaluation of the over-all system performance while considering the cascaded channels in the RF access network and RoFSO nodes can be mathematically challenging.

2. **Network planning:** The outage probability derived in **Chapter** 4 included multiple design parameters such as the radius of the coverage area, the density of RUs, the transmitted optical power, the RoFSO gain, and the length of the OF. Each of those parameters can be addressed in a separate problem and optimal value may be derived

based on the formulation of the problem and the constraints implied by the system.

3. **Other performance metrics:** The work in this thesis considered a number of performance metrics such as the data rates, **Chapter** 2, the average BER, **Chapter** 3, and the outage probability, **Chapter** 3 and **Chapter** 4. However, there are other performance metrics that can be used to quantify the quality of service and the performance of the CRAN. For example, future work may include evaluating and optimizing latency, cost, and energy-efficiency of CRANs with all-analog optical passive fronthauling. Furthermore, different criterion, other than fairness, can be adopted to motivate the optimization problem in **Chapter** 2.

4. **Downlink:** The design and optimization problems in this thesis were solved for the uplink case. Thus, a possible extension to each problem is to consider the downlink case. It is remarkable that, under certain conditions, the results obtained for the uplink can be reused for the downlink which is defined as uplink-downlink duality as done by Yu (2006). For example, in a CRAN with identical uplink and downlink sum- power, and fronthaul capacity constraints, the achievable rate regions for both uplink and downlink are the same (Liu *et al.*, 2016). Such constraints must be considered in order to extend uplink rate maximization problem in **Chapter** 2 to the downlink scenario.

5. **Link design parameters:** Other link parameters can used to motivate a different set of problems and provide new insights about the performance of the system. Firstly, if an APD is used at the detector, the resulting shot noise is a function of the signal power which changes the analyses. Secondly, digital FSO links can be deployed to avoid the clipping distortion and allow for different source coding techniques over

compress-and-forward digital RUs. Additionally, another method to address the clipping problem, is to investigate the pulse shaping of the signal and optimize the performance by choosing the optimum pulse shaping.

Appendix A

Clipping Analysis for RF/RoFSO/RoF CRAN

A.1 Introduction

The extended work in **Appendix** A includes the impact of clipping distortion that was not included in **Chapter** 3. However the clipping distortion is negligible in **Chapter** 3 under the conservative gain design in (3.2) and (3.5), a more generic model must include this distortion for any gain values. Thus, in **Appendix** A the SINR expression with the clipping distortion is derived along with the required modification in the analytical expressions derived in **Chapter** 3 to reflect that effect. Additionally, this extension includes simulation results that justify the assumption of neglecting the clipping distortion in **Chapter** 3. It also shows that other gain values can cause significant clipping distortion, i.e. not negligible, that increases the outage probability by an order of magnitude.

A.2 Analysis

The system model in **Chapter** 3 considered a conservative value of the gain to be used in the relay nodes R_1 and R_2, Fig. 3.1, prior to the clipper. The conservative gain was designed to maintain 8 standard deviations of the signal within the linear region, i.e. not clipped. Consequently, the clipping distortion was assumed to be negligible. While this assumption is acceptable for the given scenario, a more inclusive model will be introduced in this appendix with any gain value. The analyses in this section also consider the clipping distortion and show how it changes on the derivations obtained in **Chapter** 3.

Following the model in Fig. 3.1, the clipping distortion is added at the relay nodes R_1 and R_2 at the RoFSO link and RoF link respectively. The access network does not experience any clipping distortion and the received RF signal is not changed.

$$y_{\mathrm{S,R1}} = h_{\mathrm{S,R1}}x + \sum_{i=1}^{M} h_i x_i + n_{\mathrm{R1}} \tag{A.1}$$

On the next hop, the RF signal is amplified by G_1, shifted by P_{opt1}, and clipped. Then the clipped signal is converted to an intensity modulated laser signal $y_{R1\mathrm{opt}}$. The clipping distortion is modelled by a scaling factor and an added noise term using Bussgang's linear regression model (Bussgang, 1952) as discussed in **Chapter** 2. The forwarded optical signal follows

$$y_{R1\mathrm{opt}} = P_{\mathrm{opt1}} + \alpha_i G_1 y_{\mathrm{S,R1}} + n_{c_1}. \tag{A.2}$$

where the scaling factor α_1 follows

$$\alpha_1 = \mathrm{erf}\left(\frac{P_{\mathrm{opt1}}}{\sqrt{2G_1^2\sigma_{\mathrm{in}_1}^2}}\right). \tag{A.3}$$

The clipping noise term has a variance $\sigma_{c_1}^2$

$$\sigma_{c_1}^2 = P_{\text{opt1}}^2 \left(1 - \frac{\alpha_1^2 G_1^2 \sigma_{\text{in}_1}^2}{P_{\text{opt1}}^2} - \sqrt{\frac{2G_1^2\sigma_{\text{in}_1}^2}{\pi P_{\text{opt1}}^2}} e^{-\frac{P_{\text{opt1}}^2}{2G_1^2\sigma_{\text{in}_1}^2}} + \left(\frac{G_1^2\sigma_{\text{in}_1}^2}{P_{\text{opt1}}^2} - 1 \right) \text{erf}\left(\frac{P_{\text{opt1}}}{\sqrt{2G_1^2\sigma_{\text{in}_1}^2}} \right) \right) \quad \text{(A.4)}$$

where $\sigma_{\text{in}_1}^2$ is the variance of the input to the clipper. Notice that if G_1 is designed as in (3.2), then P_{opt1} is K_1 multiples of the standard deviation of the input signal. Hence, $K_1 = P_{\text{opt1}}/G_1\sigma_{\text{in}_1}$ which simplifies (A.3) and (A.4) as follows

$$\alpha_1 = \text{erf}\left(\frac{K_1}{\sqrt{2}} \right) \quad \text{(A.5)}$$

and

$$\sigma_{c_1}^2 = P_{\text{opt1}}^2 \underbrace{\left(1 - \frac{\alpha_1^2}{K_1^2} - \sqrt{\frac{2}{\pi K_1^2}} e^{-\frac{K_1^2}{2}} + \left(\frac{1}{K_1^2} - 1 \right) \text{erf}\left(\frac{K_1}{\sqrt{2}} \right) \right)}_{f_1(K_1)}. \quad \text{(A.6)}$$

It is remarkable that at a fixed K_1, the clipping noise power becomes proportional to P_{opt1}^2 only as (A.6) can be written as $\sigma_{c_1}^2 = f_1(K_1)P_{\text{opt1}}^2$.

After removing the DC bias, the received electrical signal at the relay R_2 follows

$$y_{\text{R1,R2}} = \mathcal{R}_1 h_{\text{R1,R2}} \alpha_1 G_1 y_{\text{S,R1}} + \mathcal{R}_1 h_{\text{R1,R2}} n_{c_1} + n_{\text{R2}}. \quad \text{(A.7)}$$

Similarly, $y_{\text{R1,R2}}$ is amplified by G_2, shifted by P_{opt2}, clipped, then converted to the optical domain again and retransmitted through the optical fiber to the central office. The optical signal follows

$$y_{\text{R2opt}} = P_{\text{opt2}} + \alpha_2 G_2 y_{\text{R1,R2}} + n_{c_2} \quad \text{(A.8)}$$

where

$$G_2 = \frac{P_{\text{opt2}}}{K_2\sqrt{\frac{\mathcal{R}_1^2 E\left[|h_{\text{R1,R2}}|^2\right]\alpha_1^2 P_{\text{opt1}}^2}{K_1^2} + \mathcal{R}_1^2 E\left[\mid h_{\text{R1,R2}} \mid^2\right]\sigma_{c_1}^2 + \sigma_{\text{R2}}^2}}. \tag{A.9}$$

Notice that (A.9) is different from (3.5) to account for the effect of the clipping distortion on the variance of the input to the amplifier. The gain G_2 in (A.9) is modified to maintain a constant ratio of K_2 standard deviations of unclipped signal. The clipping distortion is modelled in a similar way to (A.5) and (A.6) as

$$\alpha_2 = \text{erf}\left(\frac{K_2}{\sqrt{2}}\right) \tag{A.10}$$

and

$$\sigma_{c_2}^2 = P_{\text{opt2}}^2 \underbrace{\left(1 - \frac{\alpha_2^2}{K_2^2} - \sqrt{\frac{2}{\pi K_2^2}} e^{-\frac{K_2^2}{2}} + \left(\frac{1}{K_2^2} - 1\right)\text{erf}\left(\frac{K_2}{\sqrt{2}}\right)\right)}_{f_2(K_2)}. \tag{A.11}$$

hence $\sigma_{c_2}^2 = f_2(K_2)P_{\text{opt2}}^2$. Finally, following the same assumptions in **Chapter** 3, the received electrical signal at the detector can be written as

$$y_{\text{R2,D}} = \mathcal{R}_2\left(\alpha_2 G_2 y_{\text{R1,R2}} + 2n_{\text{NLI}}\sqrt{y_{\text{R2opt}}} + n_{c_2}\right) + n_{\text{D}}. \tag{A.12}$$

The total SINR can be written as

$$\hat{\gamma}_{\text{T}} = \frac{\hat{\gamma}_1\hat{\gamma}_2}{\hat{\gamma}_2 + \hat{\gamma}_2\hat{\gamma}_{\text{R}} + C_1^2(1 + \hat{C}_2^2/\hat{\gamma}_3)} \tag{A.13}$$

where

$$
\begin{aligned}
\hat{\gamma}_1 &= \frac{\mid h_{\mathrm{S,R1}} \mid^2 P_{\mathrm{RF}}}{\sigma^2_{\mathrm{R1}} \left(1 + \frac{f_1(K_1) C_1^2}{\alpha_1^2}\right)} \\
\hat{\gamma}_{\mathrm{R}} &= \frac{\sum_{i=1}^{M} \mid h_i \mid^2 P_{\mathrm{Ri}}}{\sigma^2_{\mathrm{R1}} \left(1 + \frac{f_1(K_1) C_1^2}{\alpha_1^2}\right)} \\
\hat{\gamma}_2 &= \frac{\left(\mathcal{R}_1^2 \mid h_{\mathrm{R1,R2}} \mid^2 P^2_{\mathrm{opt1}}\right) \left(C_1^2 f_1(K_1) + \alpha_1^2\right)}{\sigma^2_{\mathrm{R2}} \left(1 + \frac{f_2(K_2) \hat{C}_2^2}{\alpha_2}\right)} \\
\hat{\gamma}_3 &= \frac{\left(\mathcal{R}_2^2 P^2_{\mathrm{opt2}}\right) \left(\alpha_2^2 + f_2(K_2) \hat{C}_2^2\right)}{4 \mathcal{R}_2^2 P_{\mathrm{opt2}} P_{\mathrm{NLI}} + \sigma^2_{\mathrm{D}}} \\
C_1 &= K_1 \sqrt{\overline{\gamma_1} + \sum_{i=1}^{M} \overline{\gamma_{\mathrm{Ri}}} + 1} \\
\hat{C}_2 &= K_2 \sqrt{\overline{\gamma_2} \left(f_1(K_1) + \frac{\alpha_1^2}{K_1^2}\right) + 1}
\end{aligned}
\tag{A.14}
$$

By comparing (A.14) with (3.12), the effect of clipping distortion can be shown as scaling the SNRs as follows

$$
\begin{aligned}
\hat{\gamma}_1 &= \frac{\gamma_1}{\left(1 + \frac{f_1(K_1) C_1^2}{\alpha_1^2}\right)} \\
\hat{\gamma}_{\mathrm{R}} &= \frac{\gamma_{\mathrm{R}}}{\left(1 + \frac{f_1(K_1) C_1^2}{\alpha_1^2}\right)} \\
\hat{\gamma}_2 &= \gamma_2 \left(\frac{C_1^2 f_1(K_1) + \alpha_1^2}{1 + \frac{f_2(K_2) \hat{C}_2^2}{\alpha_2}}\right) \\
\hat{\gamma}_3 &= \gamma_3 \left(\alpha_2^2 + f_2(K_2) \hat{C}_2^2\right)
\end{aligned}
\tag{A.15}
$$

It is remarkable to mention that all scales are deterministic. Thus, the scales change the statistical parameters, e.g. mean and variance, while the distribution functions are the same. In

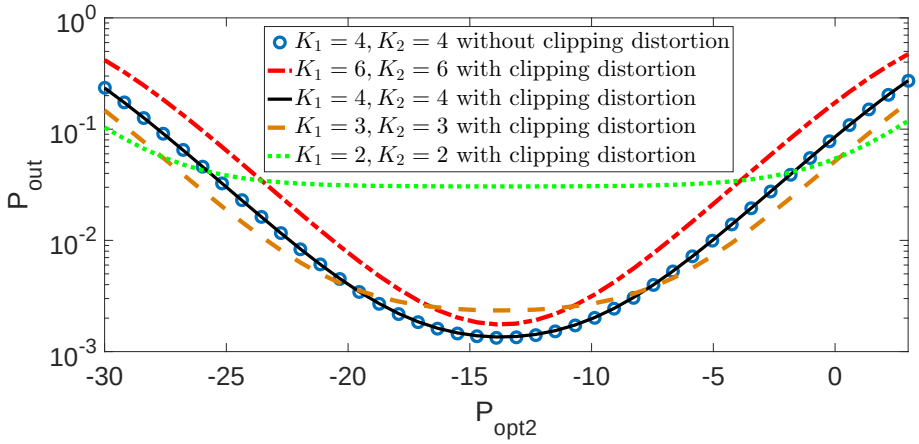

Figure A.1: P_{out} versus P_{opt2} ($\gamma_{\text{th}} = 0$ dB, $\overline{\gamma_1} = 30$ dB, $\overline{\gamma_2} = 70$ dB, $\overline{\gamma_{\text{Ri}}} = 5$ dB, $M = 0$, $\sigma_R = 0.4$, and $\zeta = 7.35$).

other words, the clipping distortion can be included in all derivations and expressions from **Chapter** 3 by substituting with the scaled parameters as obtained in (A.14) and (A.15).

A.3 Numerical Simulation

Figure A.1 shows the outage probability evaluated for different values of R_1 and R_2 gains at $K_1, K_2 \in 6, 4, 3, 2$ over a range of OF average optical power P_{opt2}. Notice that choosing a moderate value of the gain, $K_1 = K_2 = 4$ for this scenario, balances the trade-off between signal amplification and clipping distortion. Increasing the gain, i.e. decreasing $K_1, K_2 \in 3, 2$, leads to more clipping which degrades the reliability of the system. On the other hand, decreasing the gain, increasing $K_1 = K_2 = 6$, attenuates the signal which decreases the SINR leading to higher outage probability.

By observing the curves in Fig. A.1, at moderate range of the OF average optical power P_{opt2} around P^*_{opt2}, the clipping distortion dominates other sources of noise. At P^*_{opt2}, the outage probability at $K_1 = K_2 = 2$ increased by more than 10 times the outage

at $K_1 = K_2 = 4$. On contrary, for a conservative design of the gain, $K_1 = K_2 = 4$, the clipping noise is negligible and the two curves, with and without the clipping distortion, are nearly identical. Further study on the optimum design of the gain and the effect of clipping distortion are presented in **Chapter** 2 where the optimum gain was obtained numerically, and in **Chapter** 4 where an approximate analytical optimum gain was derived.

Appendix B

User Rates in RF/RoFSO/RoF CRAN with SIC Decoding

B.1 Introduction

Appendix B presents UE rate equations for another scenario when SIC is applied at the CO. As discussed earlier, Sec. 1.1, one of the key advantages of the CRAN architecture is the ability to perform joint interference mitigation techniques at the CO which in turn improves the SINR and increases the UE rates. The work in **Chapter** 3 did not consider such techniques for the tractability of the analyses, yet the extended work in **Appendix** B shows the rate equations along with a Monte-Carlo simulation for the CDF of UE rates and the average UE rates.

B.2 Analysis

The CDF of user rates in **Chapter** 3 is evaluated using the total UE-to-CO SINR. The evaluated SINR includes all interference components from UEs sharing the same band in neighboring cells. However, as discussed in **Chapter** 2, higher data rates are achievable using SIC at the CO. Thus, in this appendix, formulation of the user rates is introduced and numerical simulations are carried out to show the improvement in the CDF of UE rates.

The rate equations of uplink CRAN with SIC were studied in the literature (e.g., Zhou and Yu, 2014; Ahmed and Hranilovic, 2018) for different CRAN architectures. In **Chapter** 2, the rate equations of an uplink CRAN with SIC from (Zhou and Yu, 2014) were extended to be used for the system architecture in Fig. 2.2. Similarly, those rate equations can be modified according to the setup with three-hops RF/RoFSO/RoF in Fig. 3.1.

Define H to be the total channel matrix from $M+1$ UEs to the CO. The $M+1$ UEs are assumed to be in different cells, using the same band, and experiencing interference from each other. The channel matrix H representing the RF/RoFSO/OF can be written as

$$H = H_{\text{OF}} \times H_{\text{FSO}} \times H_{\text{RF}} \tag{B.16}$$

where H_{RF}, H_{FSO}, and H_{OF} are the channel matrices of the RF, FSO, and OF stages respectively.

For the RF access network, the diagonal elements of H_{RF}, $h_{\text{S}_\text{i},\text{R}_{1,\text{i}}}$, represent the direct channels from each of the $M+1$ UEs to the corresponding relay. The off-diagonal elements of H_{RF}, $h_{\text{S}_\text{i},\text{R}_{1,\text{k}}}$, are the channels from those UEs to the neighboring relays, i.e. interference

links between each other.

$$H_{\text{RF}} = \begin{bmatrix} h_{\text{S}_1,\text{R}_{1,1}} & h_{\text{S}_1,\text{R}_{1,2}} & \cdots & h_{\text{S}_1,\text{R}_{1,\text{M}+1}} \\ h_{\text{S}_2,\text{R}_{1,1}} & h_{\text{S}_2,\text{R}_{1,2}} & & \vdots \\ \vdots & \vdots & \ddots & h_{\text{S}_\text{M},\text{R}_{1,\text{M}+1}} \\ h_{\text{S}_{\text{M}+1},\text{R}_{1,1}} & h_{\text{S}_{\text{M}+1},\text{R}_{1,2}} & \cdots & h_{\text{S}_{\text{M}+1},\text{R}_{1,\text{M}+1}} \end{bmatrix}_{M+1\times M+1} . \tag{B.17}$$

The FSO fronthaul network does not experience interference and hence H_{FSO} is a diagonal matrix with the diagonal elements representing the direct RoFSO channel gains. The RoFSO channels, including the gain and responsivity scales, follow

$$H_{\text{FSO}} = \begin{bmatrix} \mathcal{R}_{1,1} h_{\text{R}_{1,1},\text{R}_{2,1}} G_{1,1} & 0 & \cdots & 0 \\ 0 & \mathcal{R}_{1,2} h_{\text{R}_{1,2},\text{R}_{2,2}} G_{1,2} & & \vdots \\ \vdots & & \ddots & 0 \\ 0 & \cdots & 0 & \mathcal{R}_{1,\text{M}+1} h_{\text{R}_{1,\text{M}+1},\text{R}_{2,\text{M}+1}} G_{1,\text{M}+1} \end{bmatrix}_{M+1\times M+1} . \tag{B.18}$$

Since all signals are coupled into one OF link, the OF channel matrix can be written as a diagonal matrix, H_{OF}, with equal diagonal elements representing the scaling of the RoF link $\mathcal{R}_2 G_2$.

Let Ω be a diagonal matrix that includes all noise powers from the RF, RoFSO, and RoF links as well as the GN-modelled OF nonlinearity. Noise variance from each stage is scaled

according to the path from the noise source to the CO. The total noise matrix follows

$$\Omega = \begin{bmatrix} \sigma_1^2 & 0 & \cdots & 0 \\ 0 & \sigma_2^2 & & \vdots \\ \vdots & & \ddots & 0 \\ 0 & \cdots & 0 & \sigma_{M+1}^2 \end{bmatrix} \tag{B.19}$$

where

$$\sigma_m^2 \;=\; \mathcal{R}_{1,\mathrm{m}} h_{\mathrm{R}_{1,\mathrm{m}},\mathrm{R}_{2,\mathrm{m}}} G_{1,\mathrm{m}} \mathcal{R}_2 G_2 \sigma_{R_1}^2 \;+\; \mathcal{R}_2 G_2 \sigma_{R_2}^2 \;+\; 4\mathcal{R}_2^2 P_{\mathrm{opt2}} P_{\mathrm{NLI}} \;+\; \sigma_D^2. \tag{B.20}$$

As discussed in **Chapter** 2, the i^{th} UE rate of an uplink CRAN with SIC can be expressed as

$$\log \frac{\left| \sum_{j=i}^{M+1} P_{\text{RF}} h_j h_j^H + \Omega \right|}{\left| \sum_{j>i}^{M+1} P_{\text{RF}} h_j h_j^H + \Omega \right|} \tag{B.21}$$

assuming all UEs transmit at equal power of P_{RF}. The term h_j is the j^{th} column vector from H.

Notice that the rates provided by (B.21) assume the SIC is done in the order 1^{st} to $M + 1^{th}$ UE. Thus, the remaining interfering components at each decoding step are due to the successive users only which improves the SINR.

B.3 Numerical simulation

In order to quantify the increase in UE data rates due to SIC, Monte-Carlo simulations are carried out over 10^6 instants. Each instant considers a set of $M + 1$ UEs from $M + 1$ cells transmitting signals and interfering with each other. To compare the obtained UE rates with

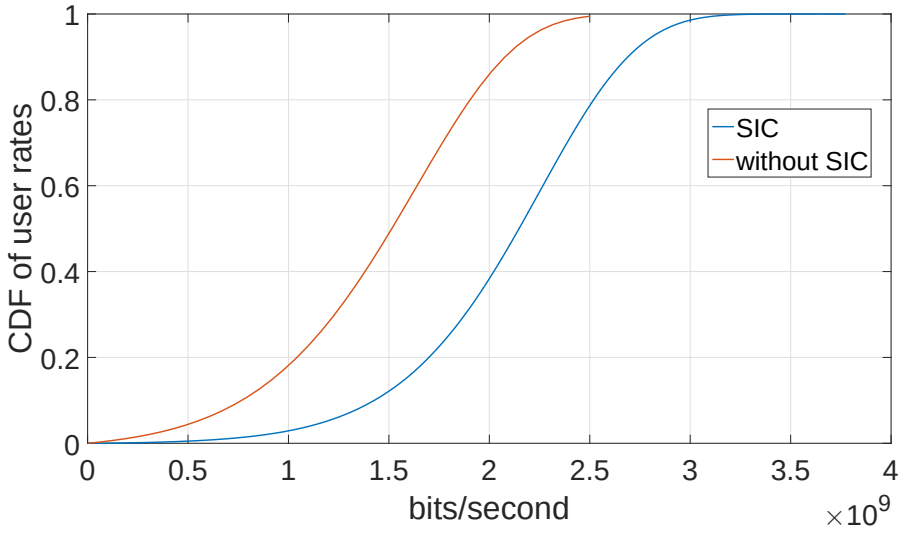

Figure B.2: CDF of User Rates ($M = 3$, $\overline{\gamma_1} = 40$ dB, $\overline{\gamma_2} = 40$ dB, $\overline{\gamma_{\mathrm{Ri}}} = 5$ dB, $R_{\mathrm{s}} = 220$ Msymbols/sec, $\sigma_{\mathrm{R}} = 0.75$, $\zeta = 7.35$, and $P_{\mathrm{opt2}} = -13.7$ dBm)

the results in **Chapter** 3, the same channel models, assumptions, and system parameters from **Chapter** 3 are used in the Monte-Carlo simulations.

Figure B.2 shows a comparison between the CDF of UE rates with and without SIC. Assuming 3 interfering UEs per UE, i.e. $M = 3$, statistics from a total of 4×10^6 UEs are used to evaluate the CDF of the rates with SIC. The other CDF curve, i.e. without SIC, is plotted using the analytical expression obtained in **Chapter** 3, (3.24). As shown in Fig. B.2, SIC improves the 50th percentile of UE rates by more than 35%.

The average UE rate with SIC is plotted in Fig. B.3 over a range of $P_{\mathrm{opt2}} \in \{-20, 5\}$ dBm. Since the RoF gain, G_2 is proportional to P_{opt2}, decreasing P_{opt2}, i.e. left half of the graph, decreases the UE rates since more attenuation impacts UE signals. On the other hand, when P_{opt2} increases, i.e. right half of the graph, it triggers more nonlinearity in the OF link which adds more nonlinear interference in the OF and hence UE rates are degraded as well. Thus, a careful choice of P_{opt2} is required to balance both effects and maximize the

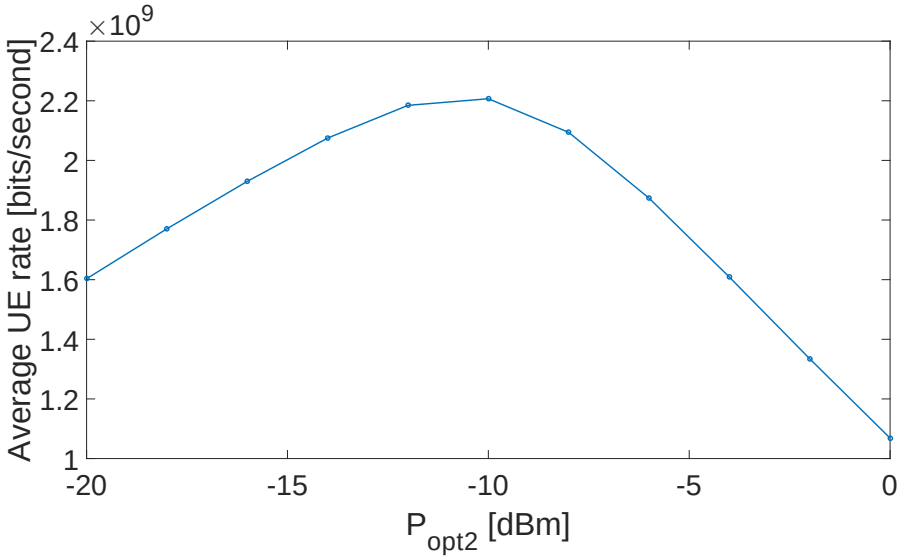

Figure B.3: Average User Rates

average UE rate.

Appendix C

P_{out} derivation with dominant n^2_{NLI}

C.1 Introduction

The dimensions and the optical power of the setup in Fig. 3.1 do not trigger severe NLI. Thus, the assumption of simplifying the SNR expression, (4.23), by ignoring the NLI squared noise term n^2_{NLI} with respect to the beating term n_{beat} is reasonable. On the contrary, the case with high n^2_{NLI} variance typically happens when the length of the optical fiber increases to be near a hundred kilometer and the total input optical power coupled in the fiber is high as well. That case was not covered in **Chapter** 4, but the outage probability for this scenario is derived in this appendix.

C.2 Analysis

For the total SNR expression given in (4.23), if the noise term n^2_{NLI} dominates, the SNR expression for the fronthaul network becomes

$$\text{SNR}_{\text{FH}} = \frac{P_{\text{RF}} K^2 G^2}{\sigma_c^2 + \frac{P_{n^2_{\text{NLI}}}}{\eta^2_{\text{OC}} \eta^2_{\text{OF}} g^2_{\text{FSO}} g^2_{\text{OF}}}}. \tag{C.22}$$

Thus, the outage probability in (4.25) can be expressed as

$$P_{\text{out}}\left(\gamma_{\text{th}}\right) = \Pr\left(g_a^4 > \frac{P_{\text{RF}} K^2 G^2 - \gamma_{\text{th}} \sigma_c^2}{2\gamma_{\text{th}} c_1^2 c_d^6 / g_l^2 g_d^2 g^2_{\text{OF}} \eta^2_{\text{OC}} \eta^2_{\text{OF}}} \right). \tag{C.23}$$

In order to obtain the PDF of g_a^4, define $\tilde{g}_a = g_a^4$. Then $\frac{dg_a}{d\tilde{g}_a} = 1/4\tilde{g}_a^{3/4}$ which, after performing the transformation of random variables, yields

$$f_{\tilde{g}_a}\left(\tilde{g}_a\right) = \frac{1}{8\tilde{g}_a \sqrt{2\pi {\sigma_d}^2}} \exp\left(-\frac{\left(\ln \tilde{g}_a + 8{\sigma_d}^2\right)^2}{128{\sigma_d}^2} \right). \tag{C.24}$$

After further simplification, it can be shown that the outage probability can be evaluated using the following integral

$$P_{\text{out}}\left(\gamma_{\text{th}}\right) = \frac{1}{8\sqrt{2\pi {\sigma_d}^2}} \int_{I_2}^{\infty} \frac{1}{\tilde{g}_a} \exp\left(-\frac{\left(\ln \tilde{g}_a + 8{\sigma_d}^2\right)^2}{128{\sigma_d}^2} \right) \mathrm{d}\tilde{g}_a \tag{C.25}$$

where

$$I_2 = \frac{P_{\text{RF}} K^2 G^2 - \gamma_{\text{th}} \sigma_c^2}{2\gamma_{\text{th}} c_1^2 c_d^6 / g_l^2 g_d^2 g^2_{\text{OF}} \eta^2_{\text{OC}} \eta^2_{\text{OF}}}. \tag{C.26}$$

Let $\phi = \ln \tilde{g}_a$, then rewriting (C.25) yields

$$P_{\text{out}}\left(\gamma_{\text{th}}\right) = \frac{e^{-\sigma_d^2/2}}{4\sqrt{2\pi{\sigma_d}^2}} \int_{\ln I_2}^{\infty} \exp\left(-\frac{\phi^2}{128\sigma_d^2} - \frac{\phi}{8}\right) \mathrm{d}\phi \tag{C.27}$$

which can be written as

$$P_{\text{out}}\left(\gamma_{\text{th}}\right) = \frac{1}{2}\text{erfc}\left(\frac{\sigma_d}{\sqrt{2}} + \frac{\ln I_2}{8\sqrt{2}\sigma_d}\right). \tag{C.28}$$

Notice that, maximizing the expression (4.34) maximizes the term $\ln I_2$ since the $\ln$ function is monotonically increasing. This, in turn, minimizes the outage probability since this term is in the argument of the erfc$(\cdot)$ function which is monotonically decreasing. Thus, the optimum gain expression derived in (4.43) is also valid for the case when n_{NLI}^2 dominates n_{beat} and the thermal noise.

Bibliography

Adamchik, V. S. and Marichev, O. I. (1990). The algorithm for calculating integrals of hypergeometric type functions and its realization in reduce system. In *Proc. Int. Symposium on Symbolic and Algebraic Computation*, pages 212–224.

Agiwal, M., Roy, A., and Saxena, N. (2016). Next generation 5G wireless networks: A comprehensive survey. *IEEE Commun. Surveys Tuts.*, **18**(3), 1617–1655.

Ahmed, K. and Hranilovic, S. (2018). C-RAN uplink optimization using mixed radio and FSO fronthaul. *IEEE/OSA J. Opt. Commun. Netw.*, **10**(6), 603–612.

Al-Dabbagh, R. K. and Al-Raweshidy, H. S. (2017). 64-GHz millimeter-wave photonic generation with a feasible radio over fiber system. *Opt. Eng.*, **56**(2), 026117–1–026117–10.

Al-Habash, R. L., Andrews, M. A., and Phillips, L. C. (2001). Mathematical model for the irradiance probability density function of a laser beam propagating through turbulent media. *Opt. Eng.*, **40**(8), 1554–1562.

Andrews, J. G., Buzzi, S., Choi, W., Hanly, S. V., Lozano, A., Soong, A. C. K., and Zhang, J. C. (2014). What will 5G be? *IEEE J. Sel. Areas Commun.*, **32**(6), 1065–1082.

Anees, S. and Bhatnagar, M. R. (2014). Performance analysis of amplify-and-forward dual-hop mixed RF/FSO systems. In *Proc. IEEE Veh. Technol. Conf.*, pages 1–5.

Anees, S. and Bhatnagar, M. R. (2015a). Information theoretic analysis of a dual-hop fixed gain AF based mixed RF-FSO system. In *International Symposium on Personal, Indoor, and Mobile Radio Communications*, pages 927–931.

Anees, S. and Bhatnagar, M. R. (2015b). Performance of an amplify-and-forward dual-hop asymmetric RF-FSO communication system. *J. Opt. Commun. Netw.*, **7**(2), 124–135.

Ansari, I. S., Al-Ahmadi, S., Yilmaz, F., Alouini, M.-S., and Yanikomeroglu, H. (2011). A new formula for the BER of binary modulations with dual-branch selection over generalized-K composite fading channels. *IEEE Trans. Commun.*, **59**(10), 2654–2658.

Ansari, I. S., Yilmaz, F., and Alouini, M.-S. (2013a). Impact of pointing errors on the performance of mixed RF/FSO dual-hop transmission systems. *IEEE Wireless Commun. Lett.*, **2**(3), 351–354.

Ansari, I. S., Yilmaz, F., and Alouini, M. S. (2013b). On the performance of hybrid RF and RF/FSO dual-hop transmission systems. In *Proc. 2nd Int. Workshop Opt. Wireless Commun.*, pages 45–49.

Ansari, I. S., Alouini, M.-S., and Yilmaz, F. (2013c). On the performance of hybrid RF and RF/FSO fixed gain dual-hop transmission systems. In *Proc. Saudi Int. Conf. Electron., Commun. and Photon.*, pages 1–6.

Awan, M. S., Csurgai-Horváth, L., Muhammad, S. S., Leitgeb, E., Nadeem, F., and Khan, M. S. (2009). Characterization of fog and snow attenuations for free-space optical propagation. *J. Commun.*, **4**(8), 533–545.

Bhatnagar, M. R. and Arti, M. K. (2013). Performance analysis of hybrid satellite-terrestrial FSO cooperative system. *IEEE Photon. Technol. Lett.*, **25**(22), 2197–2200.

Bosco, G., Poggiolini, P., Carena, A., Curri, V., and Forghieri, F. (2012). Analytical results on channel capacity in uncompensated optical links with coherent detection. *Opt. Exp.*, **20**(17), 19610–19611.

Bussgang, J. (1952). Crosscorrelation functions of amplitude-distorted Gaussian signals. *MIT Res. Lab. Tech. Rep.*, **216**, 1–14.

Cai, S., Zhang, Z., and Chen, X. (2019). Free-space optical relaying system with few-mode all-optical relay. *Opt. Commun.*, **439**, 164–170.

Checko, A., Christiansen, H. L., Yan, Y., Scolari, L., Kardaras, G., Berger, M. S., and Dittmann, L. (2015). Cloud RAN for mobile networksA technology overview. *Commun. Surveys Tuts.*, **17**(1), 405–426.

Chergui, H., Benjillali, M., and Saoudi, S. (2016). Performance analysis of project-and-forward relaying in mixed MIMO-pinhole and Rayleigh dual-hop channel. *IEEE Commun. Lett.*, **20**(3), 610–613.

Chiani, M., Dardari, D., and Simon, M. K. (2003). New exponential bounds and approximations for the computation of error probability in fading channels. *IEEE Trans. Wireless Commun.*, **2**(4), 840–845.

China Mobile (2011). C-RAN: the road towards green RAN. *White Paper*, **2**, 1–10.

Corless, R. M., Gonnet, G. H., Hare, D. E. G., Jeffrey, D. J., and Knuth, D. E. (1996). On the Lambert W function. In Advances in Computational Mathematics, volume 5, pages 329–359. US: Springer.

Dahrouj, H., Douik, A., Rayal, F., Al-Naffouri, T. Y., and Alouini, M. (2015). Cost-effective hybrid RF/FSO backhaul solution for next generation wireless systems. *IEEE Wireless Commun.*, **22**(5), 98–104.

Dehos, C., Gonzalez, J. L., Domenico, A. D., Ktenas, D., and Dussopt, L. (2014). Millimeter-wave access and backhauling: The solution to the exponential data traffic increase in 5G mobile communications systems? *IEEE Commun. Mag.*, **52**(9), 88–95.

Demestichas, P., Georgakopoulos, A., Karvounas, D., Tsagkaris, K., Stavroulaki, V., Lu, J., Xiong, C., and Yao, J. (2013). 5G on the horizon: Key challenges for the radio-access network. *IEEE Veh. Technol. Mag.*, **8**(3), 47–53.

Douik, A., Dahrouj, H., Al-Naffouri, T. Y., and Alouini, M. (2016). Hybrid radio/free-space optical design for next generation backhaul systems. *IEEE Trans. Commun.*, **64**(6), 2563–2577.

El-Fiqi, A. E., Morra, A. E., Hegazy, S. F., Shalaby, H. M. H., Kato, K., and Obayya, S. S. A. (2016). Performance evaluation of hybrid DPSK-MPPM techniques in long-haul optical transmission. *Appl. Opt.*, **55**(21), 5614–5622.

Essiambre, R.-J., Kramer, G., Winzer, P. J., Foschini, G. J., and Goebel, B. (2010). Capacity limits of optical fiber networks. *J. Lightw. Technol.*, **28**(4), 662–701.

Evans, M., Hastings, N., and Peacock, B. (2000). *Statistical Distributions*. Wiley, Hoboken, NJ, USA, 3rd edition.

Farid, A. A. and Hranilovic, S. (2007). Outage capacity optimization for free-space optical links with pointing errors. *J. Lightw. Technol.*, **25**(7), 1702–1710.

Farid, A. A. and Hranilovic, S. (2009). Link reliability, range and rate optimization for free-space optical channels. In *Proc. 10th Int. Conf. Telecommun.*, pages 19–23.

Forney, G. D. and Wei, L. F. (1989). Multidimensional constellations – Part I: Introduction, figures of merit, and generalized cross constellations,. *IEEE J. Sel. Areas Commun.*, **7**(6), 877–892.

fSONA Corporation (2017). *fSONA Corporation Website*. `http://www.fsona.com/`. Accessed: 2017.05.09.

Ge, X., Tu, S., Mao, G., Wang, C.-X., and Han, T. (2016). 5G ultra-dense cellular networks. *IEEE Wireless Commun.*, **23**(1), 72–79.

Gradshteyn, I. S. and Ryzhik, I. M. (2007). *Table of Integrals, Series, and Products*. Academic Press, 7th edition.

Gupta, A. and Jha, R. K. (2015). A survey of 5G network: Architecture and emerging technologies. *IEEE Access*, **3**, 1206–1232.

Khalighi, M. A. and Uysal, M. (2014). Survey on free space optical communication: A communication theory perspective. *IEEE Commun. Surveys Tuts.*, **16**(4), 2231–2258.

Kiasaleh, K. (2005). Performance of APD-based, PPM free-space optical communication systems in atmospheric turbulence. *IEEE Trans. Commun.*, **53**(9), 1455–1461.

Kim, S. J., Devroye, N., Mitran, P., and Tarokh, V. (2008). Comparison of bi-directional relaying protocols. In *Proc. IEEE Sarnoff Symposium*, pages 1–5.

Kong, L., Xu, W., Hanzo, L., Zhang, H., and Zhao, C. (2015). Performance of a free-space-optical relay-assisted hybrid RF/FSO system in generalized M -distributed channels. *IEEE Photon. J*, **7**(5), 1–19.

Lee, C., Sorin, W. V., and Kim, B. Y. (2006). Fiber to the home using a PON infrastructure. *J. Lightw. Technol.*, **24**(12), 4568–4583.

Lee, E., Park, J., Han, D., and Yoon, G. (2011). Performance analysis of the asymmetric dual-hop relay transmission with mixed RF/FSO links. *IEEE Photonics Technol. Lett.*, **23**(21), 1642–1644.

Li, Y., Ghafoor, S., Satyanarayana, K., El-Hajjar, M., and Hanzo, L. (2019). Analogue wireless beamforming exploiting the fiber-nonlinearity of radio over fiber based C-RANs. *IEEE Trans. Veh. Technol.*, **68**(3), 2802–2813.

Liu, L., Patil, P., and Yu, W. (2016). An uplink-downlink duality for cloud radio access network. In *Proc. IEEE Int. Symp. Inf. Theory (ISIT)*, pages 1606–1610.

M. Naboulsi, H. S. and Fornel, F. (2005). Propagation of optical and infrared waves in the atmosphere. In *Proc. Union Radio Scientifique Internationale (URSI)*, pages 1–4.

MATLAB (2016). Matlab, *version (R2015b)*. Massachusetts.

Morra, A. E. and Hranilovic, S. (2019). Mixed mmwave and radio-over-fiber systems with fiber nonlinearity. *IEEE Photon. Technol. Lett.*, **31**(1), 23–26.

Morra, A. E., Ahmed, K., and Hranilovic, S. (2017). Impact of fiber nonlinearity on 5G backhauling via mixed FSO/fiber network. *IEEE Access*, **5**, 19942–19950.

Najafi, M., Jamali, V., Ng, D. W. K., and Schober, R. (2017). C-RAN with hybrid RF/FSO fronthaul links: Joint optimization of RF time allocation and fronthaul compression. In *Proc. IEEE Global Commun. Conf.*, pages 1–7.

Park, J., Lee, E., Park, G., Roh, B., and Yoon, G. (2013). Performance analysis of asymmetric RF/FSO dual-hop relaying systems for UAV applications. In *Proc. IEEE Military Commun. Conf.*, pages 1651–1656.

Park, S., Simeone, O., Sahin, O., and Shamai, S. (2013). Joint precoding and multivariate backhaul compression for the downlink of cloud radio access networks. *IEEE Trans. Signal Process.*, **61**(22), 5646–5658.

Pesek, P., Bohata, J., Zvanovec, S., and Perez, J. (2016). Analyses of dual polarization WDM and SCM radio over fiber and radio over FSO for C-RAN architecture. In *Proc. 25th Wireless and Opt. Commun. Conf.*, pages 1–4.

Petkovic, M. I. (2015). Performance analysis of mixed RF/FSO systems. In *Proc. 23rd Telecommun. Forum*, pages 293–300.

Petkovic, M. I., Cvetkovic, A. M., Djordjevic, G. T., and Karagiannidis, G. K. (2015). Partial relay selection with outdated channel state estimation in mixed RF/FSO systems. *J. Lightw. Technol.*, **33**(13), 2860–2867.

Petkovic, M. I., Cvetkovic, A. M., Djordjevic, G. T., and Karagiannidis, G. K. (2017). Outage performance of the mixed RF/FSO relaying channel in the presence of interference. *Wireless Pers. Commun.*, **96**(2), 2999–3014.

Pham, A. T., Trinh, P. V., Mai, V. V., Dang, N. T., and C-T Truong (2015). Hybrid free-space optics/millimeter-wave architecture for 5G cellular backhaul networks. In *Proc. Opto-Elec. Commun. Conf.*, pages 1–3.

Poggiolini, P., Carena, A., Curri, V., Bosco, G., and Forghieri, F. (2011). Analytical modeling of nonlinear propagation in uncompensated optical transmission links. *IEEE Photon. Technol. Lett.*, **23**(11), 742–744.

Poggiolini, P., Bosco, G., Carena, A., Curri, V., Jiang, Y., and Forghieri, F. (2012). A detailed analytical derivation of the GN model of non-linear interference in coherent optical transmission systems. *arXiv:1209.0394 [physics]*.

Poggiolini, P., Bosco, G., Carena, A., Curri, V., Jiang, Y., and Forghieri, F. (2014). The GN-model of fiber non-linear propagation and its applications. *J. Lightw. Technol.*, **32**(4), 694–721.

Saito, Y., Kishiyama, Y., Benjebbour, A., Nakamura, T., Li, A., and Higuchi, K. (2013). Non-orthogonal multiple access (NOMA) for cellular future radio access. In *Proc. IEEE 77th Veh. Technol. Conf.*, pages 1–5.

Samimi, H. (2019). Outage analysis of mixed dual-hop RF-FSO communication system over fading channels with pointing errors. *Wireless Personal Commun.*, pages 1–13.

Samimi, H. and Uysal, M. (2013). End-to-end performance of mixed RF/FSO transmission systems. *J. Opt. Commun. Netw.*, **5**(11), 1139–1144.

Sanderovich, A., Shamai, S., Steinberg, Y., and Kramer, G. (2008). Communication via decentralized processing. *IEEE Trans. Inf. Theory*, **54**(7), 3008–3023.

Sanderovich, A., Shamai, S., and Steinberg, Y. (2009a). Distributed MIMO receiver-achievable rates and upper bounds. *IEEE Trans. Inf. Theory*, **55**(10), 4419–4438.

Sanderovich, A., Somekh, O., Poor, H. V., and Shamai, S. (2009b). Uplink macro diversity of limited backhaul cellular network. *IEEE Trans. Inf. Theory*, **55**(8), 3457–3478.

Sauer, M., Kobyakov, A., and George, J. (2007). Radio over fiber for picocellular network architectures. *J. Lightw. Technol*, **25**(11), 3301–3320.

Shieh, W. and Chen, X. (2011). Information spectral efficiency and launch power density limits due to fiber nonlinearity for coherent optical OFDM systems. *IEEE Photon. J.*, **3**(2), 158–173.

Siddique, U., Tabassum, H., Hossain, E., and Kim, D. I. (2015). Wireless backhauling of 5G small cells: Challenges and solution approaches. *IEEE Wireless Commun.*, **22**(5), 22–31.

Simon, M. K. and Alouini, M.-S. (2000). *Digital Communication over Fading Channels*. Wiley, Hoboken, NJ.

Simon, M. K. and Alouini, M.-S. (2005). *Digital Communication over Fading Channels*, volume 95. John Wiley & Sons.

Singh, J., Ponnuru, S., and Madhow, U. (2009). Multi-Gigabit communication: The ADC bottleneck. In *Proc. IEEE Int. Conf. on Ultra-Wideband*, pages 22–27.

Smadi, M. N., Ghosh, S. C., Farid, A. A., Todd, T. D., and Hranilovic, S. (2009). Free-space optical gateway placement in hybrid wireless mesh networks. *IEEE/OSA J. Lightw. Technol.*, **27**(14), 2688–2697.

Soleimani-Nasab, E. and Uysal, M. (2016). Generalized performance analysis of mixed RF/FSO cooperative systems. *IEEE Trans. Wireless Commun.*, **15**(1), 714–727.

Soleimani-Nasab, E., Matthaiou, M., Ardebilipour, M., and Karagiannidis, G. (2013). Two-way AF relaying in the presence of co-channel interference. *IEEE Trans. Commun.*, **61**(8), 3156–3169.

Song, X., Yang, F., and Cheng, J. (2013). Subcarrier intensity modulated optical wireless communications in atmospheric turbulence with pointing errors. *J. Opt. Commun. Netw.*, **5**(4), 349–358.

Tan, Z., Yang, C., and Wang, Z. (2017). Energy consume analysis for ring-topology TWDM-PON front-haul enabled cloud RAN. *J. Lightw. Technol.*, **35**(20), 4526–4534.

Tipmongkolsilp, O., Zaghloul, S., and Jukan, A. (2011). The evolution of cellular backhaul technologies: Current issues and future trends. *IEEE Commun. Surveys Tuts.*, **13**(1), 97–113.

Trinh, P. V., Thang, T. C., and Pham, A. T. (2017). Mixed mmWave RF/FSO relaying systems over generalized fading channels with pointing errors. *IEEE Photon. J.*, **9**(1).

Usman, M., Yang, H. C., and Alouini, M. S. (2014). Practical switching-based hybrid FSO/RF transmission and its performance analysis. *IEEE Photon. J*, **6**(5), 1–13.

Wake, D., Nkansah, A., and Gomes, N. J. (2010). Radio over fiber link design for next generation wireless systems. *J. Lightw. Technol*, **28**(16), 2456–2464.

Wang, G., Gu, R., Zhang, J., Li, H., and Ji, Y. (2016a). Asynchronous delivery oriented efficient resource allocation in TWDM-PON enabled fronthaul. In *Proc. IEEE Online Conf. Green Commun. (OnlineGreenComm)*, pages 45–50.

Wang, X., Thota, S., Tornatore, M., Chung, H. S., Lee, H. H., Park, S., and Mukherjee, B. (2016b). Energy-efficient virtual base station formation in optical-access-enabled cloud-RAN. *IEEE J. Sel. Areas Commun.*, **34**(5), 1130–1139.

Wang, X., Cavdar, C., Wang, L., Tornatore, M., Zhao, Y., Chung, H. S., Lee, H. H., Park, S., and Mukherjee, B. (2016c). Joint allocation of radio and optical resources in virtualized cloud RAN with CoMP. In *Proc. IEEE Global Commun. Conf.*, pages 1–6.

Weathercanada (2017). Weather, climate and hazards - canada.ca. `https://www.canada.ca/en/services/environment/weather.html`. Accessed: 2017.05.03.

Wolfram Research (2017). *The Wolfram Functions Site*. `http://functions.wolfram.com`. Accessed: 2017.05.09.

Yu, W. (2006). Uplink-downlink duality via minimax duality. *IEEE Trans. Inf. Theory*, **52**(2), 361–374.

Yu, W., Kwon, T., and Shin, C. (2011). Adaptive resource allocation in cooperative cellular networks. In *Cooperative Cellular Wireless Networks*, pages 233–256. Cambridge University Press.

Zedini, E., Ansari, I. S., and Alouini, M.-S. (2014). On the performance of hybrid line of sight RF and RF-FSO fixed gain dual-hop transmission systems. In *Proc. 2014 IEEE Global Commun. Conf.*, pages 2119–2124.

Zedini, E., Ansari, I. S., and Alouini, M.-S. (2015a). Performance analysis of mixed Nakagami-m and Gamma-Gamma dual-hop FSO transmission systems. *IEEE Photon. J.*, **7**(1), 1–20.

Zedini, E., Ansari, I. S., and Alouini, M.-S. (2015b). Unified performance analysis of mixed line of sight RF-FSO fixed gain dual-hop transmission systems. In *Proc. IEEE Wireless Commun. Netw. Conf.*, pages 46–51.

Zedini, E., Soury, H., and Alouini, M.-S. (2016). On the performance analysis of dual-hop mixed FSO/RF systems. *IEEE Trans. Wireless Commun.*, **15**(5), 3679–3689.

Zhang, J., Dai, L., Zhang, Y., and Wang, Z. (2015). Unified performance analysis of mixed radio frequency/free-space optical dual-hop transmission systems. *J. Lightw. Technol.*, **33**(11), 2286–2293.

Zhang, X., Cheng, W., and Zhang, H. (2014). Heterogeneous statistical QoS provisioning over 5G mobile wireless networks. *IEEE Network*, **28**(6), 46–53.

Zheng, D., Li, Y., Chen, E., Li, B., Kong, D., Li, W., and Wu, J. (2016). Free-space to few-mode-fiber coupling under atmospheric turbulence. *Opt. Express*, **24**(16), 18739–18744.

Zhou, Y. and Yu, W. (2014). Optimized backhaul compression for uplink cloud radio access network. *IEEE J. Sel. Areas Commun.*, **32**(6), 1295–1307.

Zhou, Y. and Yu, W. (2016). Fronthaul compression and transmit beamforming optimization for multi-antenna uplink C-RAN. *IEEE Trans. Signal Process.*, **64**(16), 4138–4151.

Zixiang Xiong, Liveris, A. D., and Cheng, S. (2004). Distributed source coding for sensor networks. *IEEE Signal Processing Magazine*, **21**(5), 80–94.